Università degli Studi di Palermo

AREA QUALITÀ, PROGRAMMAZIONE E SUPPORTO STRATEGICO
SETTORE STRATEGIA PER LA RICERCA
U. O. DOTTORATI

Scienze Molecolari e Biomolecolari
Dipartimento di Scienze e Tecnologie Biologiche Chimiche e Farmaceutiche (STEBICEF)
Settore Scientifico Disciplinare - SSD:CHIM/08

Development of natural and synthetic compounds as kinase inhibitors targeting cancer cells and cancer stem cells

IL DOTTORE
Dott. FABIO SCIANO'

IL COORDINATORE
Chiar.ma Prof.ssa GIOVANNA PITARRESI

IL TUTOR
Chiar.ma Prof.ssa PATRIZIA DIANA

IL CO TUTOR
Preg.ma Dott.ssa STELLA MARIA CASCIOFERRO

CICLO XXXV
ANNO CONSEGUIMENTO TITOLO 2023

INDEX

Introduction 3

Pancreatic ductal adenocarcinoma 4

Pancreas physiology 4

Pancreatic ductal adenocarcinoma 5

Standard treatments and chemoresistance of Pancreatic Ductal Adenocarcinoma 7

PDAC conventional chemotherapy 8

Chemoresistance in Pancreatic ductal adenocarcinoma 8

Role of protein kinases 11

Protein Tyrosine Kinases families 13

Focal adhesion kinase: structure and activity 14

FAK promotes cancer invasion and metastasis 16

Role of FAK as a potential target in PDAC 18

Healthcare crisis: the antimicrobial resistance 21

Bacterial biofilm 24

Strategies to combat microbial biofilm 27

Imidazo[2,1-b][1,3,4]thiadiazoles 33

Imidazo[2,1-*b*][1,3,4]thiadiazole: A Promising Bioactive Scaffold in Medicinal Chemistry 33

Imidazo[2,1-*b*][1,3,4]thiadiazole: antiproliferative activity. 34

Aim of the study 42

Chemistry section 49

Biology section 65

Antiproliferative activity 65

Biological assays on Pancreatic Ductal Adenocarcinoma cells 76

Cells viability assays 76

Effect on cell cycle 81

Antimigratory activity 83

PamGene Kinases array 86

Anti-biofilm activity 90

EXPERIMENTAL SECTION 93

Chemistry 93

Biology 139

References 145

Introduction

Cancer is major public healthcare issue all around the world, it occupies the second position as leading cause of lethal disease after cardiovascular illness. The 5-year relative survival rate of all cancers combined increased between the mid-1970s and 2011 from 49% to 68% overall, from 50% to 68% in White people, and from 39% to 63% in Black individuals[1]. In 2020, tumor incidence registered 19,292,789 new cases all around the world, and high mortality in both sexes (9,958,133). In 2020, the WHO ranking of the five top incident human tumors includes: breast (2,261,419), lung (2,206,771), colonrectum (1,931,590), prostate (1,414,259) and stomach (1,089,103). These malignancies represent the 46.14% of the whole new year cases.[2] In the last decades, the development of successful treatment methods and early diagnostic markers had a huge impact on reduction of mortality rates, especially in not invasive cancer. In regional cancer, the survival rate is higher for female breast cancer (86%), colonrectum (72%), and lung cancer (60%)[3]. Whereas, metastatic cancers follow a different trend, indeed five years survival rate for invasives cancers are significantly lower , i.e. female breast cancer (29%), colonrectum (15%), and lung cancer (6%), representing a major challenge in cancer therapy.[3]

Pancreatic cancer is an outstanding example of early-stage metastatic challenging cancer, despite lower world incidence (495,773; 3%), pancreatic cancer maintains a high mortality rate, with 11% in 5-years overall survival rate. As the forecast of 2022 showed, the pancreatic cancer estimated cases are in eighth and tenth (3%) positions, respectively in women and men.[3] Moreover, it is alarming that pancreatic cancer ranked in third position for estimated death in both sexes, even if mortality has increased slowly in men, from 12.1 (per 100,000) in 2000 to 12.7 in 2019 but remained relatively stable in women at 9.3 to 9.6 per 100,000[3].

Treatment approaches to support oncological patients strictly depend on tumors type and on the progression of the disease, which has large impact on treatment strategy (surgery, radiotherapy, or chemotherapy)[4] and the consequent follow up.

Pancreatic ductal adenocarcinoma

Pancreas physiology

The pancreas is a composite gland, which has exocrine and endocrine functions. The endocrine part is composed by islets of Langerhans. Four different cell types constitute the Islet (alpha, beta, delta and epsilon). Alpha and beta cells constitute the 85% of the islet and regulate the glucose level in blood stream. Indeed, alphas induce the release of glucagon in hypoglycaemia condition, while elevated blood glucose levels determine the release of insulin by beta cells. The 4% of islet is formed by delta cells that release somatostatin, regulating alpha and beta cells activity. Finally, epsilon cells produce Ghrelin, involved in regulating body's energy balance. Exocrine portion is composed by acinar cells (Acini) which produce and transport enzymes that are released into small ducts and then pass through larger central pancreatic duct, from which they are drained into the bile duct, and then to the duodenum (the first part of the small bowel)[5]. In duodenum, pancreatic juice supports the digestion of complex macromolecules of food. Consequently, pancreatic activities are essential involved in digestive function and the hormonal regulation. Thus, any problems and malfunctions of pancreas lead to some specific treatable diseases such as diabetes or other dysfunctions, which sometimes may advance to pancreatitis and tumour initiation[6].

In pancreatic gland, neoplasia can arise from both sides[7]:

- Exocrine: many tumours of the pancreas arise in the exocrine part. Under the microscope these cancer tissues look like pancreatic ducts and that is why they are known as Pancreatic Ductal Adenocarcinoma
- Endocrine: less frequently, tumours arise from the endocrine component of the pancreas and these endocrine tumours are called "pancreatic neuroendocrine tumours" or "islet cell tumours" for short[8].

The 95% of pancreatic cancer diagnoses are Pancreatic ductal adenocarcinoma (PDAC)[9].

Pancreatic ductal adenocarcinoma

Pancreatic ductal adenocarcinoma diagnoses are closely correlated with age; thus incidence rise in elder people (>50 y.o.)[10]; also family disease history has impact on the neoplasm onset (5-10%)[11]. Therefore, associated environmental risks are smoking tobacco and alcohol abuse, in fact smokers have twofold to threefold higher risk of developing pancreatic cancer than non-smokers[12]. Pancreatic diseases such as diabetes mellitus, are recognized as risk factor for early-stage pancreatic cancer; additionally, long term diabetes mellitus approximately doubles the risk of pancreatic cancer.[13]

Early spread with local diffusion and metastasis to distant organs are the main features which make this tumour so lethal. Even though, surgery remains the only chance of cure for PDAC,[14] for mentioned reasons only few patients (15-20%) are eligible for surgical resection[15], whereas the greatest part of patients is diagnosed too late when neoplasm is locally advanced or metastatic, not allowing surgical resection.[16]

Acinar cells, responsible for the secretion of digestive enzymes, are characterized by intrinsic plasticity and have a key role in ductal cell metaplasia induction: this metaplastic process known as acinar-ductal metaplasia, occurs during acute-chronic pancreatitis and may represent an initial step towards the pancreatic intraepithelial neoplasia formation[17]

Mainly, pancreatic cancers originate from three different types of precursor lesions: intraductal papillary mucinous neoplasms (IPMNs), mucinous cystic neoplasms (MCNs) and pancreatic intraepithelial neoplasia (PanIN). MCNs are mucin-producing cyst-forming epithelial neoplasms of the pancreas with a peculiar stromal tissue; IPMNs are non-invasive mucin-producing epithelial tumours, usually characterized by formation of long finger-like papillae; PanINs are non-invasive small epithelial tumours, located in the smaller pancreatic ducts, and characterized by cytological and architectural atypia.[18–20]

KRAS (Kirsten rat sarcoma virus) mutations have been identified as leading cause of PDAC early lesion initiation (PanIN1). Other common mutations include inactivation of cyclin-dependent kinase inhibitor 2 (CDKN2) (in

around 90% of PDAC cases) and Mothers against decapentaplegic homolog 4 (SMAD4/DPC4) (~55%), BRCA2, MutL homolog 1 (MLH1) or protease serine 1 (PRSS1) alteration; thus, the 50–70% of PDAC cases which carry mutations in the tumour protein 53 (TP53) gene lead to a quickly progression from PanIN stage to the malignant form of PDAC.[21]

Therefore, pancreatic ductal adenocarcinoma development is marked by three different progression stages defined by histologic abnormalities of the ductal epithelium.[22] PDAC progression ranges from PanIN1A and PanIN-1B to PanIN-2 and PanIN-3, showing the increasing loss of cellular function and nuclear morphology.[23] Each stage is characterized by early gene mutations activation; and the results show that activating mutations in KRAS are a relatively early event and are present in >99% of PanIN-1 lesions.[24] Early PanIN-2 lesions have CDKN2A inactivating mutations;[25] PanIN-3 lesions show inactivating mutations in TP53 and SMAD4.[26] (Fig.1)

The last stage PanIN-3 appears to be a precursor lesion of the invasive illness and it is intrinsically linked with the progression to invasive pancreatic cancer.[27] All stages which lead to PDAC morphology development are closely bound to accumulation of numerous mutations which drive to several dysregulated pathways. Overall, around 60 mutations in 12 different signalling pathways accompany the development of aberrant ducts in PDAC.[23] Prevalent genetic mutations in PDAC are associated with genes such as KRAS, CDKN2A (encoding p16), TP53 and SMAD4.[28] For many years, the development of KRAS inhibitors did not reach the expected outcomes. Recently, Janes et al. reinforced KRAS back in the forefront as a potential pharmacological target by discovering a new potent covalent inhibitor (ARS-1620) through structure-based design study on the $KRAS^{G12C}$ S-IIP-binding site.[29,30] The breakthrough discovery led to promising novel approach for development of KRAS inhibitors for tumour treatment, including PDAC.[31,32]

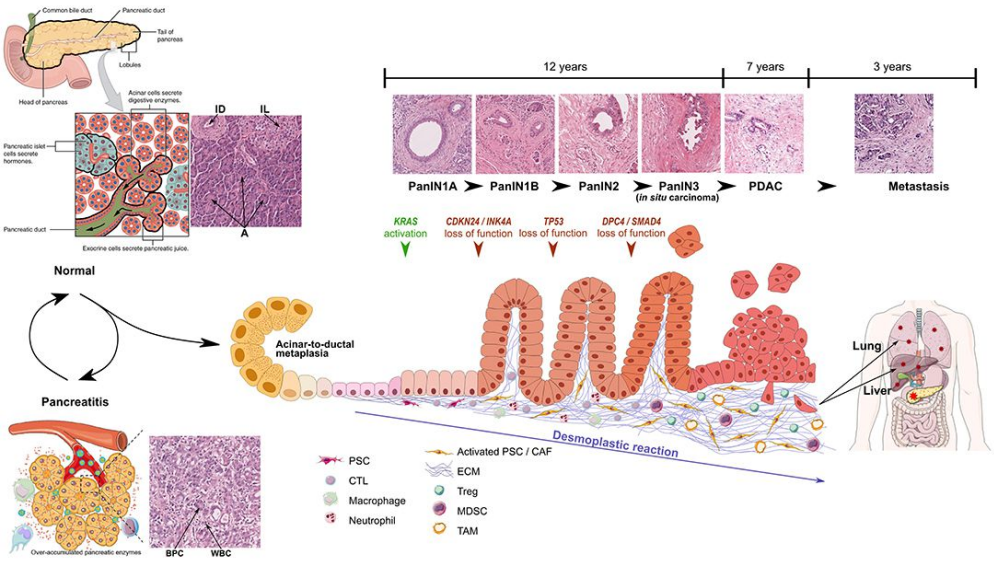

Figure 1 Scheme of pancreatic accumulation of mutations and following steps which lead to Pancreatic ductal adenocarcinoma.[33]

Standard treatments and chemoresistance of Pancreatic Ductal Adenocarcinoma

Pancreatic ductal adenocarcinoma (PDAC), also known as Pancreatic Cancer or Pancreatic adenocarcinoma (PC), is among the most lethal human cancers, with the lowest 5-year survival rate of all cancers (~ 10%)[3]. PDAC is a relatively uncommon tumor, with approximately 60,430 new diagnoses expected in 2021 in the US, but with rapidly increasing incidence passing from 0.5% to 1.0% per year[34].

According to estimates the numbers of PDAC cases are going to increase until to get the second position as cancer related death by the 2030.[3] It is characterized by silent progression and symptoms absence which make challenging its detection in early stages, due to these reasons its diagnosis usually arrives only in later stages of the disease, when metastasis is already spread, the possible approaches available are narrow, and chemotherapy represent only option[35].

Many reasons stand behind the high PDAC mortality, such as: lack of treatments and high resistance to chemotherapies[16,36], lack of efficient diagnostic methods, the use of early diagnostic markers with low sensitivity and specificity[37],

widespread metastasis[38,39] and complex composition of tumor microenvironment.[40]

PDAC conventional chemotherapy

Currently, Gemcitabine is the first line therapy for PDAC since it was approved by FDA in 1997.[41] Gemcitabine is nucleoside analog, in particular its structure derives from deoxycytidine (dC), thus it is also known as 2',2'-difluoro-2'-deoxycytidine (dFdC). Gemcitabine mechanism induces the block of cell proliferation, inhibiting DNA and RNA synthesis pathways,[42–44] and causing the arrest in phase G1/S of the cell cycle.[45] In the last decade, due to PDAC chemotherapy resistance, new clinical chemotherapies have been adopted: FOLFIRINOX, which is a combination of four different antitumor agents (oxaliplatin, irinotecan, leucovorin, and 5-fluorouracil), led to an increase of the survival rate of 4.3 months, passing from 6.8 to 11.1 months in PDAC patients.[46,47] Concurrently, significant increase of adverse effects incidence was detected: grade 3 or 4 of neutropenia, febrile neutropenia, thrombocytopenia, diarrhea, and sensory neuropathy, as well as grade 2 alopecia. *Nab*-paclitaxel, an albumin-stabilized paclitaxel formulation,[48] is active on microtubule stabilization, it blocks cells in G2/M phase of the cell cycle resulting in cell death[49]. Nab-paclitaxel/Gemcitabine combination therapy has been used since 2011 in PDAC patients, leading to extension and progression the free and overall survival rate.

Chemoresistance in Pancreatic ductal adenocarcinoma

Chemotherapy, used alone or in combination with radiotherapy, is considered the most effective and widely used modality in treating cancers. Cancer drug resistance is a major problem for chemotherapy treatment.[50] The reduction of drug absorption and increased drug efflux are the main cell chemoresistance mechanisms.[51]

Pancreatic ductal adenocarcinoma is characterized by a strong resistance mechanism against the first line treatment.[52] Gemcitabine is high hydrophilic molecule that cannot pass through cells membrane bilayers; therefore, it penetrates membrane using carriers. Gemcitabine can use several human

nucleoside transporters (NTs), Concentrative Nucleoside Transporters (hCNTs) and human Equilibrative Nucleoside Transporters (hENTs).[45]

Moreover, the hCNTs family is sodium-dependent and regulate unidirectional cellular transport of nucleosides including Gemcitabine; whereas hENTs carriers mediate intracellular sodium-independent uptake of dFdC.[53] In particular, hENT1 has high affinity with Gemcitabine but low capacity, instead hENT2 has lower affinity for Gemcitabine but higher capacity.[54] The dFdC is carried into the cytoplasm where it is mainly phosphorylated by deoxycytidine kinase (dCK) and by Thymidine Kinase 2 (TK2), in Gemcitabine monophosphate, which undergoes two further phosphorylations catalyzed by other cytosol enzymes, the uridine/cytidine monophosphate kinase 1 (CMPK1) and the nucleoside diphosphate kinase (NDPK). The process led, first, to the formation of Gemcitabine diphosphate (dFdCDP), and subsequently to its active form, Gemcitabine triphosphate (dFdCTP), which is now able to inhibit the ribonucleotide reductase (RNR) and the DNA double strand.[55] (Fig. 2)

The inhibition of RNR determines the depletion of the deoxyribonucleotide pools mainly dGTP, followed by dATP and dCTP. The reduction of dCTP pools, causing a reduction of dCK inhibition, increases gemcitabine phosphorylation. Additionally, decreased dCTP pools will also promote the incorporation of Gemcitabine into DNA since dCTP and dFdCTP compete for DNA synthesis,[43] blocking DNA synthesis or binding DNA and inducing double strand break.[45]

Into the cytoplasm, Gemcitabine can be inactivated through deamination catalyzed by two enzymes: deoxycytidine deaminase (CDA) responsible for the reaction from dFdC to dFdU and deoxycytidylate deaminase (dCMP), which inactivates dFdCMP turning it to dFdUMP. Interestingly, Gemcitabine has been described as inhibitor of Thymidylate Synthetase (TS), the inhibition pathway is due to similarity of the deaminated product of gemcitabine dFdUMP with 2-deoxyuridine monophosphate (dUMP), which is the natural substrate of TS.[44]

The poor outcome of PDAC patients is closely bound to the high drug resistance of this tumor and the lack of new efficient therapies.[52] Due to the long pathway, the several transports and the transformations needed by Gemcitabine, various resistance mechanisms have been developed by the malignancy. High

chemoresistance in PDAC could be acquired and intrinsic, and it is mainly caused by nucleoside transporters[56], nucleoside enzymes[57] and tumor microenvironment[58].

As aforementioned, Gemcitabine can pass the membrane trough specialized transmembrane nucleoside transporters (NT). First resistance mechanism to overcome is mediated by this family of carriers NT (i.e. hCNT1, hCNT2 and hCNT3, hCNT4).[59] The transporters hCNT1, hCNT2 are directly correlated with Gemcitabine uptake and cytotoxic activity, indeed their dysregulation is the main causes of Gemcitabine chemoresistance.[60] Downregulation and following decrease of expression of these carriers on membrane cause low and inefficient intra-cellular concentration of Gemcitabine[61].

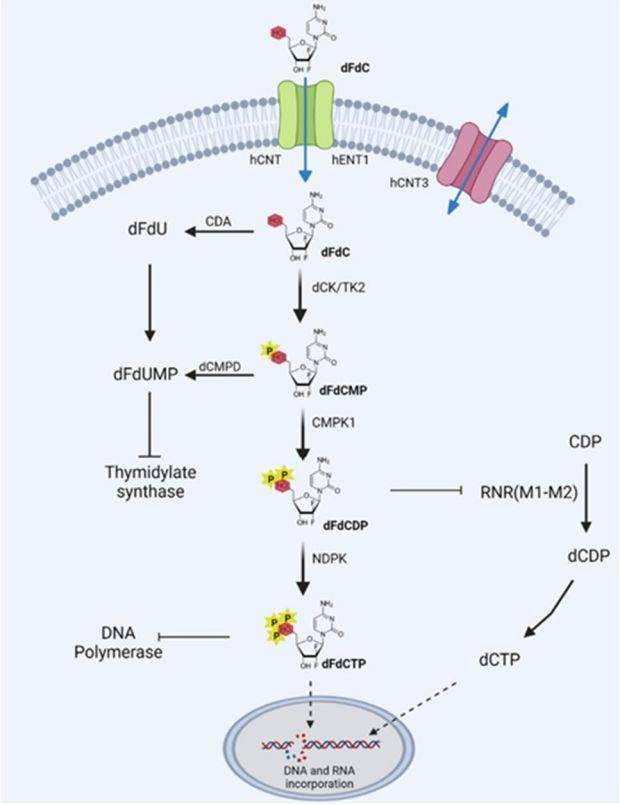

Figure 2. Gemcitabine mechanisms of action.

Other resistance mechanisms against Gemcitabine action are mediated into cells cytoplasm, one of these is provided by deoxycytidine kinase (dCK), a cytosolic enzyme responsible for Gemcitabine phosphorylation and activation.[62]

The deficiency of deoxycytidine kinase (dCK), which mediate the first Gemcitabine phosphorylation, is cause of acquired resistance, resulting in lower values of concentration of the Gemcitabine activated form in cytoplasm.[63,64] In PDAC, Gemcitabine resistance is also mediated by ribonucleotide reductase (RNR), a key role enzyme in DNA synthesis pathway. RNR catalyzes the formation of deoxyribonucleotides[65] from ribonucleotides; at the same time it is responsible for DNA repair process. RNR structure has two subunits, M1 and M2. The M1 subunit plays the main role in RNR activity.[66] Nevertheless both subunits are correlated with Gemcitabine resistance when high expressed. A recent meta-analysis revealed that patients with high RNRM1 expression had poorer OS and DFS rates than those with lower RNRM1 expression[67]. Resistance mechanism is also led by the tumor microenvironment in Pancreatic Ductal Adenocarcinoma (PDAC) which can constitute from 50% up to 80% of the total tumor mass.[68] Recently, TME has been described for its preponderant role in chemoresistance via several mechanisms.[69–72]

Tumor Microenvironments is composed by all surrounding interstitial tissues where the cancer represents the core of this thick structure. PDAC microenvironment is composed by Pancreatic stellate cells (PSCs), cancer associated fibroblasts (CAFs), myeloid/derived suppressor cells (MDSCs), and tumor associated macrophages (TAMs) which constitute the biggest part of the cellular components in TME. [40]

Role of protein kinases

Protein kinases (PTKs) play crucial tasks in a variety of biological processes, in signalling cascade of normal and cancer cells, such as growth, differentiation, metabolism, and apoptosis,[73] thus, PTKs are considered one of the most promising and investigated family for targeted therapies in medical and pharmacological research in the last 20 years.[74] In drug development, the interest in protein kinases as target has been growing up since FDA approved Imatinib, the first released tyrosine kinase inhibitor drug (i.e., Bcr-Abl) used in chronic myeloid leukemia (CML) in 2001. Strikingly, the 5-year relative survival rate for CML increased from 22% in the mid-1970s to 71% for patients diagnosed between 2011 and

2017, and most CML patients treated with Imatinib, or other tyrosine-kinase inhibitors are experiencing near-normal life expectancy.[75] Owing to protein kinases dysregulation in several illness and the beneficial therapeutically results, PTKs inhibitors are fascinating research topics in anticancer chemotherapy.[76] PTKs have essential roles in all multicellular eukaryotic organism;[77] they catalyze the reaction of phosphorylation from ATP to a specific serine, threonine, or tyrosine residue, which have crucial relevance in several cellular mechanisms.[78] In 2002, Manning et al. identified and listed 518 protein-kinases in human genome.[79] Furthermore, PTKs are involved in many different cellular functions such as regulating metabolism, viability, proliferation, differentiation, cell surviving, apoptosis and migration within several cell types.[80] As such, dysregulation of PTKs signaling can lead to many different human diseases, and PTKs overexpression have been detected in several types of human tumors, such as lung, ovarian, colon and pancreatic cancers.[81–83] In the last 20 years, FDA approved more than 68 new PTKs inhibitors for treatment of many diseases such as: organ transplantation and autoimmune diseases (e.g., glaucoma, rheumatoid arthritis) as well as solid and liquid cancers.[84] (Fig. 3)

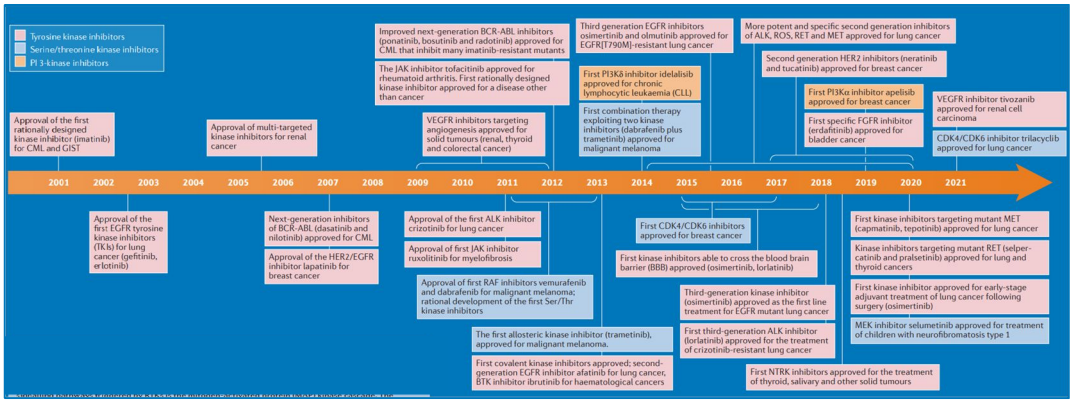

Figure 3. Timeline of the most relevant protein kinase inhibitors discoveries and approvals by FDA[85]

Noteworthy, among FDA protein kinases approved drugs, twelve target protein-serine/ threonine protein kinases, four are directed against dual specificity protein kinases (MEK1/2), the remaining 52 inhibit tyrosine kinases: thirteen block non-receptor protein-tyrosine kinases, and 39 target receptor protein-tyrosine kinases.

Interestingly, a major part of protein kinase inhibitors (58 out of 68) are clinically used to treat oncological patients.[86]

Protein Tyrosine Kinases families

Among 518 protein kinases present in human being, 90 belong to protein-tyrosine kinases family (PTKs). Human protein-tyrosine kinases are basically sorted in two categories by their cell position and structure: receptor tyrosine kinases (RTKs) and non-receptor tyrosine kinases (NRTKs).[76]

The group of receptor tyrosine kinase contains 58 enzymes which own transmembrane and extracellular domains, through which RTKs can recognize extracellular ligands and activate a cytoplasmic domain. Tyrosine kinase receptors (RTKs) are divided into 20 sub-families (EGFR, Insulin, PDGFR, VEGFR, FGFR, CCK, NGFR, HGFR, EPHR, AXL, TIE, RYK, DDR, RET, ROS, LTK, ROR, MUSK, LMR, Undetermined).[87] The 20 families are grouped by common structures and organized by similarities regarding their conserved and unique extracellular domain. The common structure of receptors tyrosine kinases consists of extracellular domain, transmembrane domain, and cytosolic domain. In the extracellular part the amino acids sequences of RTKs extracellular domains define ligands and sub-family membership. The trans-membrane domain consists in an α-helix, which place RTKs into the cell membrane playing a key role for dimer formation and receptor chains stabilization.[88] Finally, cytoplasmic domain contains a specific tyrosine kinase required for the catalysis of ATP-dependent phosphorylation of receptor chains. Cytoplasmic portion is the core of signal transduction, it usually contains two domains: a juxta membrane region (40–80 amino acids), where tyrosine kinase proper domain is located, and a C-terminal region. The active site is organized in 2 lobes of 12 subdomains connected by the kinase insert domain. The orientation and position of the activation loop, located into tyrosine kinase lobe, determines the active or inactive status of the protein. Additionally, ATP site is located between two lobes, and in its inactive form it binds the cation Mg^{2+}.[89] The small N-terminal lobe is responsible to orient, stabilize and make ATP complex ready. Meanwhile, the large C-terminal lobe has

a key role in the autophosphorylation process, in fact this lobe catalyzes the reaction moving a phosphoryl group (PO_3^{2-}) from ATP to the protein substrate.[90]

Moreover, non-receptor tyrosine kinases (NRTK) family are encoded by 33 genes and can be divided into nine sub-families: Abl, Fes/Fer, Syk/Zap70, Jak, Tec, Fak, Ack, C-Src, and Csk.[77] Unlike RTKs, the non-receptor tyrosine kinases, have not extracellular domain or transmembrane spanning domain, but they could be free into cells cytoplasm, attached to the inner membrane or inside the nucleus in their inactive conformation. NRTKs are regulated via autophosphorylation, like RTKs, or through phosphorylation mechanisms mediated by other NRTK or different kinases, which activate the downstream pathways.[88]

Non receptor tyrosine kinases and PTKs have similar catalytic domain. Non receptor tyrosine kinase classes contain a N-terminal portion where the two lobes interact with ATP, and C-terminal binds substrates or peptides in the activation process. Furthermore, it contains the activation loop where tyrosine groups can be phosphorylated. In the inactivated conformation of NRTK, the tyrosine residues are maintained hidden, and they can only be shown after the correct ligand interaction, which leads to a conformation change.[91] An important difference with RTKs is the presence in NRTKs of inter- and intra-molecular non catalytic domains which mediate the interactions with other PTKs, playing a key role in their functional modulation. The greatest part of non- receptor tyrosine kinases subfamilies shares a common domain organization; mainly they contain SH2 or SH3 domains or both, and a kinase domain. Some exceptions are FAK and JAK, which do not have SH domains. SH2 domain is involved in specific binding with phosphotyrosil residues, besides SH3 binds to specific proline-rich motifs present in many proteins.[92,93]

Focal adhesion kinase: structure and activity

Focal adhesion kinase (FAK) belongs to a sub-family of non-receptor tyrosine kinase discovered in 1992. Currently, FAK is a main interest protein kinase target in cancer research. Focal adhesion kinase family is constituted by two proteins: FAK (or FAK1) and PYK2 (or FAK2). Focal adhesion kinase (FAK) is a cytoplasmic non-receptor protein tyrosine kinase which was isolated for the first

time by co-immunoprecipitation of tyrosine-phosphorylated proteins from cells transformed with Rous sarcoma virus v -Src.[94] FAK has a key role in many regulating and signaling intracellular mechanisms such as proliferation, adhesion and survival but it is mainly involved in cell motility pathways. FAK is highly related with focal adhesion functions, creating interaction points between cells and its extracellular matrix (ECM).

Hence, FAK represents a signaling hub integrating information received from: i) extracellular matrix (ECM) integrin interactions ii) growth factor receptor signaling iii) G-protein-coupled receptor signaling and iv) mechanical forces imposed on the cell and transmitted by the cytoskeleton.[95,96]

Next to aforementioned NRTK general structure, FAK structure contains many differences. The primary structure of (125kDa) can be divided in three different portions. The N-terminal FERM (4.1 protein, Erzin, Radixin, Moesin homology) domain is composed by 3 lobes (F1,F2,F3); it consists in approximately 300 amino acids residues which whom FAK is anchored to intracellular membrane.[97] Thus, FERM is involved in bind mechanisms with receptors tyrosine kinase such as growth factor receptors (EGFR or PDGFR). During the inactive conformation FERM domain covers the central kinase domain, which is the key portion of FAK signalling, and where 6 tyrosine phosphorylation sites are present.[98] Between kinase domain and C-terminal focal adhesion targeting (FAT) domain, there is a spacer of 220-residue proline-rich low-complexity region. FAT domain contains the residues to interact with primary adhesion plaque components such as Paxillin and Talin.[99] (Fig. 4)

The interaction of integrin clusters with transmembrane receptors represents the main activation pathway for FAK, which leads to adhesions and cell spreading processes.[100] Integrin signaling determines a conformation change which leads to FAK kinase domain exposure, allowing the phosphorylation of its main site Y397 and the following phosphorylation cascade of the other Tyr sites of FAK initiating downstream signaling, which provide high affinity binding site for the SH2 domain of c-Src family kinases.[101]

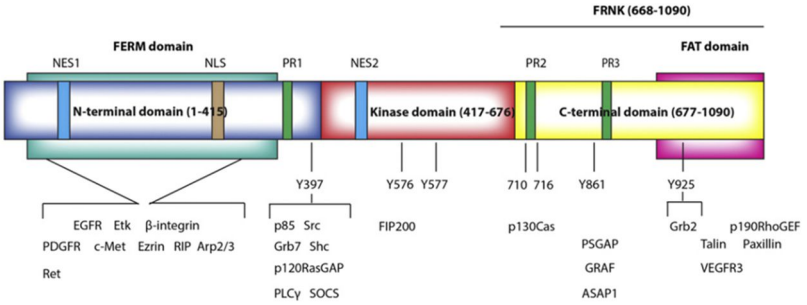

Figure 4. Focal adhesion primary structure: N-terminal FERM (4.1 protein, Erzin, Radixin, Moesin homology), C-terminal focal adhesion targeting (FAT) and central main kinase domain.

Therefore, interaction between Y397-activated FAK and c-Src leads to tyrosine phosphorylation cascade in multiple sites of FAK, resulting in cytoskeletal changes and activation of other downstream signaling pathways that regulate cell adhesion, migration and survival.[102]

FAK promotes cancer invasion and metastasis

Focal adhesion kinase has been found overexpressed and activated in several tumors including ovarian, cervical, kidney, lung, brain, colon, breast, skin and pancreatic cancer.[103] Furthermore, in the last years, overexpression of FAK has been strongly associated with PDAC. Chatzizacharias and coworkers, in 2010 published a clinical study on 65 PDAC patients showing how FAK was overexpressed in 78.46% of patients, and how that dysregulation leads to a poor survival rate and to an increasing insurgence of pancreatic cancer, especially in stages M and T.[104] Accordingly, dysregulate activity of FAK mediates tumor aggression to other tissues, indeed it is considered the main player in migration and angiogenesis processes, facilitating tumors metastasis. Several studies have confirmed FAK pro-metastatic role and the increased chemo-resistance to Gemcitabine induced by FAK in Pancreatic cancer (PC).[105,106] Furthermore, FAK is involved in several downstream signaling pathways with many different mediators of cell migration. In particular, FAK-Src interaction activates phosphorylation of p130cas, that contains SH2 binding site, in order to increase

cell migration signaling. Then, phosphorylated Cas can bind Crk regulating membrane ruffling and cell migration.[107]

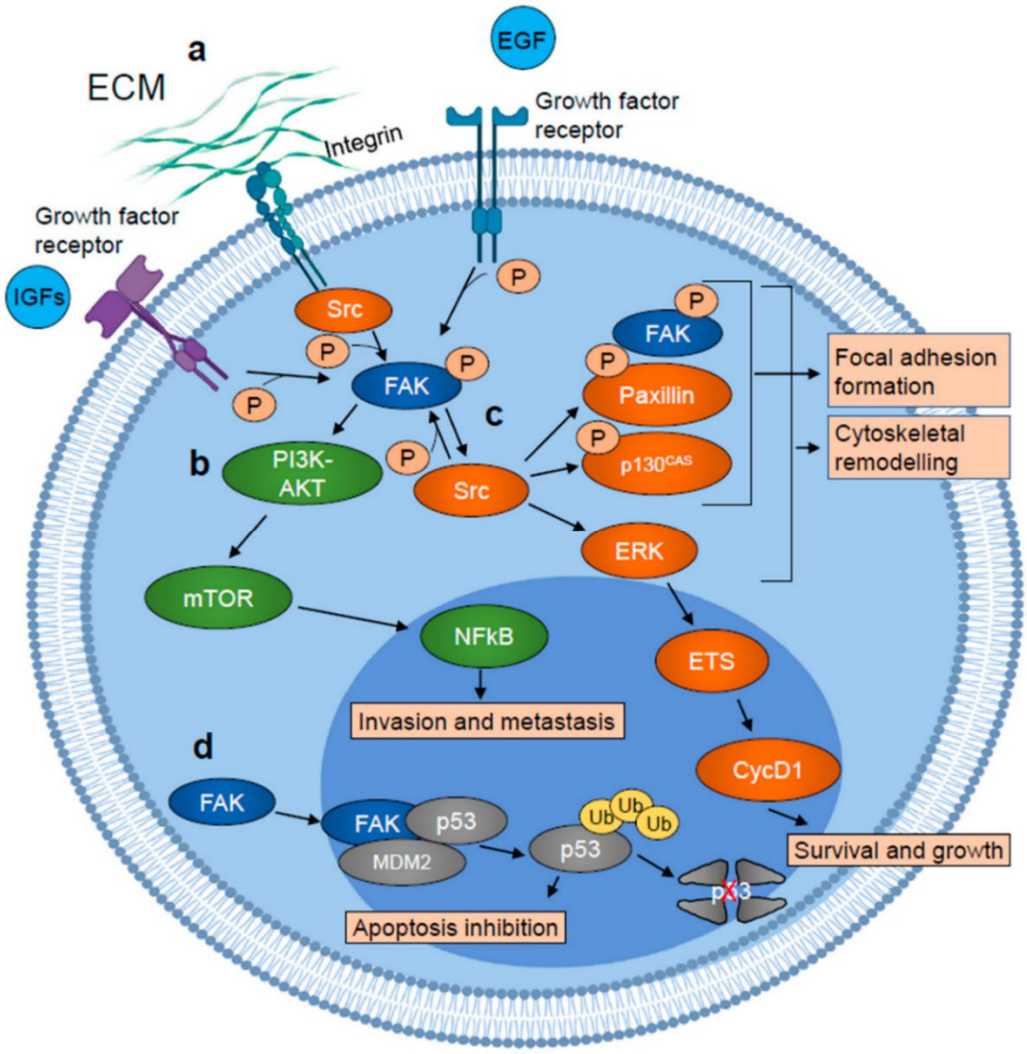

Figure 5. Focal adhesion kinase pathways Schematic representation of FAK involvement in tumor growth and metastasis. (a) In response to the activation of integrins and growth factor receptors, FAK undergoes autophosphorylation and is then triggered by Src. (b) Active FAK stimulates tumor cell invasion and metastasis, activating PI3K-AKT-mTOR signaling cascade, which results in increased NFkB transcriptional activity. (c) Additionally, phosphorylated/active FAK induces SRC-dependent phosphorylation of paxillin and p130cas, which results in the formation of a focal adhesion complex containing phosphorylated/active FAK, paxillin, and p130cas which lead to cytoskeletal remodeling and focal adhesion formation/turnover. SRC also stimulates ERK

signaling cascade which results in the ETS transcription factor-dependent induction of cyclin D1 (CycD1) expression which in turn promotes tumor cell survival and growth. (d) In the nucleus FAK promotes cell survival by acting as scaffold protein for the p53–MDM2 interaction, inducing p53 ubiquitination and its proteasomal degradation which results in apoptosis inhibition.[108]

FAK also plays a key role in migration mechanism mediating the interaction with PI3K and Grb2, the FAK/PI3K and FAK/Grb7 complexes. In addition, migration and invasion are also promoted by FAK via the v-C-Src-Cas-Crk signaling cascade, which regulate membrane ruffling and cell migration through DOCK180 and Rac. [109,110] Furthermore, in cancer cells FAK mediates Src phosphorylation of endophilin A2 to decrease its interaction with dynamin, which results in reduced internalization of MT1-MMP and consequent stimulation of the invasive activity of v-Src transformed cells.[111] Besides, FAK regulates cells functions in kinase independent manner, in particular it was discovered that FAK might work in the nucleus to help p53 connecting with Mdm2 and facilitating its ubiquitination and destruction.[112] To summarize, FAK mediates and regulates several functions both in normal and cancer cells, including typical neoplastic dysregulated process such as proliferation, survival, angiogenesis and metastasis, becoming likely a suitable target for a variety of diseases that are highly dependent on these biological processes.

Role of FAK as a potential target in PDAC

The development of tyrosine kinase inhibitors showed several benefits during the past 20 years, such as increased selectivity and higher activity towards resistant cancer types.[85-86]

Protein kinase inhibitors can be sorted in 6 classes (Type I-VI), depending on protein binding site and kind of interaction. Tyrosine kinases inhibitors:

- Type-I targets ATP site in a competitive way. However, these compounds can inhibit only the active conformation of PTKs because ATP pocket is usually unreachable in the inactive form.[113]

- Type-II inhibitors can bind the ATP site close regions, blocking protein kinases also in their inactive conformation. Due to the conservative primary structure of TKs, type I and type II inhibitors have usually shown lack of selectivity.[113]
- Type-III inhibitors can inactive PTKs binding an allosteric site and showing better selectivity than other classes.[113]
- Type IV are non-competitor inhibitors, they target allosteric substrate such as Type III inhibitors, but in this case binding residues which are more distant from ATP site.[114]
- Type V, also known as bivalent molecules, can bind two different sites of the kinase active pocket. In this way, they inactivate the protein.[115]
- Type VI inhibitors gathers all the molecules which can bind protein tyrosine kinase in a covalent way.[114]

Since discovery, targeting Focal adhesion kinase had a huge impact in new drugs development, due to its upregulation in many invasive cancers compared to primary and not metastatic tissues.[116,117] Even though, in the last years many FAK inhibitors (FAKi) have been ongoing in preclinical and clinical trials. Recently, due to its role in invasion and metastasis, FAKi have been tested, alone or in drug combination in many clinical trials for PDAC treatment. FAK inhibitors can be divided in two classes: selective and unselective inhibitors, which can inhibit both FAK and Pyk2.[118]

Focal adhesion kinase inhibitors main target three different sites of FAK structure: ATP binding site (in competitive or not competitive manner), FAK-FAT domain or FAK-FERM domain. Defactinib, is a potent FAK/Pyk2 inhibitor, active on ATP binding site, it has been studied in many different trials against solid tumor, including Pancreatic cancer. Defactinib monotherapy failed in its battle against tumor, however it has widely been used as combination therapy. Despite Defactinib underwent in more than 21 clinical studies for different diseases, two more trials are planned to test it against PDAC.[119,120]

GSK2256098, GlaxoSmithKline designed FAKi targets Tyr397 site, after several *in vitro* encouraging results on many solid and liquid tumors, including promising

results on PDAC cells inhibiting cell motility.[102] GSK2256098 is now in phase II of the clinical study in combination with trametinib for treatment of advanced PDAC (NCT02428270).

VS-6062 (also known as PF-00562271) is a novel dual inhibitor of FAK and Pyk2; it has been evaluated in clinical trials against advanced solid tumors including head & neck, prostate, and pancreatic cancer in phase I trial (NCT00666926), showing non linear PTK and supporting that further clinical studies for FAK inhibitor are needed.

Pancreatic Ductal adenocarcinoma drug resistance is a concrete worldwide problem. In the last years several new drugs have been developed to overcome resistance mechanisms which make PDAC chemotherapy treatment a challenging clinical issue. Protein tyrosine kinases have crucial roles in many cancers including PDAC. Although PTKs dysregulation has been strongly correlated with tumour genesis and cancer progression. PTK have been identified as promising combination or alternative approach to conventional cancer therapies due to bypass resistance mechanism. Furthermore, protein kinases have shown broad effects, targeted cellular pathways and affected not only tumour cells but also, matrix and proteins that surround tumour mass, in order to arrest its growth and expansion.

FAK have shown intrinsic presence in several intracellular and extracellular pathways, promoting oncogenic and metastasis mechanism, and emphasizing the attractiveness of non-receptor tyrosine kinase as target.

Healthcare crisis: the antimicrobial resistance

In recent years, antimicrobial resistance has been rapidly rising at global scale. The widespread from one country to another is unstoppable all around the globe, super bugs and multidrug resistant bacteria have become a challenge to overcome. The increased number of bacterial populations unaffected by drugs is closely associated with antibiotic widespread resistance, caused by the misuse and abuse of antibiotics and antimicrobial in many fields, such as human healthcare, agriculture, aquaculture, animal farming, veterinary medicine, pest control and pharmaceutical industry.[121] In contrast, it is important to consider that the molecular pathways behind antimicrobial resistance versus drugs were present since ancient times. Those mechanisms of bacteria defence are known as *intrinsic resistance*. Antibiotic resistance development is the most dangerous weapon used by microorganism, which led to endemic superbugs and multidrug-resistant bacteria in many parts of the world.[122] Collectively, antimicrobial-resistant pathogens caused more than 2.8 million infections and over 35 000 deaths annually from 2012 to 2017, according to the Centers for Disease Control and Prevention (CDC) Antibiotic Resistance Threats in the United States Report published in 2019.[123] It is estimated that globally approximately 700,000 deaths are attributed annually to antimicrobial resistance, and this could rise to 10 million deaths per year by 2050.[124] Additionally, Antimicrobial multidrug resistant ESKAPE bacteria (*Enterococcus faecium, Staphylococcus aureus, Klebsiella pneumoniae, Acinetobacter baumannii, Pseudomonas aeruginosa,* and *Enterobacter species*)[125], which developed resistant drug mechanisms against more of three antibiotics, represent the first cause of nosocomial chronic infections and one of the most challenging pathogens to threat in human healthcare field. The acquisition and spread of antimicrobial resistance reduced therapeutic options of severe infections, causing increasing death rates, and alarming the global healthcare system.[126] Microorganisms mainly acquire antimicrobial resistance by two mechanisms: either pick-up/transfer of resistance genes from other bacteria or gene mutation of pre-existing or acquired genes. For instance, a clear inquiry about the current scenario has been revealed by the dangerous misuse of antibiotics in treatment of SARS-CoV-2 infections. In

particular, the increasing number of invasive procedures associated with the use of antibiotics, steroidal anti-inflammatory and other immunomodulatory drugs and the overcrowding in health care settings may lead to an increase in Healthcare-Associated infections.[127] Furthermore, it is well documented that increased antibiotic use is related with higher resistance rates, as countries with low rates of antimicrobial resistance also report lower rates of antimicrobial consumption.[128]

According to Joon-Hee[129], resistance mechanisms can be classified as intrinsic, acquired, or adaptive.

- Innate resistance is due to natural microorganism profiling and it is also known as intrinsic resistance. Examples of it include the antigenic resistance to glycopeptides displayed by Gram-negative bacteria because of the permeability of the outer membrane present in the Gram-negative bacterial cell envelope.[130]
- In contrast, acquired resistance is defined as the microorganism resistance exhibited by previously sensitive bacterium which acquired a resistance mechanism by either a mutation or the acquisition of new genetic material only after the exposure to an external source, for example drugs contact.[131]
- Adaptive resistance is defined as the resistance to one or more antibiotics. It is induced by a specific environmental signal (e.g., stress, growth state, pH, concentrations of ions, nutrient conditions, sub-inhibitory levels of antibiotics). Contrary to intrinsic and acquired resistance, adaptive resistance is transient. Adaptive resistance, which allows bacteria to respond more rapidly to antibiotic challenge, generally reverts to the original state once the inducing signal is removed.[132,133] Adaptive resistance seems to be the result of modulations in gene expression as a response to environmental changes. Rather than being caused by genetic alterations, which usually produce irreversible phenotypes; adaptive resistance may be the result of epigenetic changes. Specifically, it has been suggested that DNA methylation by the DAM methylase could be responsible for the presence of different gene expression profiles in a bacterial population and could provide the heterogeneity and epigenetic

heredity of gene expression, essential for adaptive resistance.). Modulation of the expression of efflux pumps and porins have been implicated in the emergence of adaptive resistance.[134]

Bacteria developed multiple strategies to escape from multiple drugs, making infections even more challenging diseases to treat. In addition, bacteria spread those mechanism in multiple ways, even though different strains. For example, resistance genes, which encode modified β-lactamases, can be transferred rapidly and efficiently horizontally. The horizontal gene transfer is the main mechanism through which bacteria can rapidly and widely exchange gene; this process can occur through three main mechanisms:

- Transformation: this genetic recombination mechanism characterizes only small number of bacteria, which are able to incorporate free DNA fragments from a dead bacterium into its chromosome.[135,136]
- Transduction: transduction involves the transfer of genetic material between a donor and a recipient bacterium by a bacteriophage.
- Conjugation: this is probably the most important mechanism of horizontal gene transfer. It involves the transfer of genetic material from one bacterial cell to another by direct physical contact between the cells. Genetic material is exchanged as plasmid among two or more bacteria, from the donor cell to the recipient cells, through as sex pili. From the simple conjugation event, bacteria can exchange through single plasmid multidrug resistance mechanism at once. The assembly of multiple resistance genes on a single plasmid is mediated by mobile genetic elements (transposons, integrons, and Insertion Sequence Common Region- ISCR-elements).

In summary, resistance to antibiotics is typically led by common different mechanisms developed by cells which can act in different ways depending on drugs mechanisms of action. as common result, bacteria enlarge efficient escape methods: drugs destruction or modification, target alterations (target replacement, target site mutations, target site enzymatic alterations, target site protection, target overproduction or target bypass), and reduced antibiotic accumulation due to

either decreased permeability and/or increased efflux.[122] However, antibiotic crisis is not only attributed to antimicrobial multidrug resistance of planktonic microorganisms, indeed antimicrobic crisis is closely related with other convenient mechanisms and survival strategies used by bacteria to escape from conventional antimicrobial treatment. The microbial biofilm is most relevant and diffused strategy.

Bacterial biofilm

Microbial biofilms are one of the oldest and best organized ancient model of organism life mode of the Earth.[137] Biofilms are very complex structures, made by one or more variety of microbial population such as Gram-positive and Gram-negative, motile and non-motile, aerobic and anaerobic, facultative bacteria, and fungi. Biofilms are surface-attached microbial community, surrounded and enclosed by 3D self-secreted structure made by polysaccharides, proteins, lipids and extracellular DNA, known as extracellular polymeric substances matrix (EPS). The EPS regulates homeostasis of the microenvironment performing many functions, such as acting as nutrients filter, allowing close cells contact and communication, and performing as a physical barrier demonstrating a significant higher tolerance to antimicrobial agents rather than nonadherent planktonic cells.[138] Biofilm provides microbes several benefits such as: defence from host immune system or antimicrobial drugs, hydrate environment, high extracellular enzymatic activity and in particular high microbe density with leads to coordination of virulence factor via quorum sensing.[139] Bacterial biofilm plays a key role in human resistant infections; indeed it is has been estimated that 80-90% of human infection are biofilm-associated. This statistic has become even more alarming considering that bacterial cells in biofilm are 1000-fold more resistant to conventional therapies than corresponding planktonic form. Nonetheless, biofilm infections are characterized by chronicity and extreme resistance to drugs treatments.[140] Biofilm are involved in different diseases, such as cystic fibrosis, wounds, otitis media, pneumonia, and osteomyelitis. Furthermore, biofilm represents the main cause of nosocomial chronic infections, indeed the biofilm

can adhere and persist on biotic or abiotic surfaces such as medical devices or implants, valves, stents and shunts, or catheters and endoscopes.[141]

Biofilm development is a complex cyclic-multistep process which starts from and finish to planktonic cells. Biofilm formation process is usually divided in 4 steps: first step concerns adhesion mechanism to biotic or abiotic surfaces; once adhered, free planktonic cells switch to biofilm phenotype expression. Afterward, cells begin to proliferate and to secret EPS. At this point, the biofilm maturation leads to 3D structures development in which the EPS matrix provides a multifunctional and protective scaffold, enabling via intra and extracellular chemical signalling to organize microenvironments where microorganisms coexist within polymicrobial and social interactions (competitive and synergistic). In the last stage, when biofilm formation is completed, cells begin 'dispersal' mechanisms, whereby cells leave the biofilm to re-enter the planktonic phase and wide spread to colonize other surfaces.[142] (Fig. 6)

1. Initial adhesion
2. Robust adhesion
3. biofilm maturation
4. Cell dispersion

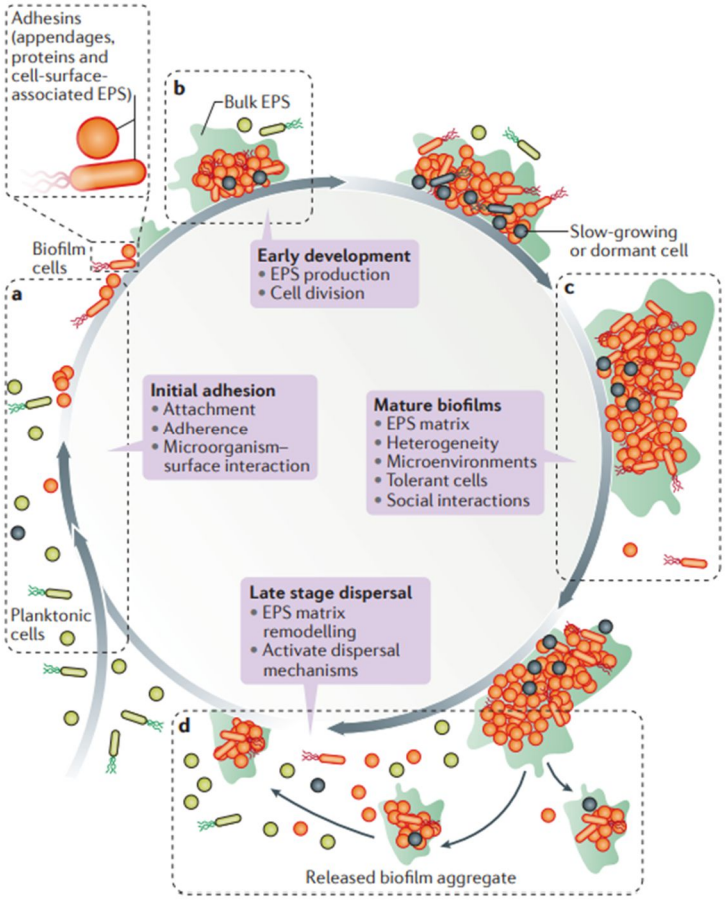

Figure 6. Biofilm development. a) early adhesion: planktonic microorganisms express needed protein to surface adhesion b) biofilm development: microorganisms start to cooperate and secrete EPS proteins matrix c) biofilm is formed, inhabitant cells communicate each other and exchange information; dormant cells are present into the agglomerate d) dispersion: free planktonic cells are released by the biofilm.[142]

The biofilm gathers several necessary features for MDR widespread. The high complexity of biofilm and the close contact among different cells including high density of eDNA found into biofilm are all clues of the high ability of horizontal gens transfer, which allow rapidly the widespread of antibiotic resistance among different bacteria strains.[126] The reduced antibiotic susceptibility exhibited by biofilm-embedded cells, do not depend only on the EPS barrier, but it has multifactorial origin and can vary according to the species and genetic makeup of the organisms, the developmental stage of the biofilm and the environmental

conditions.[143,144] The reasons of higher antibiotic resistance in biofilm are combined drug resistance mechanisms expressed by planktonic and those due to biofilm structure: restriction of antibiotic penetration by the ECM, the secretion of antibiotic-modifying enzymes, extracellular DNA, and other macromolecules into the ECM, the accumulation of filamentous bacteriophages which promote the formation of liquid crystalline structures, differential metabolic activity, the emergence of dormant cells, biofilm-associated upregulation of bacterial efflux, enhanced horizontal gene transfer and mutation frequency, and interactions between different bacterial species within mixed-species biofilms.[144–146]

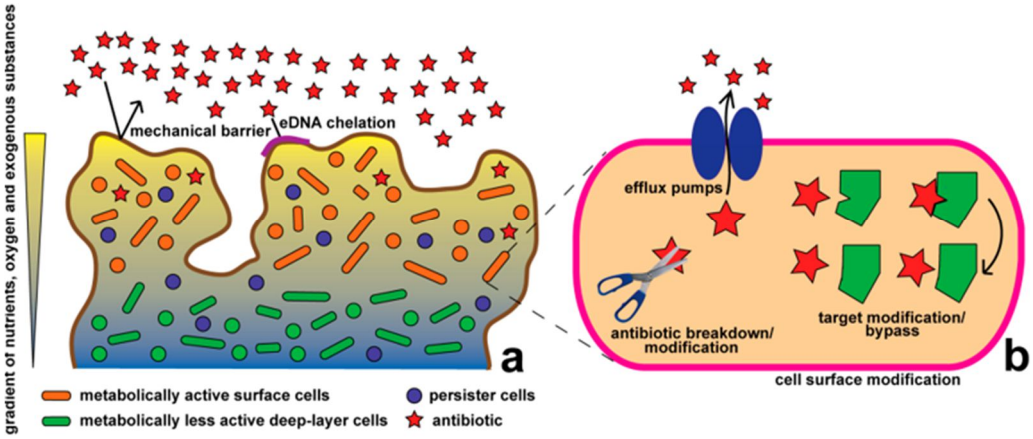

Figure 7. Schematic representation of biofilm established resistance mechanisms (a) and resistance mechanism exhibited by microbial inhabitants of biofilm (b).

Strategies to combat microbial biofilm

Development on novel molecules for treatment of biofilm related infections is current challenge. This circumstance demands new strategies for biofilm-associated infections, and currently, researchers focus on the development of antibiofilm agents thus new specific drugs able to directly target biofilm structure. Antibiofilm agents can act through two different mechanisms of action: by inhibition of biofilm formation or by disrupting biofilm architecture. Therefore, our knowledge about biofilm is still limited, several efforts lead to the identification of numerous targets and pathways which can be used to inactivate biofilm virulence.

The first developed inhibition strategy targets mechanisms involved during the early steps of biofilm formation. Initial attachment can be blocked following two approaches, thus acting on the surface to which microbes will attach or treating microbial cells to block their attachments mechanisms. Some "physical" strategy has been developed, indeed certain imprint 3D pattern surface or change surface proprieties e.g. hydrophilic might inhibit or delay microbial attach to surfaces.[147–149] Another purpose to block microbial attachment is pre-conditioning of surface by chemicals such as surfactant.[150] These approaches include small molecules able to inhibit Quorum Sensing stimuli generated by chemicals signalling, that repress the expressions of microbial adhesion molecules[151], inhibit the biofilm matrix synthesis[152], antagonize QS signals[153], or kill bacteria in biofilms. [154]

Table 1 Summary of targets and mechanism of potential anti-biofilm agents acting on biofilm formation.

Targets Mechanisms	Related to targets	Effects on biofilm	Ref.
Autoinducers of QS system AHL AIP AI-2	i) Degradation ii) Inhibition of synthesis iii) Competitive interference with signals iv) Interference with receptors	Interference with formation Interference with motility Altered biofilm structure	140,155–160
Second messengers c-di-GMP	i) Inhibition of synthesis ii) Interference with receptors iii) Direct degradation iv) Downregulation	Interference with transition from planktonic to sessile phenotype	161–164
c-di-AMP	i) Inhibition of synthesis ii) Interference with receptors iii) Direct degradation iv) Downregulation	Interference with formation	165,166
Environmental stress sensing (p)ppGpp	Inhibition of synthesis	Interference with formation	167
Sortase A (SrtA)	inhibition of the synthesis of cell wall associated proteins (MSCRAMMs)	Prevention of adhesion Interference with formation	168,169
Type 1 fimbriae (FimH) and other appendages	i) Inhibition of synthesis ii) Interference with receptors iii) Direct degradation iv) Downregulation	Prevention of adhesion Interference with formation	170–172
Environmental stress sensing (p)ppGpp	i) Inhibition of synthesis	Interference with antibiotic tolerance	167
Toxin/Antitoxin (TA) systems	Effect on c-di GMP pathway	Dispersion Interference with persister cells formation	173
PQS	i) by inhibiting the biosynthesis ii) by targeting PqsR	Distruption of biofilm integrit	174–178

Table 2 Summary of targets and mechanisms of potential anti-biofilm agents acting on existing biofilm.

Targets Mechanisms	Related to targets	Effects on biofilm	Ref.
LecA and LecB	Direct inhibition	Prevention of adhesion Interference with formation	[179–183]
Matrix components i	i) Degradation of eDNA ii) Degradation of polysaccharides iii) Degradation of proteins	Detaching adherent cells Dispersion Destruction	[139,142]
Autoinducers of QS system AHL AIP AI-2	i) Degradation ii) Inhibition of synthesis iii) Competitive interference with signals	Altered biofilm structure Interference with antibiotic tolerance Dispersion	[184,185]
Second messengers c-di-GMP	iv) Inhibition of synthesis v) Interference with receptors vi) Downregulation v) Direct degradation	Dispersion Interference with antibiotic tolerance Inhibition of matrix components	[186]
c-di-AMP	i) Inhibition of synthesis ii) Interference with receptors iii) Direct degradation iv) Downregulation	Interference with antibiotic tolerance Inhibition of matrix components	[165,166]

Due to the high diffusion of chronic nosocomial infections biofilm-related, the development of novel small molecules able to interfere with the biofilm architecture is strongly required.[187] However, preformed biofilm can be destroyed by interfering with biofilm structures and inducing their detachments. Certainly, preformed biofilm, due to full completed EPS envelope is more difficult to disrupt inducing biofilm detachment. Mainly two conditions are required to achieve preformed biofilm degradation: matrix polymers must be degraded[188] or cells must be persuaded to disperse.[189] The most efficient strategies to eliminate the

biofilm preformed adhesion are; 1) sloughing, 2) erosion, and 3) seeding dispersal.[190]

When sloughing involves stripping-off of biofilms as a lump from surfaces and results in rapid mass loss. The erosion is slower than sloughing, and it is a gradual process that involves continuous detachment of single cell or small portion from external area of biofilm. The seeding dispersal, unlike those passive processes, refers to an active process to rapidly discharge single cells from the central region of biofilm, leaving central hollow cavities.

Albeit, seeding dispersal seems to be most effective approach to destroy biofilm, but it remains a complex method because of the presence of dormant inactive cells which compose the central core of the biofilm structure. The dormant cells express an extra drug resistant mechanism due to a particular phenotype that make them inert or less susceptible to pharmacological substances.[191]

In summary, the biofilm persistence in the environment and in the host is due to the high microbial cell density which also includes 'persister cells,' characterized by a dormancy state, e.g. adapted quiescent cells with reduced response to stimuli including antimicrobial drugs. The EPS matrix preserves microbial cells from external stressful impulses and promotes the horizontal genetic exchange. As aforementioned the biofilm microorganisms develop protection from the host immune system and tolerance to antimicrobials through different mechanisms. Tolerance toward antimicrobials, unlike resistance which is genetic-based and can be acquired through point mutations or horizontal gene transfer mechanisms such as conjugation, transformation, or phage transduction.

Owing to the lack of biofilm efficient therapeutical strategies along with prevalent risk of drug resistance to conventional therapy, the development of novel small molecules able to facilitate the dispersion of preformed biofilms or inhibit the formation of new biofilms *in vivo* has become an urgent medical need.[192]

Imidazothiadiazoles represent a well-known promising scaffold in antimicrobial field and have been recently reported as precious resource in the battle against multidrug resistance bacteria and biofilm.[193] Indeed, antimicrobial activity is the

most known and evaluated during the years regarding for imidazothiadiazole. Since many imidazothiadiazole showed high potency against biofilm of Gram positive and Gram-negative bacteria strains. My research interest was also directed towards the identification of novel antibiofilm agents to be used in the treatment of chronic biofilm-related infections.

Imidazo[2,1-*b*][1,3,4]thiadiazoles

During the last decade, numerous new biological pathways were discovered, and medicinal chemistry advances brought to faster and larger synthetic production and biological evaluation of novel scaffold against various diseases. Among multiple natural, synthetic and semisynthetic scaffold evaluated, the fused bicyclic heteroaromatic ring imidazo[2,1-*b*][1,3,4]thiadiazole showed fascinating and promising pharmaceutical properties.

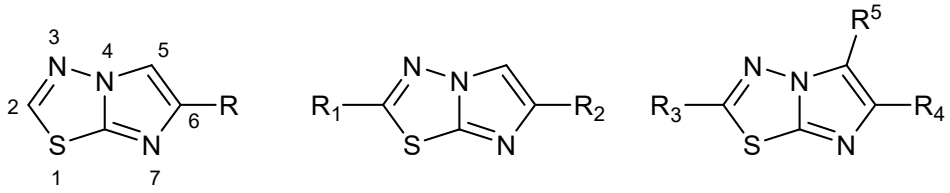

1 **2** **3**

Figure 8. General structures of mono-, bi- and tri-substituted imidazo[2,1-*b*][1,3,4]thiadiazoles

Matsukawa and co-workers in 1952 described the synthetic pathway for the synthesis of 2,6-bisubstituted-imidazo[2,1-*b*][1,3,4]thiadiazoles. The reaction involves 2-amino[1,3,4]thiadiazole derivatives and the appropriate α-haloketones dissolved and refluxed in absolute ethanol.[194] Nowadays, this reaction still remain widely employed for the preparation of these compounds.

Imidazo[2,1-*b*][1,3,4]thiadiazole: A Promising Bioactive Scaffold in Medicinal Chemistry

Nitrogen-bridgehead (Ring Junction) bicyclic heteroatomic rings have always aroused huge interest for their wide range of biological activities. Imidazo[2,1-*b*][1,3,4]thiadiazole derivatives showed interesting physicochemical and biological properties due to the planar and rigid heteroaromatic ring system, characterized by four heteroatoms and two condensed heterocycles with different π-conjugation. Therefore, after its discovery, imidazo[2,1-*b*][1,3,4]thiadiazole scaffold has attracted both academic and pharmaceutical industry research. Indeed over the years, ever more novel compounds containing imidazo[2,1-*b*][1,3,4]thiadiazole scaffold have been synthetized to evaluate its biological

properties. During the last 60 years, the synthesis and biological activities of numerous imidazo[2,1-*b*][1,3,4]thiadiazoles variously substituted in position C-2, C-5 or C6 have been largely described in literature. Among the imidazo[2,1-*b*][1,3,4]thiadiazoles previously synthesized the 2,6-bisubstituted- and 2,5,6 trisubstituted derivatives showed the most promising biological activities. Design and evaluation on thousands compounds bearing imidazo[2,1-*b*][1,3,4]thiadiazole moiety led to identification of multiple biological activities in pharmaceutical field including anticancer[194] antioxidant[195] , antifungal[196], antimicrobial[197] anticonvulsants[198], antihypertensive[199], antituberculosis[200], and anti-inflammatory.[201]

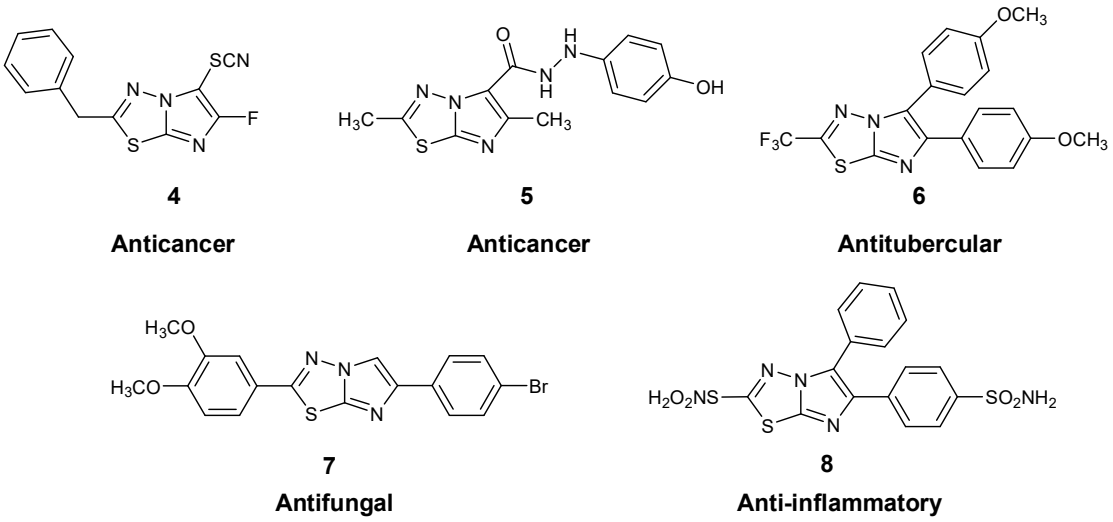

Figure 9. Chemical structures and biological activities of some imidazothiadiazoles

Imidazo[2,1-*b*][1,3,4]thiadiazole: antiproliferative activity.

Anticancer activity for imidazo[2,1-*b*][1,3,4]thiadiazole compounds was firstly described by Gadad et al in the early 2000,[202] almost 50 years later its discovery. During the last 20 years, imidazothiadiazoles reached impressive results due to efforts in structure modification which led to interesting antiproliferative results against several human tumours. Since 1999 to 2003, firstly Gadad then Terzioglu[203] tested some 2,5-alkyl-6-aryl-substituted imidazo[2,1-

b][1,3,4]thiadiazoles on the 60 cell lines of NCI panel of human cancer, reporting modest IC_{50} values in the range of hundreds micromolar ($log10^{-4}$) against most of them.

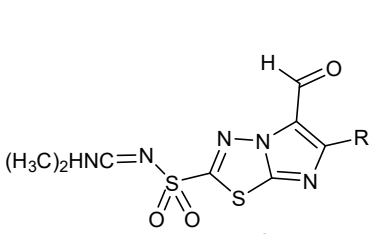

9a-g

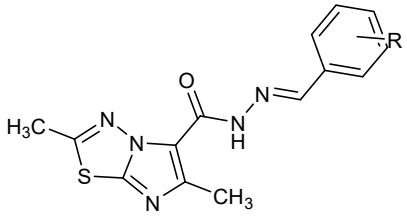

10a-g

a, C_6H_5,
b, 4-Br-C_6H_4,
c, 4-Cl-C_6H_4,
d, 4-NO_2-C_6H_4,
e, 4-C_6H_5-C_6H_4,
f, 3-coumarinyl,
g, 5-(4-NO_2-C_6H_4)$^{-2}$-furyl

a, H;
b, 4-$CH_3C_6H_5$;
c, 2-OHC_6H_4;
d, 4-$CH_3OC_6H_5$;
e, 4-BrC_6H_4;
f, 4-ClC_6H_4;
g, 4-FC_6H_4;
h, 4-NO_2C_6H

Figure 10. Imidazo[2,1-*b*][1,3,4]thiadiazole **9** and **10** with moderate antiproliferative activity.

Years later , intense Structure Activity Relationship (SAR) studies led to novel more potent imidazo[2,1-*b*][1,3,4]thiadiazole derivatives rather than the previously synthetized.

Karki et al.[204] (2011) evaluated a series of 2,6 diarialkyl-5-substituted-6-aryl-imidazo[2,1-*b*][1,3,4]thiadiazole on human T-cell leukemia cell line (CEM). Imidazothiadiazole analogues **11** and **12** exhibited moderate cytotoxicity with IC_{50} values in the ranges of 10–16 and 8– 26 μg/mL, respectively against CEM cell line.

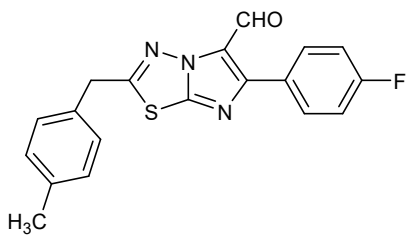

11

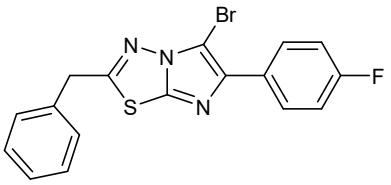

12

Figure 11. Imidazo[2,1-*b*][1,3,4]thiadiazole with improved antiproliferative activity on human T cell leukemia cell line

In 2012, Noolvi et al.[194] published *in vitro* anticancer activity of a series of 2,6-disubstituted imidazo[2,1-*b*][1,3,4]thiadiazoles of type **13**. Compounds **13d** showed potent antiproliferative activity reporting IC_{50} values of 0.114 and 0.743nM against HOP-92 (non-small cell lung) and CAKI-1 (renal) cancer cell lines, respectively.

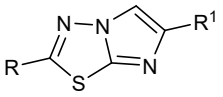

13a-l

R= 4-CH_3O-C_6H_4
2-Cl-5-NO_2-C_6H_3
R^1= C_6H_5,
2,4-$(OH)_2$-C_6H_3,
3-NH_2-C_6H_4,
4-OCH_3-C_6H_4,
4-NH_2-C_6H_4
4-$(OH)_2$-C_6H_3,
3-NH_2-C_6H_4

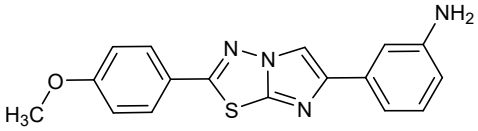

13d

Figure 12. 2,6-bisubstituted imidazothiadiazole derivatives **13** with potent antiproliferative activity

Subsequently, Kumar et al.[205], evaluated the influence of many substitutions in position C-5 of imidazothiadiazole scaffold on the antiproliferative activity against different cancer cells belonging to nine subpanels of human tumours (Leukemia, NSCLC, Colon, CNS, Melanoma, Ovarian, Renal, Prostate and Breast). Among The new trisubstituted compounds, derivative **15d** showed GI_{50} values in the range 1.2 - 4.4 μM on the whole panel. Compound **15d**, bearing formyl group in position 5, was selected for further biological evaluation, which confirmed the ability of this class of compounds to induce cell death by stimulating caspase 3 and 8 activation.

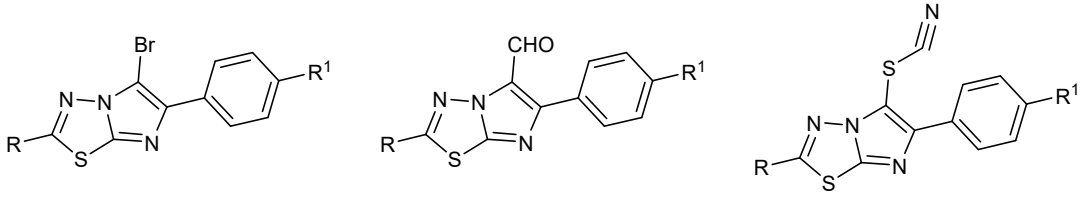

14a-f

a, R = benzyl, R' = H
b, R = benzyl, R' = Cl
c, R = benzyl, R' = NO_2
d, R= benzyl, R' = Br
e, R= cyclohexylethyl, R' = F
f, R = ethyl, R' = Cl

15a-f

a, R = benzyl, R' = H
b, R = benzyl, R' = Cl
c, R = benzyl, R' = NO_2
d, R= benzyl, R' = Br
e, R= cyclohexylethyl, R' = F
f, R = ethyl, R' = Cl

16a-e

a, R = benzyl, R' = H
b, R = benzyl, R' = Cl
c, R = benzyl, R' = NO_2
d, R= benzyl, R' = Br
e, R= benzyl, R' = OCH_3

Figure 13. 2,5,6-trisubstituted imidazothiadiazole derivatives with nanomolar antiproliferative activity

Kamur et al.[206] prepared a third generation of Karki's analogues compounds, inspired by the most potent compound previously described, synthetizing imidazothiadiazole derivatives substituted with a 4-chlorobenzyl moiety in position C2, and with different heterocycles in position 6. Compound **4i,** bearing a coumarin-3-yl group, emerged as the most potent compound against a panel of three different cancer cell lines including the murine leukemia cells L1210, the human T-lymphocyte cells CEM and the human cervix carcinoma cells HeLa. eliciting IC_{50} values in the values in the range 0.75-0.90 μM. Cell cycle studies, DNA fragmentation and Annexin V-FITC staining suggested that **4i** induces apoptosis without arresting cell cycle.

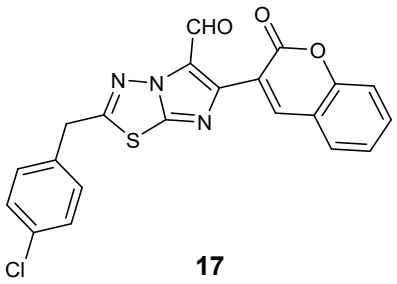

17

Figure 14. Chemical structure of imidazothiadiazole **17**.

Kamal et co-workers[207] in 2014 evaluated for the first time the antiproliferative activity of a series of 3,5,6-substituted imidazo[1,2-*b*][1,3,4]thiadiazole compounds, bearing in position C-5 a heteroaromatic ring, such as a 5,6-substituted-indolin-2-one. Compounds **7, 11** and **15** displayed potent cytotoxicity

activity with IC_{50} ranging from 1.1 to 3.2μM. The most potent compounds proved to strongly inhibit tubulin polymerization with IC_{50} values from 0.15 to 2.11 μM. Recently, Kamal group described interesting antiproliferative activity towards different human cancer cell lines for a new series of imidazo[2,1-*b*][1,3,4]thiadiazole **18**. Among them, conjugates **18a-c** exhibited the most potent antiproliferative activity with GI_{50} values ranging from 0.13 to 3.8 μM. Cell cycle analysis highlighted that the treatment with **18a-c** resulted in accumulation of cells in G2/M phase, inhibition of tubulin assembly, disruption of microtubule network.

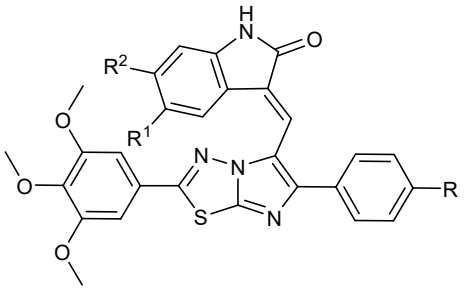

18a, R= CH_3; R^1= F; R^2 =H;
18b, R= H; R^1= Cl; R^2 =H;
18c, R= H; R^1= H; R^2 =Cl

Figure 15. Potent trisubstituted imidazothiadiazoles **18.**

In 2015, imidazothiadiazoles analogues were reported for their kinase inhibition, in particular against transforming growth factor-β type-I receptor kinase (ALK5), which mediates many signals involving in cell proliferation, survival and angiogenesis. In particular, compound **19d** showed the highest ALK5 inhibition, exhibiting an IC_{50} of 1.2 nM. Additionally, compound **19d** showed a marked selectivity towards the P38α kinase with significant percentage of inhibition (91%) at10 μM.[208]

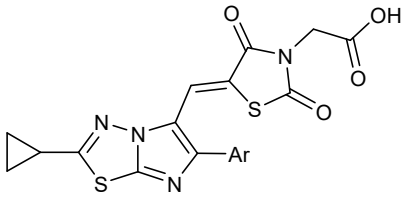

19a, R= C_6H_5;
19b, R= 2,4-Cl-C_6H_3;
19c, R= 4-Br-C_6H_4;
19d, R= 4-F-C_6H_4;
19e, R= 4-Cl-C_6H_4;
19f, R=2,4-OH-C_6H_3;

Figure 16. Imidazothiadiazole **19** as inhibitor of ALK5.

During the last years, the research group in which I have carried out my PhD focused on the synthesis and the antiproliferative activity evaluation of novel 2,6-disubstituted imidazo[2,1-*b*][1,3,4]thiadiazoles of type **20** and **21**.[193,209–212] In particular, the newly synthetized derivatives were substituted in position C-2 with 3-indolyl group[213] and in position C-6 with a substituted phenyl group or a thiophen ring. All compounds **20** and **21** were tested against the National Cancer Institute full panel of about 60 human tumour cell lines and against Pancreatic Ductal Adenocarcinoma cell lines, which are not present in NCI panel, including immortalized cells, primary PDAC cells and Gemcitabine resistant clone cells. All compounds showed a good antiproliferative activity with IC_{50} in the micromolar and sub-micromolar range against all tested cancer cells.

The four compounds **20a-b** and **21a-b** with most potent antiproliferative activity are reported in figure 17. Compounds **21** were selected for further biological studies to better evaluate their antitumor activity and mechanism of action on PDAC cells. Firstly, imidazothiadiazole derivatives (Fig. 17) evaluated on two-dimensional cytotoxicity assay. Compounds **20** and **21**, showed potent antiproliferative activity ranging micromolar and sub micromolar activity. In particular, remarkably cytotoxic activity with the half maximal inhibitory concentration values (IC_{50}) were shown by **20a** and **20b** against pancreatic tumour cells, including immortalized cell line SUIT-2, PANC-1, CAPAN-1, a gemcitabine resistant clone PANC-1GR and a primary cell culture PDAC-3.

Against the PDAC cells panel derivatives **20a** and **20b** displayed IC_{50} values between 0.85-2.7 μM and 0.99-2.2 μM, respectively.

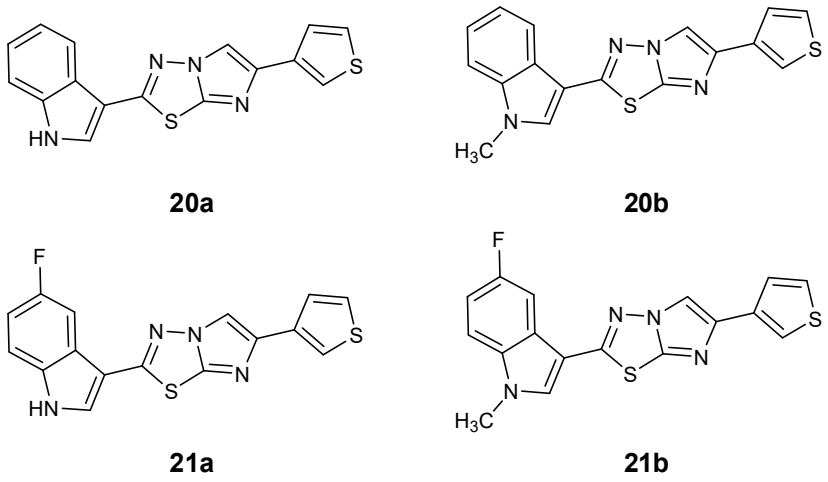

Figure 17. Chemical structures of the most potent imidazothiadiazoles derivatives **20, 21.**

Therefore, compounds containing 5-fluoro-indoles **21a** and **21b** ranged IC_{50} low micromolar values 1.78-5.1 μM and 2.1-4.86 μM against aforementioned cells. The promising compounds were also tested on 3D spheroids model formed by PDAC-3 cells at 5 times IC_{50} concentration; this *in vitro* assay that can better replicate the intricate biology and architecture of solid tumour which develop in three dimensions. The spheroids exposed to compounds **20a-b** maintained their activity also on the more complex model, inducing the decrease of growth fold changes compared to untread 3D cell model According, to the promising antiproliferative activity compounds were tested by *in vitro* wound healing assay to investigate the capability of these compounds to reduce invasion and migration mechanism of the PDAC cells. Once again, PDAC cells were treated with imidazothiadiazoles at $4xIC_{50}$ concentration; after 24hours, imidazothiadiazoles showed notable antimigratory activity, reducing the motility of the treated cells compared to the untreated control. Furthermore, in order to investigate the mechanism of action, the compound **20a** was further investigated via high-throughput analysis with the PamGene tyrosine kinase peptide substrate array (PamChip). The SUIT-2 cells were treated with $5xIC_{50}$ concentration of **20a** revealing the ability of this imidazothiadiazole analogue to inhibit 45 tyrosine

kinases, with specific selectivity against Focal adhesion Kinase (FAK), non-receptor tyrosine kinase involved in cell survival, cells migration and tumour mass growth. Finally, the mechanism of FAK inhibition was confirmed by the quantitative analysis the Enzyme-Linked Immunosorbent Assay (ELISA), which highlighted a reduction of the FAK phosphorylation at tyrosine residue 397 (FAK [pY397]), essential for the kinase activity of this protein.[193,209–212]

In summary, in the last decades imidazothiadiazoles received great attention as scaffold for the development of novel molecules of pharmaceutical interest. Among the different biological activities described, the anticancer properties reached fascinating results, opening future promising perspectives for this class of compounds.

Aim of the study

Considering the interesting antiproliferative and antibiofilm activities shown by lead compounds imidazo[2,1-*b*][1,3,4]thiadiazoles **22** (Figure 1), the aim of my PhD project was to analyse structural changes of the lead compounds in order to investigate the structural relevance of each moiety and and their effect on the biological/antiproliferative activity.

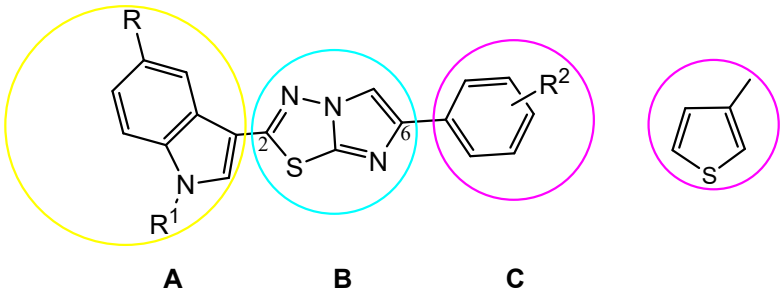

22

Figure 18. Chemical structure of imidazo[2,1-*b*][1,3,4]thiadiazoles **22**

Changes made to lead compound general structures can be divided according to the exchanged moiety in three different categories:

1. Changes on central nucleus B
    - Series of [1,3,4]thiadiazole[3,2-*a*]pyrimidin-5-ones (22 compounds), in which the imidazole ring of the central nucleus was replaced by the hexatomic pyrimidinone heterocyclic ring.
    - Series of imidazo[2,1-*b*][1,3]thiazoles (13 compounds), in which central 1,3,4-thiadiazole has been replaced with its isostere 1,3-thiazole .
2. Changes on the nucleus A
    - Series of analogues imidazo[2,1-*b*][1,3,4]thiadiazoles, replaced in position 2 with an 7-azaindolic (16 compounds) or 1,3-thiazole ring (5 compounds)
3. Changes on the nucleus C
    - Two series of 5-substituted-3-(-6-methyl-imidazo[2,1-*b*][1,3,4]thiadiazol-2-yl)-1*H*-indole analogues bearing in position

C6 2-furanyl (10compounds) and 1,4-benzodioxane-6-yl (10 compounds).

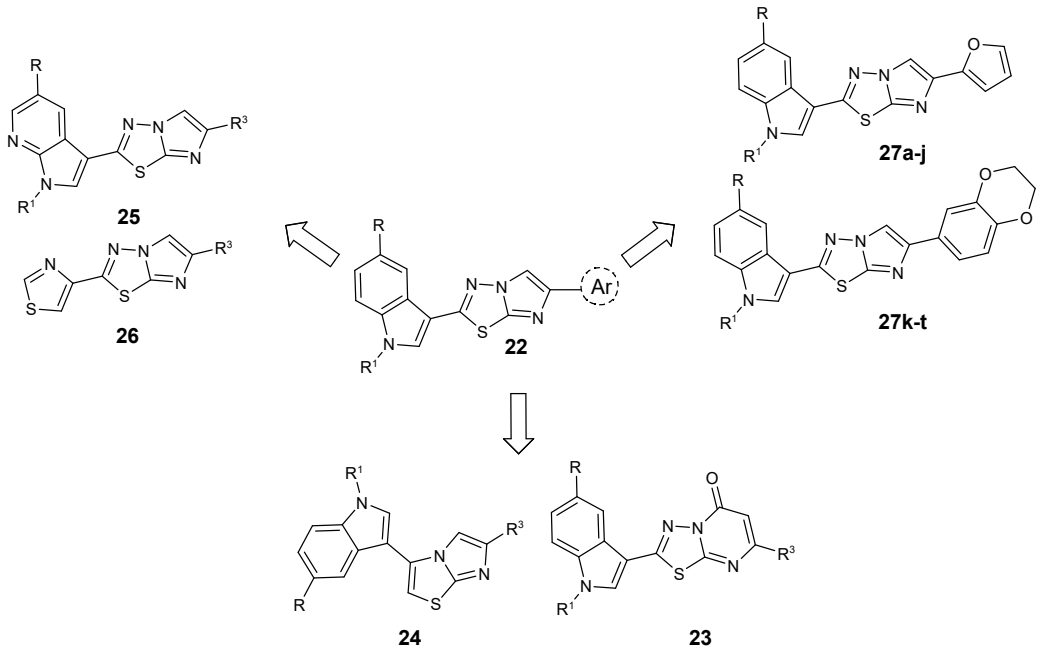

Figure 19. Schematic representation of the structural modifications made on the lead compound **22**.

Changes on the nucleus B

Initially, we started studying the influence of structural modifications of the central core biological activity by synthesizing a new series of [1,3,4]thiadiazolo[3,2-a]pyrimidin-5-ones.

Heterocycles compounds have always had huge relevance in drug discovery. The six membered nitrogen ring pyrimidine is the building unit of essential biological structures such as DNA and RNA. Therefore, bicyclic pyrimidine-fused derivatives, such as triazolopyrimidines, furopyrimidines, pyridopyrimidines, pyrrolopyrimidines, pyrimidoazepines, quinazolines, purines, and pteridines, were found to exhibit remarkable anticancer[214,215], antimicrobial[216], antiviral[217], anti-analgesic[218] ,inflammatory[219] and antimalarial[219] activities.

During the years, a growing interest has been focusing even more on 5,6-bicyclic heteroatomic rings; in particular, bicyclic systems which bear pyrimidines and pyrimidines. In the last decade, the Trapidil which bears pyrimidine condensed

with 5 membered heterocycle ring (Figure 3) was marketed (2011) as a vasodilator and antiplatelet drug.[220] In 2008, Essramycin, the first [1,2,4]triazolo[1,5-a]pyrimidin-5-one antibiotic drug, was isolated from marine Streptomyces species.[221] Moreover, [1,3,4]thiadiazolo[3,2-a]pyrimidin-5-ones derivatives **25** and **26** were described for their antimicrobial and antiproliferative activity.[222]

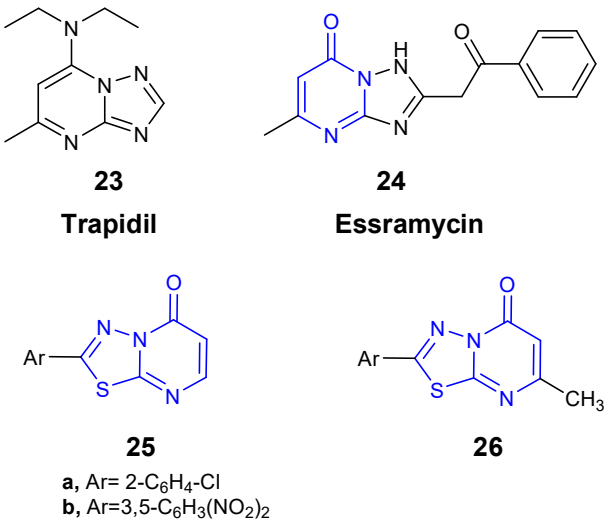

Figure 20. Chemical structures of pyrimidine and pyrimidinone fused compounds reported for antiproliferative activity.

1,3-Thiazole ring, equally to its bioisostere 1,3,4-thiadiazole, has been found in several natural compounds, increasing the interest for its synthetic or semisynthetic applications in medicinal chemistry. During the years, many compounds bearing thiazoles moiety have been described for their activities on wide spectrum of diseases. The analogues fused heterocycle imidazo[2,1-*b*]thiazole derivatives have been reported in the literature for their wide biological activity, in particular imidazothiazole are described as anticancer[223,224], antibacterial[225] and antioxidant.

According to literature, imidazo[2,1-*b*]thiazole derivatives showed potent efficacy against many human cancer cell lines. Furthermore, some imidazothiazoles derivatives are already approved by FDA. Levamisole **27**, a well-known immunomodulator and anthelminthic drug, and YM-201627 (**28**), an anticancer drug, are two examples of orally active imidazo[2,1-*b*]thiazole derivatives.

Additionally, antiproliferative studies demonstrated that imidazo[2,1-*b*]thiazole derivatives mainly inhibit cancer cell growth acting through protein kinase inhibition or tubulin inhibition.[226,227]

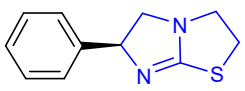

27

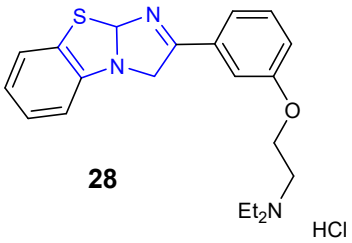

28

Figure 21 Commercial imidazo[2,1-*b*]thiazole analogues.

To accomplish our aim, the study proceed evaluating the role of the imidazo[2,1-*b*][1,3,4]thiadiazole of the lead compounds. A new series containing the bicyclic bio isostere imidazo[2,1-*b*]thiazole was prepared. The novel compounds contain 3,5-disubistuted-imidazo[2,1-*b*]thiazole, instead of imidazo[2,1-*b*][1,3,4]thiadiazole, which bears substituted indoles in position C-3 while different substituted phenyl analogues or 3-thiophenyl in position C-5.

Changes on the nucleus A

Indole, also known as benzopyrrole, is an important heterocyclic ring of pharmaceutical interest due to its several well-known biological activities.[213] The role of the indole nucleus for the biological activity was evaluated by replacing it with its isostere 1*H*-pyrrolo[3,2-*b*]pyridine, also known as 7-azaindole, exhibited many relevant biological activities such as, cytotoxic, anti-angiogenic, anti-CRTh2 receptor, anti-Alzheimer disease, and many others.[228] The presence of the nitrogen atoms on the scaffold provides suitable sites for bidentate hydrogen bonds with the hinge region of different kinases, including Focal adhesion kinase.[229]

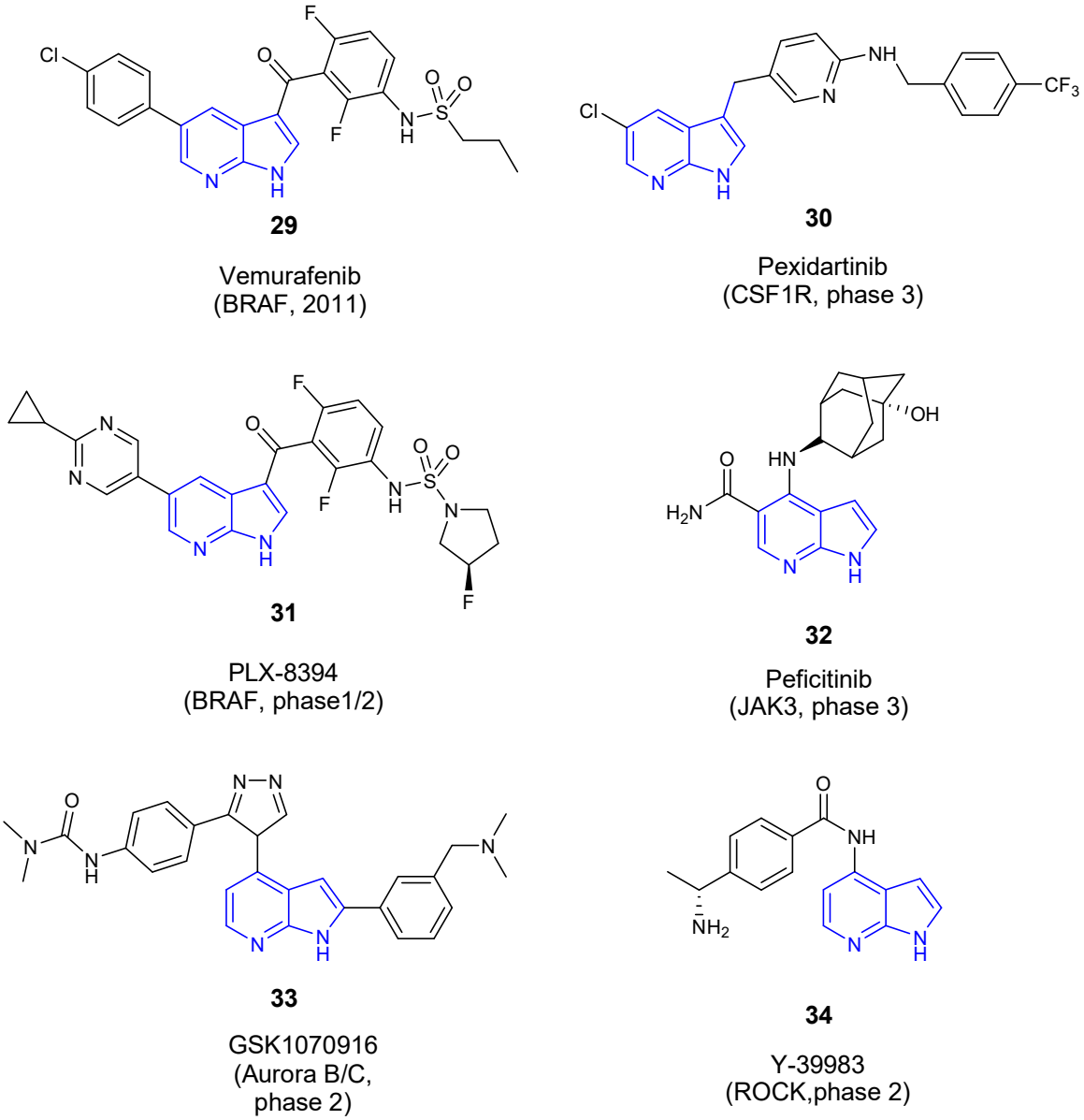

Figure 22. Chemical structures of 7-azaindole derivative compounds with antiproliferative and protein kinase inhibitory activity

Furthermore, many scaffold bearing 7-azaindoles in the last decades arrived in clinical phases as kinase inhibitors. Among them Vemurafenib B-RAF kinase (serine–threonine kinase [STK]) inhibitor, has been already FDA approved (2011) as first drug bearing 7-azaindole kinase inhibitor for treatment of melanoma. Other compounds reported are currently in clinical phase as inhibitors of different kinases, including serine/threonine kinases and tyrosine kinases. (Fig. 22)

The effect on the biological activity of the introduction of the heteroaromatic ring 1,3-thiazole in position C-2 was also evaluated. 1,3-thiazole has been proven to be fascinating building block for the design and synthesis of pharmacologically active derivatives.[230] Many compounds bearing thiazoles have been found to have antioxidant[231], anti-inflammatory[232], antibacterial[233], antifungal[234] , antiviral[235], anticonvulsant[236] properties. Numerous thiazole analogues showed extremely strong anti-cancer activity. Examples of selective drugs with antiproliferative and tyrosine kinase inhibitory action are Dabrafenib and Dasatinib.[237,238] As result of the interesting antiproliferative activity and kinases inhibitor shown by 1,3-thiazole derivativities, we decided to synthetize new imidazothiadiazoles which bound this 5-membered heteroaromatic ring in position C2.

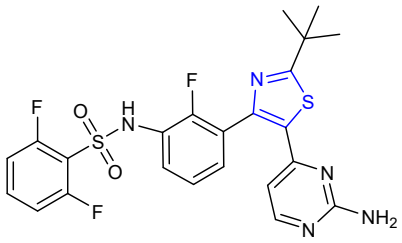

35

Dabrafenib

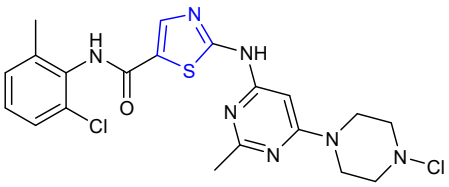

36

Dasatinib

Figure 23. Chemical structures of 1,3-thiazole derivative compounds antiproliferative and protein kinase inhibitory activity

Changes on the nucleus C

Finally, we thought to investigate the effect of the substitution in position C-6 by synthesizing two series bearing a 2-furanyl ring, or a 1,4-benzodioxane in that position. These two scaffolds were selected based on their interesting pharmaceutical properties described in literature. In particular, 1,4-benzodioxane, which is described as promising moiety for kinase inhibition in particular against Focal adhesion kinases. During the last decades, Y.-T. Duan[239,240] research group produced many compounds containing 1,4-benzodioxane moiety with FAK inhibition activity.[241]

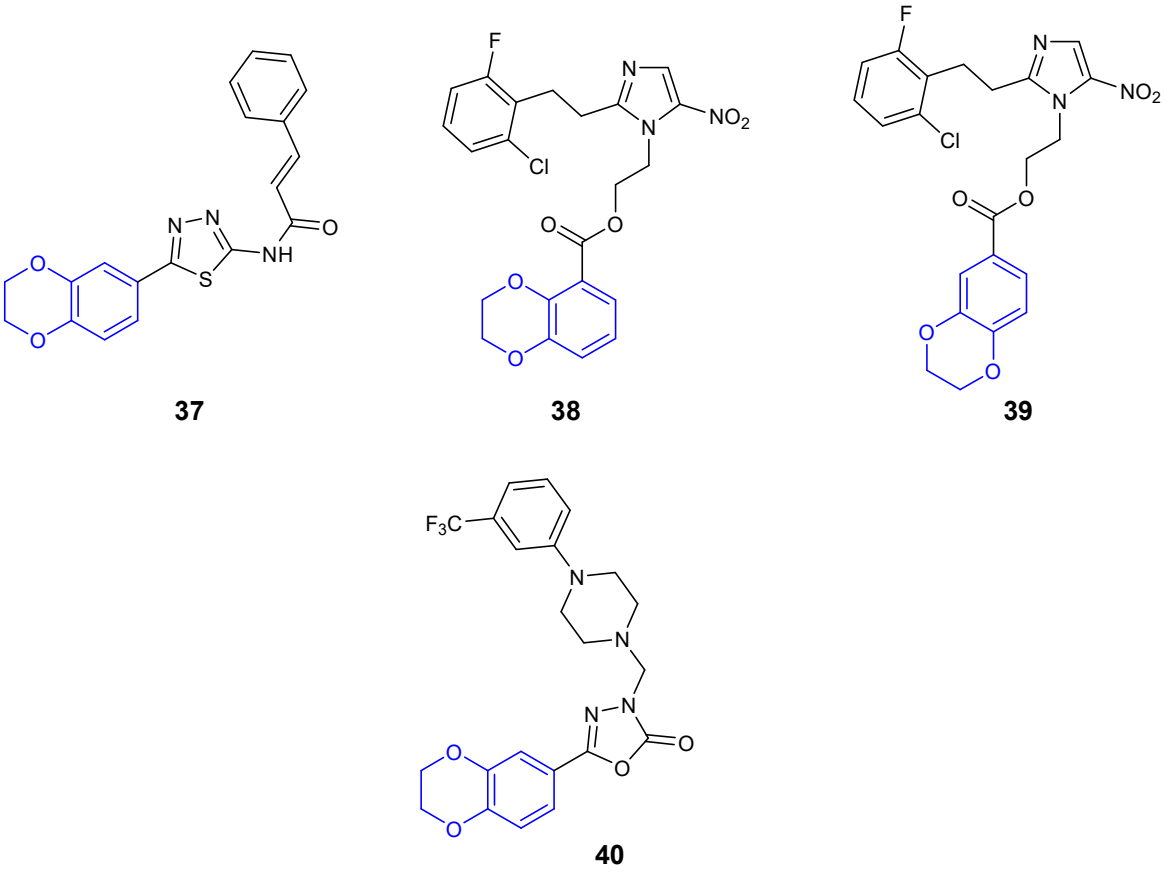

Figure 24. Chemical structures of 1,4-benzodioxane derivatives compounds with antiproliferative and protein kinase inhibitory activity.

Chemistry section

Compound **23a-v** were efficiently synthetized following the synthetic procedure reported in Scheme 1.

Scheme 1. Synthetic scheme of nucleus B exchange with introduction of [1,3,4]thiadiazolo[3,2-*a*]pyrimidin-5-one.

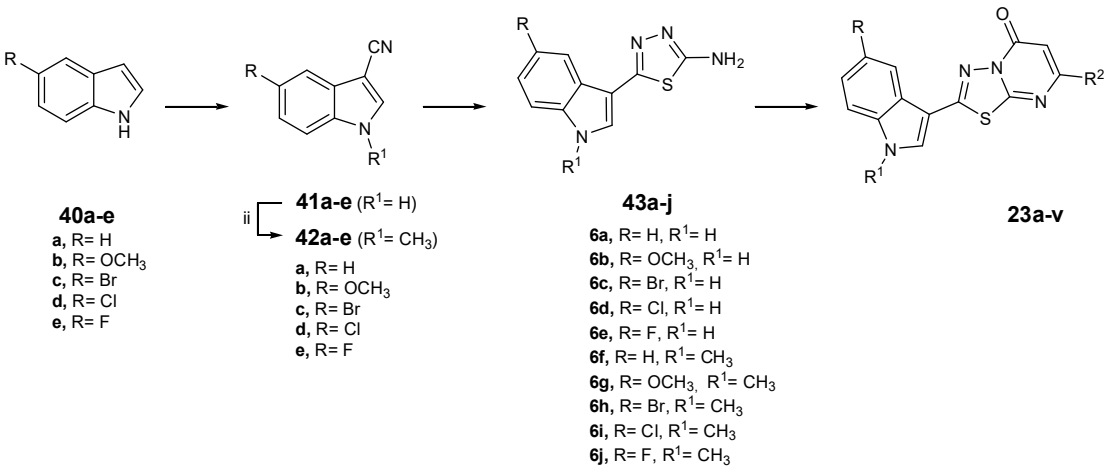

In particular, compounds **23a-v** were prepared starting from the commercially available 5-substituted indoles **40a-e** which were reacted with chlorosulfonylisocyanate (CSI) in anhydrous acetonitrile, to give the corresponding sulphonylchlorides which allow to reach the carbonitrile only after addition of dimethylformammide (DMF) by promoting losing sulfuric anhydride (SO_3), DMF and hydrochloric acid (HCl). The reaction, stirred at temperature between 0°C and 5°C afforded the desired compounds **41a-e** in excellent yields (90-98%).

Scheme 2. Synthesis of 5-substituted-1*H*-indole-3-carbonitrile.

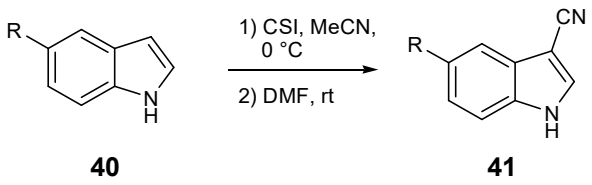

Table 1. 5-substituted-1*H*-indole-3-carbonitrile **41.**

Compound	R	Yield%
41a	H	90
41b	OCH_3	90
41c	Br	98
41d	Cl	90
41e	F	90

N1-methyl-3-carbonitrile **42a-e** were obtained in excellent yields through the reaction of derivatives **41a-e** with dimethyl carbonate in anhydrous DMF, using K_2CO_3 as base, at 130 °C for 3.5 h.

Scheme 3. Synthesis of 5-substituted-1-methyl-indole-3-carbonitrile.

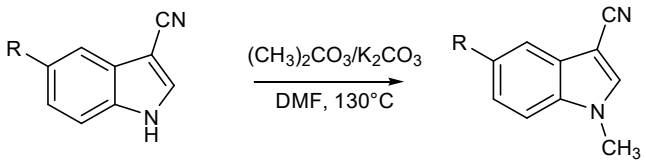

41a-e **42a-e**

Table 2. 5-substituted-1-methyl-indole-3-carbonitrile **42.**

Compound	R	Yield%
42a	H	97
42b	OCH_3	90
42c	Br	98
42d	Cl	95
42e	F	92

The preparation of the key intermediates, 2-amino-thiadiazoles **43a-j,** was afforded heating derivatives **41a-e** and **42a-e** with thiosemicarbazide in trifluoracetic acid at 75 °C, for 2h. After this time, the reaction mixture was neutralized with $NaHCO_3$ solution, and compounds **43a-j** were collected by vacuum filtration and washed with diethyl ether.

Scheme 4. Synthesis of 1,5-substituted(indol-3-yl)-[1,3,4]thiadiazol-2-ylamine

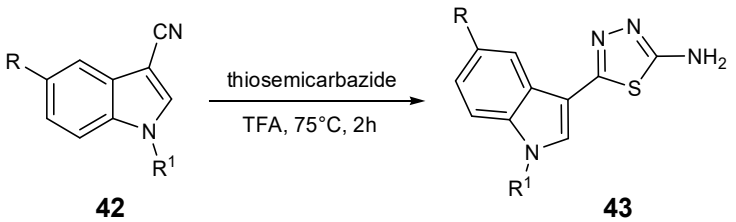

42 **43**

Table 3. 1,5-substituted-(indol-3-yl)-[1,3,4]thiadiazol-2-ylamine **43.**

Compound	R	R^1	Yield%
43a	H	H	98
43b	OCH_3	H	98
43c	Br	H	92
43d	Cl	H	98
43e	F	H	98
43f	H	CH_3	90
43g	OCH_3	CH_3	95
43h	Br	CH_3	99
43i	Cl	CH_3	100
43j	F	CH_3	95

Final products 2,7-disubstituted-[1,3,4]thiadiazol[3,2-a]pyrimidin-5-one **23** were prepared, in acid conditions by the reaction between compounds **43a-j** with the commercial 3-oxo-3-phenyl-propionic acid ethyl ester for compounds **23a-j**, and with the thiophenyl β-ketoester **45** in polyphosphoric acid (PPA) to prepare compounds **23m-v** Whereas compounds **23k-l,** were prepared refluxing compound **43a** and **43f** in acetic acid with 3-oxo-butyric acid ethyl ester.

Scheme 5. Synthesis of final compounds 2,7-disubstituted[1,3,4]thiadiazolo[3,2-*a*]pyrimidin-5-one**.**

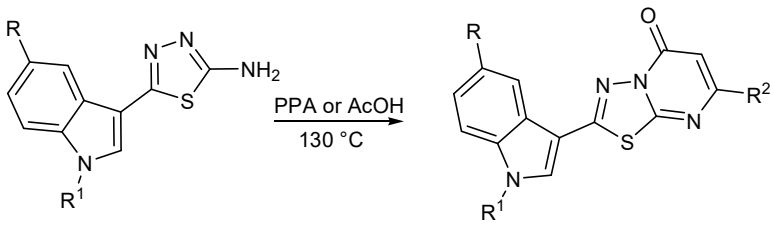

43 **23**

Table 4. 2,7-Disubstituted[1,3,4]thiadiazolo[3,2-*a*]pyrimidin-5-one**.**

Compound	R	R^1	R^2	Yield%
23a	H	H	Ph	55
23b	OCH_3	H	Ph	41
23c	Br	H	Ph	48
23d	Cl	H	Ph	36
23e	F	H	Ph	42
23f	H	CH_3	Ph	46
23g	OCH_3	CH_3	Ph	30
23h	Br	CH_3	Ph	32
23i	Cl	CH_3	Ph	39
23j	F	CH_3	Ph	45
23k	H	H	CH_3	30
23l	H	CH_3	CH_3	28
23m	H	H	3-thiophenyl	36
23n	OCH_3	H	3-thiophenyl	25
23o	Br	H	3-thiophenyl	29
23p	Cl	H	3-thiophenyl	27
23q	F	H	3-thiophenyl	31
23r	H	CH_3	3-thiophenyl	33
23s	OCH_3	CH_3	3-thiophenyl	23
23t	Br	CH_3	3-thiophenyl	25
23u	Cl	CH_3	3-thiophenyl	23
23v	F	CH_3	3-thiophenyl	32

The appropriate β-ketoester derivative 2-bromo-1-thiophen-3-yl-ethanone **45** was obtained in good yield 70%, starting from 3-acetyl thiophene **44** reacts with NaH

and diethyl carbonate in DMF to produce, after column chromatography, the oily product**.** The high sensibility of this reaction has required distillation following Voghel procedure to make anhydrous diethyl carbonate before its usage.

Scheme 6. Synthesis of 3-oxo-3-thiophen-3-yl-propionic acid ethyl ester.

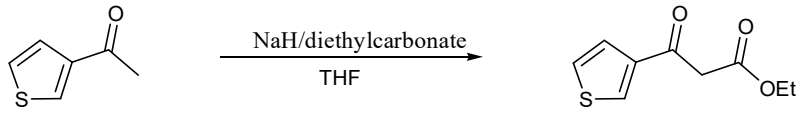

44 **45**

Scheme 7. Synthetic scheme of nucleus B exchange with introduction of imidazo[2,1-*b*]thiazole.

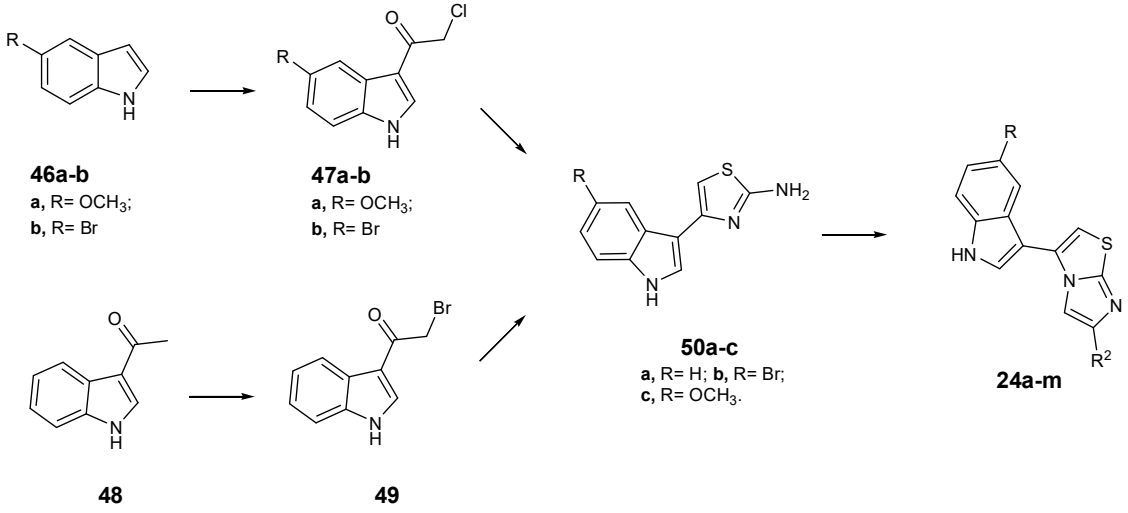

46a-b
a, R= OCH_3;
b, R= Br

47a-b
a, R= OCH_3;
b, R= Br

50a-c
a, R= H; **b,** R= Br;
c, R= OCH_3.

24a-m

48 **49**

The haloacetyl derivatives 2-chloro-1-(1*H*-indol-3-yl)-ethanone **47a-b** and 2-bromo-1-(1*H*-indol-3-yl)-ethanone **49** were prepared following two different methods to avoid the undesired product of N-alkyl indole **53.**

Scheme 8.

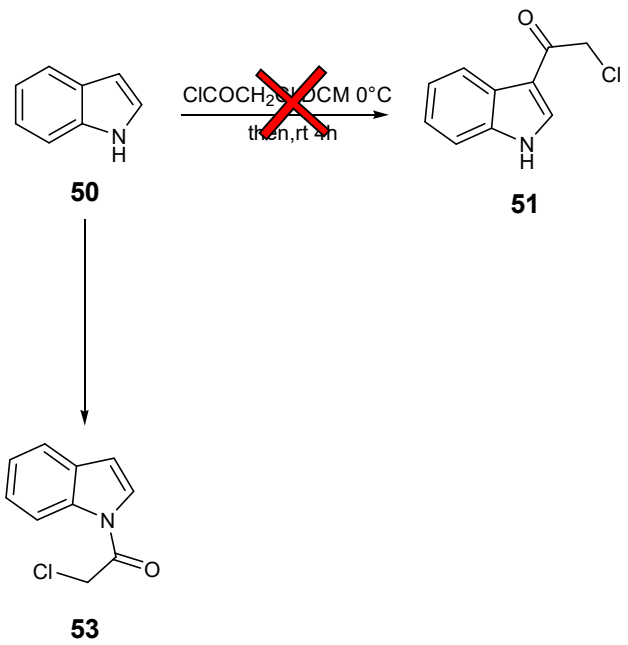

2-bromo-1-(1*H*-indol-3-yl)-ethanone **49** was obtained by dissolving commercially available 3-acetyl indole **48** in anhydrous methanol, while bromine was added dropwise in order halogenate Cα to reach a final good yield (70%).

Scheme 9. Synthesis of 2-bromo-1-(1*H*-indol-3-yl)-ethanone.

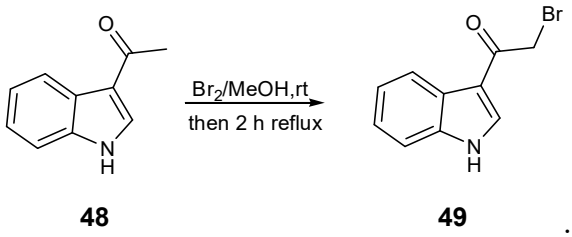

Besides, indoles substitute in position C-5 with electron withdrawing groups, such as a methoxy group or a bromine atom (**46a-b)** were suitable for the Friedel-Craft acylation in standard condition at 0 °C with chloroacetylchloride and aluminium chloride ($AlCl_3$), as acid of Lewis, under nitrogen atmosphere, and stirred for 4-6h to finally obtain the derivatives **47** in moderate yield (40-50%)

Scheme 10. Synthesis of 2-chloro-1-(1*H*-indol-3-yl)-ethanone **47.**

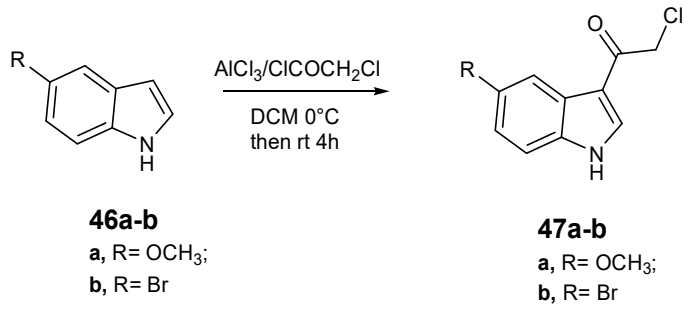

46a-b
a, R= OCH_3;
b, R= Br

47a-b
a, R= OCH_3;
b, R= Br

Then both haloacetyl derivatives, according to Hantzsch reaction condition, were refluxed in anhydrous ethanol with thiourea to prepare 4-(5-substitute-1*H*-indol-3-yl)-thiazol-2-ylamine derivatives **50a-c** in good yield (60-70%).

Scheme 11. Synthesis of 4-(5-substituted-1*H*-indol-3-yl)-thiazol-2-ylamine **50a-c.**

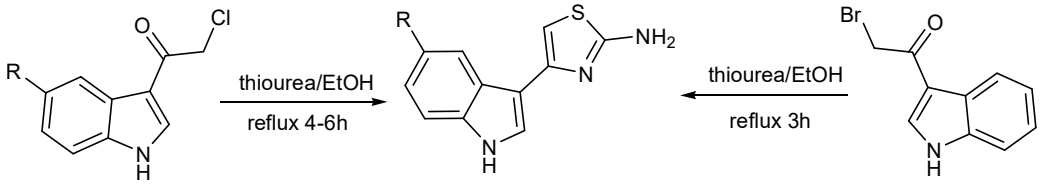

47a-b
a, R= OCH_3;
b, R= Br

50a-c
a, R= H; **b,** R= Br;
c, R= OCH_3.

49

Synthesis of final products 5-subtituted-3-(6-aryl-imidazo[2,1-*b*]thiazol-3-yl)-*1H*-indole **24a-n** were performed by reacting **50a-c** in anhydrous ethanol with commercial 2-bromo-acetophenone derivatives or the synthetized 2-bromo-1-thiophen-3-yl-ethanone **21.**

Scheme 12. Synthesis of 5-subtituted-3-(6-aryl-imidazo[2,1-*b*]thiazol-3-yl)-1*H*-indole **24.**

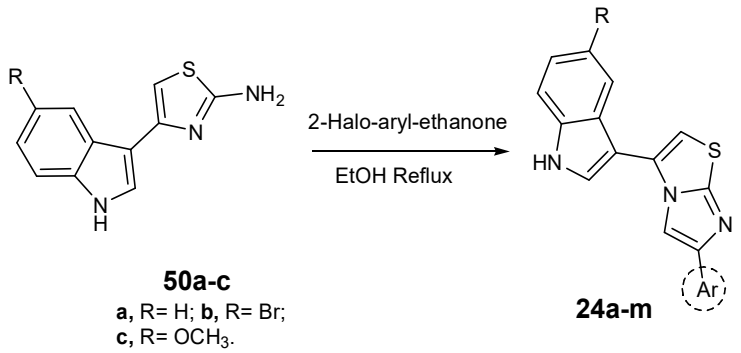

50a-c
a, R= H; **b,** R= Br;
c, R= OCH_3.

24a-m

Table 5. 5-subtituted-3-(6-aryl-imidazo[2,1-*b*]thiazol-3-yl)-1*H*-indole **24.**

Compound	R	R^1	Yield%
24a	H	C_6H_5	17
24b	H	3-Thiophenyl	15
24c	H	2,5-OCH_3-C_6H_3	20
24d	H	4-F-C_6H_4	22
24e	Br	C_6H_5	16
24f	Br	3-Thiophenyl	13
24g	Br	2,5-OCH_3-C_6H_3	15
24h	Br	4-F-C_6H_4	20
24i	Br	3'-OCH_3-C_6H_4	10
24j	OCH_3	C_6H_5	16
24k	OCH_3	3-Thiophenyl	13
24l	OCH_3	4-F-C_6H_4	15
24m	OCH_3	2,5-OCH_3-C_6H_3	18

The intermediate 2-bromo-1-thiophen-3-yl-ethanone **54** was afforded by the bromination of the 3-acetylthiophene **44** in anhydrous dichloromethane, and recrystallized in EtOH/H_2O to obtain white crystals in good yield. (60%)

Scheme 13. Synthesis of 2-bromo-1-thiophen-3-yl-ethanone **54.**

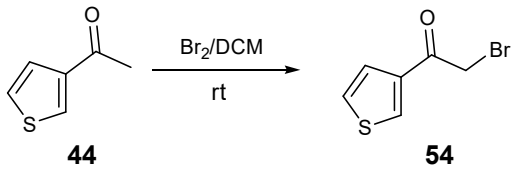

Compounds **25a-o** were achieved starting from commercially available **55a** as reported in scheme 14.

Scheme 14. Synthetic scheme of nucleus A exchange with introduction of 7-azaindole.

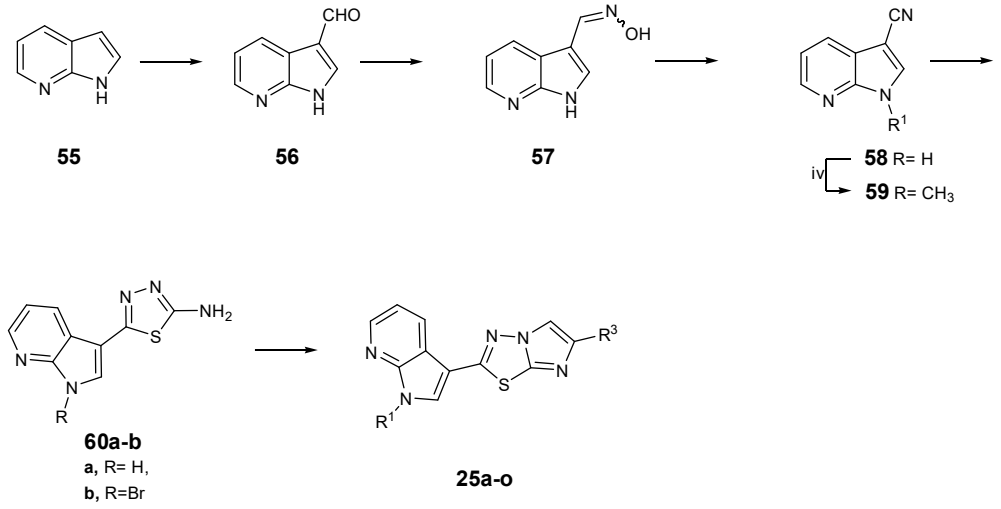

Starting from the commercially available 7-azaindole **55** which was turned into their 3-formaldehyde analogues **56** by reacting with hexamethylenetetramine hydrochloride in acetic acid/water solution (1:2), and heated at 120°C until total consumption of the starting materials (1-2h). The reaction was quenched with ice cold water to afford the final compounds in good yield (85%).

Scheme 15. Synthesis of 1*H*-pyrrolo[2,3-*b*]pyridine-3-carbaldehyde **56.**

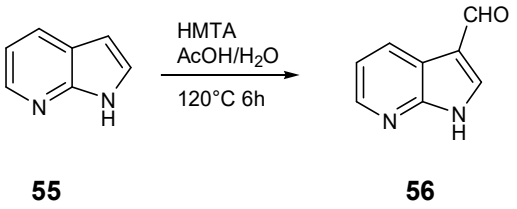

The oxime intermediate **57** was synthetized by treating 1*H*-pyrrolo[2,3-*b*]pyridine-3-carbaldehyde **56** with hydroxylamine hydrochloride , in

hydroalcoholic solution EtOH/H_2O (2:1) in presence of a weak base as Na_2CO_3. 1*H*-pyrrolo[2,3-*b*]pyridine-3-carbaldehyde oxime **57** was obtained in excellent yield (90%) and used for next reaction without any purification.

Scheme 16. Synthesis of 1*H*-pyrrolo[2,3-*b*]pyridine-3-carbaldehyde oxime **57**

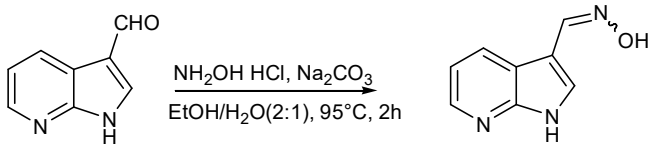

56 **57**

Preparation of **58** were carried out through the reaction of compounds **57** with acetic anhydride at 130 °C 6h, to obtain 1-acetyl-1*H*-pyrrolo[2,3-*b*]pyridine-3-carbonitrile reaction intermediate, which was deacetylated through refluxing crude compound in methanol/NaOH 1M solution for 2h, to finally get the desired 1*H*-pyrrolo[2,3-*b*]pyridine-3-carbonitrile **58**

Scheme 17. Synthesis of 1*H*-pyrrolo[2,3-b]pyridine-3-carbonitrile **58**

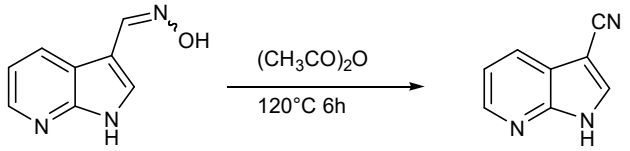

57 **58**

The N-methylation reaction to afford derivatives **59** was performed at room temperature in excellent yields (85%) with iodomethane (CH_3I) in presence of potassium t-butoxide (t-BuOK) as base and tris [2- (2-methoxyethoxy) ethyl] amine (TDA-1) as a phase transfer catalyst.

Schem 18. Synthesis of 1-methyl-pyrrolo[2,3-*b*]pyridine-3-carbonitrile **59.**

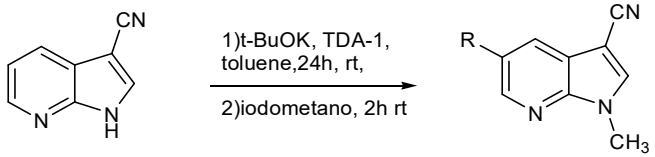

58 **59**

The preparation of rings **60a-b** was performed with the same aforementioned procedure used for indole analogues, by the heating with thiosemicarbazide in

trifluoracetic acid at 75 °C for 2h. The precipitated solid was filtered under vacuum and washed with diethyl ether to obtain 5-(1*H*-pyrrolo[2,3-*b*]pyridin-3-yl)-[1,3,4]thiadiazol-2-ylamine **60a-b** in excellent yield (80-85%).

Scheme 19. Synthesis of 5-(1*H*-pyrrolo[2,3-*b*]pyridin-3-yl)-[1,3,4]thiadiazol-2-ylamine **60a-b.**

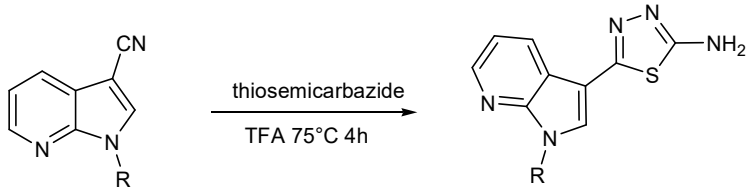

58, R= H;
59, R= CH_3;

60a-b
a, R= H;
b, R= CH_3;

Final compounds 6-substituted-imidazo[2,1-*b*][1,3,4]thiadiazol-2-yl-1*H*-pyrrolo[2,3-*b*]pyridine **25a-o** (Table 6) were obtained in ethanol with α-haloketones refluxed in anhydrous ethanol at 80°C for 24h, in moderate and good yield (50-70%)**.**

Scheme 20. Synthesis of 6-substituted-imidazo[2,1-*b*][1,3,4]thiadiazol-2-yl-1*H*-pyrrolo[2,3-*b*]pyridine **25a-o**

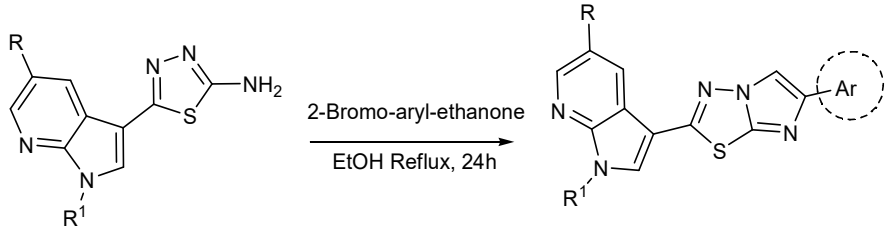

60a-c **25a-o**

Table 6. 6-substituted-imidazo[2,1-*b*][1,3,4]thiadiazol-2-yl-1*H*-pyrrolo[2,3-*b*]pyridine **25**

Compound	R	Ar	Yield%
25a	H	C_6H_5	42
25b	H	4F-C_6H_4	40
25c	H	2,5- OCH_3-C_6H_3	27
25d	H	3'-OCH_3-C_6H_4	36
25e	H	3-Thiophen-yl	25
25f	H	3-Pyridin-yl	31
25g	H	1,4-Benzodioxan-6-yl	39
25h	CH_3	C_6H_5	24
25i	CH_3	2,5- OCH_3-C_6H_3	37
25j	CH_3	3-Thiophen-yl	21
25k	CH_3	3-Pyridin-yl	25
25l	CH_3	1,4-Benzodioxan-6-yl	40
25m	CH_3	4-Pyridin-yl	28
25n	CH_3	2-Furan-yl	45
25o	CH_3	3'-OCH_3-C_6H_4	30

All 2-bromo-phenyl-ethanone derivates used for the final reaction were commercially available, whereas 2-bromo-heteroaryl-ethanone compounds were synthetized by bromination of their acetyl analogues.

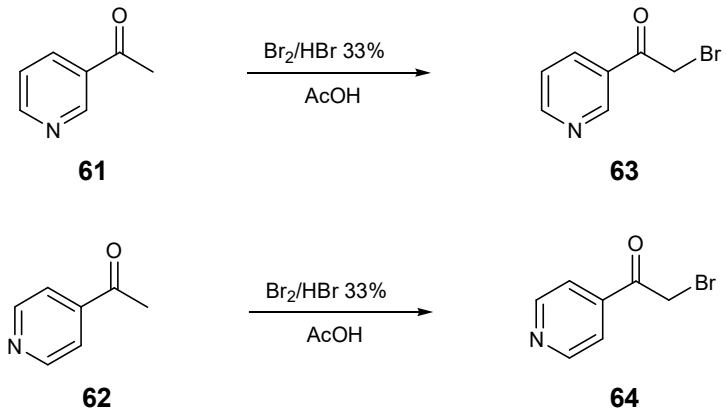

Scheme 21. Synthesis of 2-bromo-pyridinyl-ethanone **63,64.**

2-bromo-1-pyridin-3-yl-ethanone **63** and 2-bromo-1-pyridin-4-yl-ethanone **64** were obtain with the same synthetic procedure. The commercial pyridine acetyl derivatives **61, 62** were dissolved and stirred in acetic acid and bromine in HBr 33% was added dropwise at 0°C. The mixture was heated for 2 h at 40°C, then 75°C for 2h. Compounds **63** and **64** were obtained after the appropriate work-up and purified by trituration in diethyl ether. Yield (90-95%)

Scheme 22. Synthesis of 2-bromo-1-(2,3-dihydro-benzo[1,4]dioxin-6-yl)-ethanone **66.**

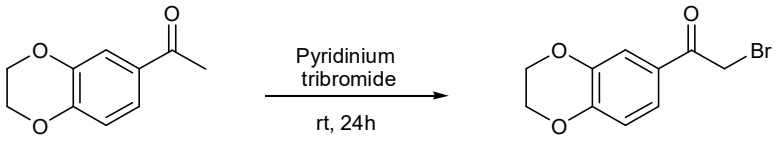

65 **66**

2-bromo-1-(2,3-dihydro-benzo[1,4]dioxin-6-yl)-ethanone intermediate **66** was obtained starting from commercially available 1-(2,3-dihydro-benzo[1,4]dioxin-6-yl)-ethanone **65** dissolved in methanol and properly brominated using pyridinium tribromide to yield the desired mono-brominated compound in good yields (60%) after hot recrystallization process in ethyl acetate.

Scheme 23. Synthesis of 1-furan-2-yl-ethanone **68**.

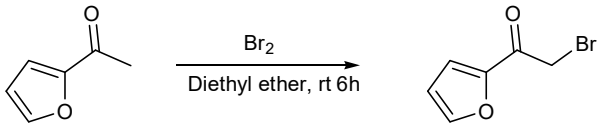

67 **68**

The bromoacetyl derivative **68** was obtained as reported in scheme 24. Bromine was added dropwise at rt to a solution of commercial 1-furan-2-yl-ethanone in diethyl ether and stirred for 12h. Crude product was obtained after the extraction and neutralization with solution of $Na_2S_2O_3$ and was purified by flash chromatography to yield the desired 2-bromo-1-furan-2-yl-ethanone in excellent yield 95%.

Scheme 24. Synthetic scheme of nucleus A exchange with introduction of 1,3-thiazole.

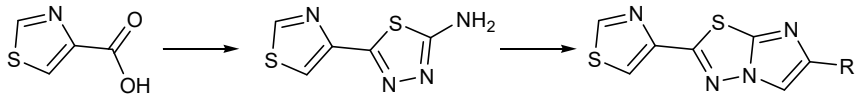

69 **70** **26a-e**

Imidazo[2,1-*b*][1,3,4]thiadiazole analogues **26a-e** were synthetized starting from commercially available 4-carboxylic-1,3-thiazole **69** acid and passing from key intermediate 5-thiazol-4-yl-[1,3,4]thiadiazol-2-ylamine **70.**

Scheme 25. Synthetic of 2-amino-[1,3,4]thiadiazoles **70.**

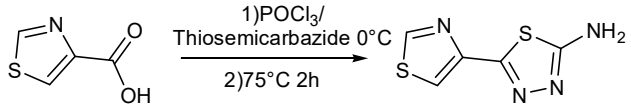

69 **70**

Unlike other aforementioned 2-amino-[1,3,4]thiadiazoles, derivate 5-thiazol-4-yl-[1,3,4]thiadiazol-2-ylamine, was obtain via one-pot reaction with $POCl_3$ and thiosemicarbazide, in order to obtain the unstable acyl chloride that immediately reacted with thiosemicarbazide to afford desiderate compound **70.**

Scheme 26. Synthesis of 6-substituted-l-3-thiazol-4-yl-imidazo[2,1-*b*][1,3,4]thiadiazole **26.**

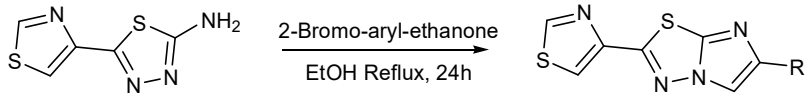

70 **26a-e**

Finally, 2-amino[1,3,4]thiadiazole **70** was reacted in anhydrous ethanol with various 2-bromo-aryl-ethanone derivatives to yield final compounds **26a-e.**

Table 7. 6-substituted-l-3-thiazol-4-yl-imidazo[2,1-*b*][1,3,4]thiadiazole **26.**

Compound	R	Yield %
26a	4-F-C_6H_4	40
26b	2,5- OCH_3-C_6H_3	33
26c	3'-OCH_3-C_6H_4	34
26d	3-Thiophenyl	40
26e	4-CF_3-C_6H_4	52

Scheme 27. Synthetic scheme of nucleus C exchange with introduction of 2-furan and 1,4-benzodioxane.

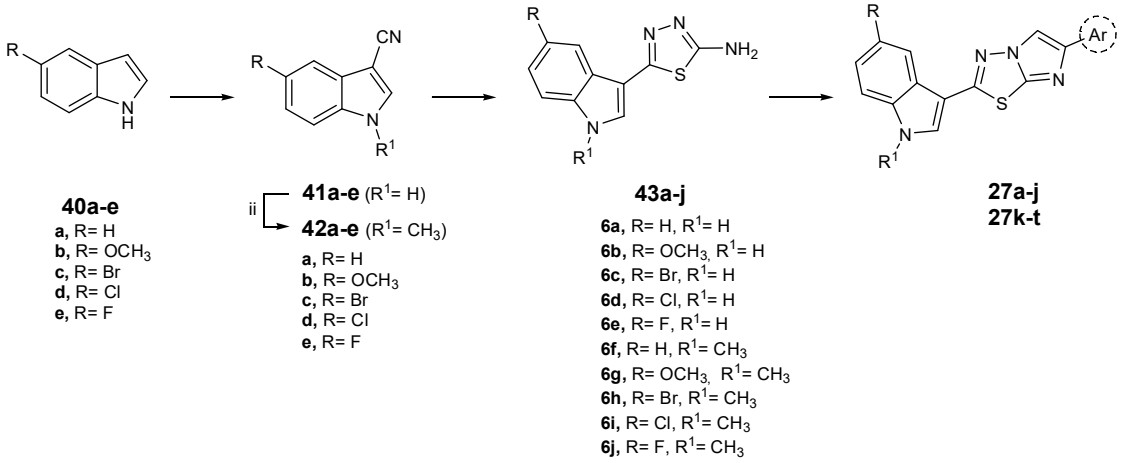

Imidazothiadiazole **27a-k** were synthetises following the already described procedure via intermediate **43a-j** using the same synthetic processes showed for pyrimidinones **23**. Final compounds were gained by heating compounds **43a-j** in anhydrous ethanol with respectively 2-bromo-1-furan-2-yl-ethanone **68** or 2-bromo-1-(2,3-dihydro-benzo[1,4]dioxin-6-yl)-ethanone **66** for 16-25h.

Table 8. 3-(6-furan-2-yl-imidazo[2,1-*b*][1,3,4]thiadiazol-2-yl)-1*H*-indole **27a-j** and 3-[6-(2,3-dihydro-benzo[1,4]dioxin-6-yl)-imidazo[2,1-*b*][1,3,4]thiadiazol-2-yl]-1*H*-indole **27k-t**

Compound	R	R^1	R^2	Yield%
27a	H	H	2-furan-yl	22
27b	OCH_3	H	2-furan-yl	20
27c	Br	H	2-furan-yl	35
27d	Cl	H	2-furan-yl	28
27e	F	H	2-furan-yl	40
27f	H	CH_3	2-furan-yl	36
27g	OCH_3	CH_3	2-furan-yl	38
27h	Br	CH_3	2-furan-yl	35
27i	Cl	CH_3	2-furan-yl	38
27j	F	CH_3	2-furan-yl	45
27k	H	H	1,4-bezodioxan-6-yl	40
27l	OCH_3	H	1,4-bezodioxan-6-yl	27
27m	Br	H	1,4-bezodioxan-6-yl	31
27n	Cl	H	1,4-bezodioxan-6-yl	44
27o	F	H	1,4-bezodioxan-6-yl	50
27p	H	CH_3	1,4-bezodioxan-6-yl	38
27p	OCH_3	CH_3	1,4-bezodioxan-6-yl	27
27r	Br	CH_3	1,4-bezodioxan-6-yl	35
27s	Cl	CH_3	1,4-bezodioxan-6-yl	44
27t	F	CH_3	1,4-bezodioxan-6-yl	30

Biology section

Antiproliferative activity

The purpose of my PhD project was to develop novel *small molecules* with improved antiproliferative and antimigratory activity compared to lead compound.

The antiproliferative activity of all synthesized compounds was evaluated by the National Cancer Institute (NCI, Bethesda MD) on the full panel of cancer cell lines. Preliminary, the compounds are tested on NCI panel of 60 tumour cell line, according with their protocol, at the single dose of 10^{-5} M.

The full NCI 60 cell panel includes: five leukemia cell lines, nine non-small cell lung cancer cell lines, seven colon cancer cell lines, six central nervous system cancer cell lines, eight melanoma cell lines, six ovarian cancer cell lines, eight renal cancer cell lines, two prostate cancer cell lines and breast cancer cell lines (including one with P-glycoprotein overexpression). The One-dose data was reported as a mean graph of the percent growth of treated cells. The number reported for the one-dose assay is growth relative to the no-compound control, and relative to the time zero number of cells. This allows detection of both growth inhibition (values between 0 and 100) and lethality (values less than 0). For example, a value of 100 means no growth inhibition. A value of 30 would mean 70% growth inhibition. A value of 0 means no growth during the experiment. A negative value means lethality.

To clarify following results: a value of 100 means no growth inhibition, a value of 30 would mean 70% growth inhibition, a value of 0 means not growth during the experiment, a negative value means lethality, a value of -100 means all cells are dead. NCI results are also expressed as: the concentration that causes 50% growth inhibition (IC50 value), the GI50 measures the growth inhibitory power of the test agent, the TGI signifies a cytostatic effect and the LC50, which signifies a cytotoxic effect.

Thiadiazopyrimidinone derivatives **23** generally showed weak-moderate growth inhibition (Fig. 25). Whereas some compounds showed selective cytotoxicity against specific sub panels such as: breast cancer (HS 578T), Central Nervous

System (SNB-75 and NCI-H522), Melanoma (MDA-MB-435), Non-Small Cell Lung Cancer (HOP-92), ovarian (OVCAR-3) and renal cancer(A498). In particular, compound **23g** showed interesting activity against renal cancer cell line A498 with a percentage of growth of 4.32% and proved to be very potent against melanoma and CNS cancer cell line exhibiting -23.78% of growth on MDA-MB-435 and -34.05% on NCI-H522

Melanoma (MDA-MB-435), Non-Small Cell Lung Cancer (HOP-92), ovarian (OVCAR-3) and renal cancer (A498). Compound **23g** showed interesting activity against renal cancer cell line A498 scoring 4.32% growth value compared to the untreated control. Furthermore, **23g** showed cytotoxicity activity against melanoma and CNS cancer cell line reaching -23.78% on MDA-MB-435 and growth of -34.05% on NCI-H522.

Figure 25 One dose mean graph of **23g** against NCI tumor cells: leukemia (red), non-small cell lung cancer cell (blue), colon cancer cell lines (green), central nervous system cancer cell lines (grey), melanoma cell lines (orange), ovarian cancer cell lines (purple), renal cancer cell lines (yellow), prostate cancer cell lines (light blue) and breast cancer cell lines (pink).

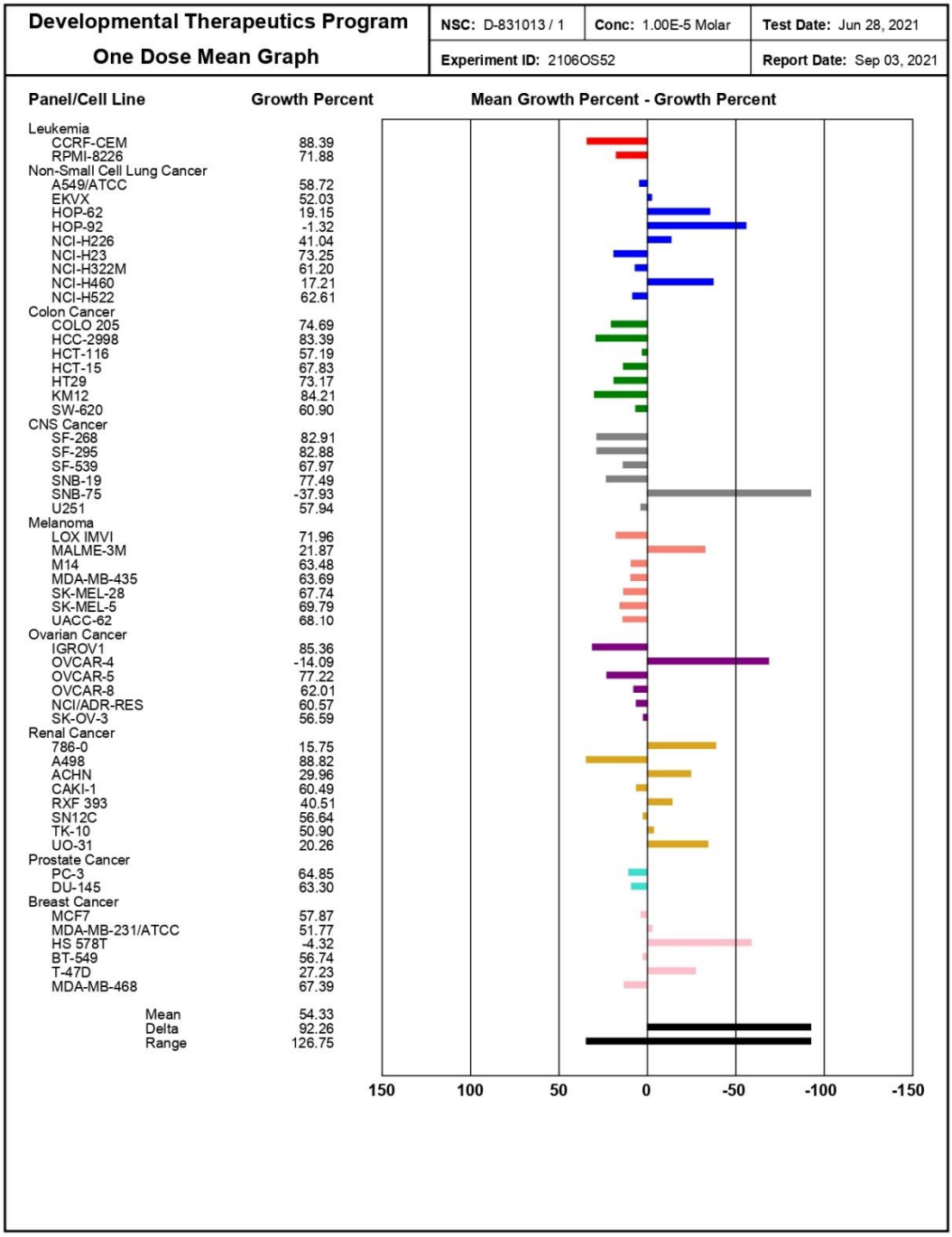

Also, derivatives **23e** and **23j,** which differ only in the N-indole methylation in compound **23j**, elicited interesting antiproliferative activity. Compound **23e,** in fact, showed a good cytotoxic activity against NSLC cells HOP-92 (-1.32%) breast cancer subpanel cells HS 578T (-4.32%), ovarian cancer cell line OVCAR-4 (-19.04%), showing the highest potency against CNS cancer cells SNB-75 (-37.93%). The N-methylated analogues **23j** maintained comparable activity towards HOP-92 cell line (3.43%), and on CNS tumour cell NCI-H522 (-37.42%).

Whereas the highest result was obtained against CNS cancer cells SNB-75 (-37,93%). Interestingly the N-methylated analogues **23j** maintained comparable activity on HOP-92 (3.43%), and cytotoxicity activity on CNS tumour but this time on a different cell type indeed the activity was similar on NCI-H522 (-37.42%).

Figure 26 One dose mean graph of **23e** against NCI tumor cells: leukemia (red), non-small cell lung cancer cell (blue), colon cancer cell lines (green), central nervous system cancer cell lines (grey), melanoma cell lines (orange), ovarian cancer cell lines (purple), renal cancer cell lines (yellow), prostate cancer cell lines (light blue) and breast cancer cell lines (pink).

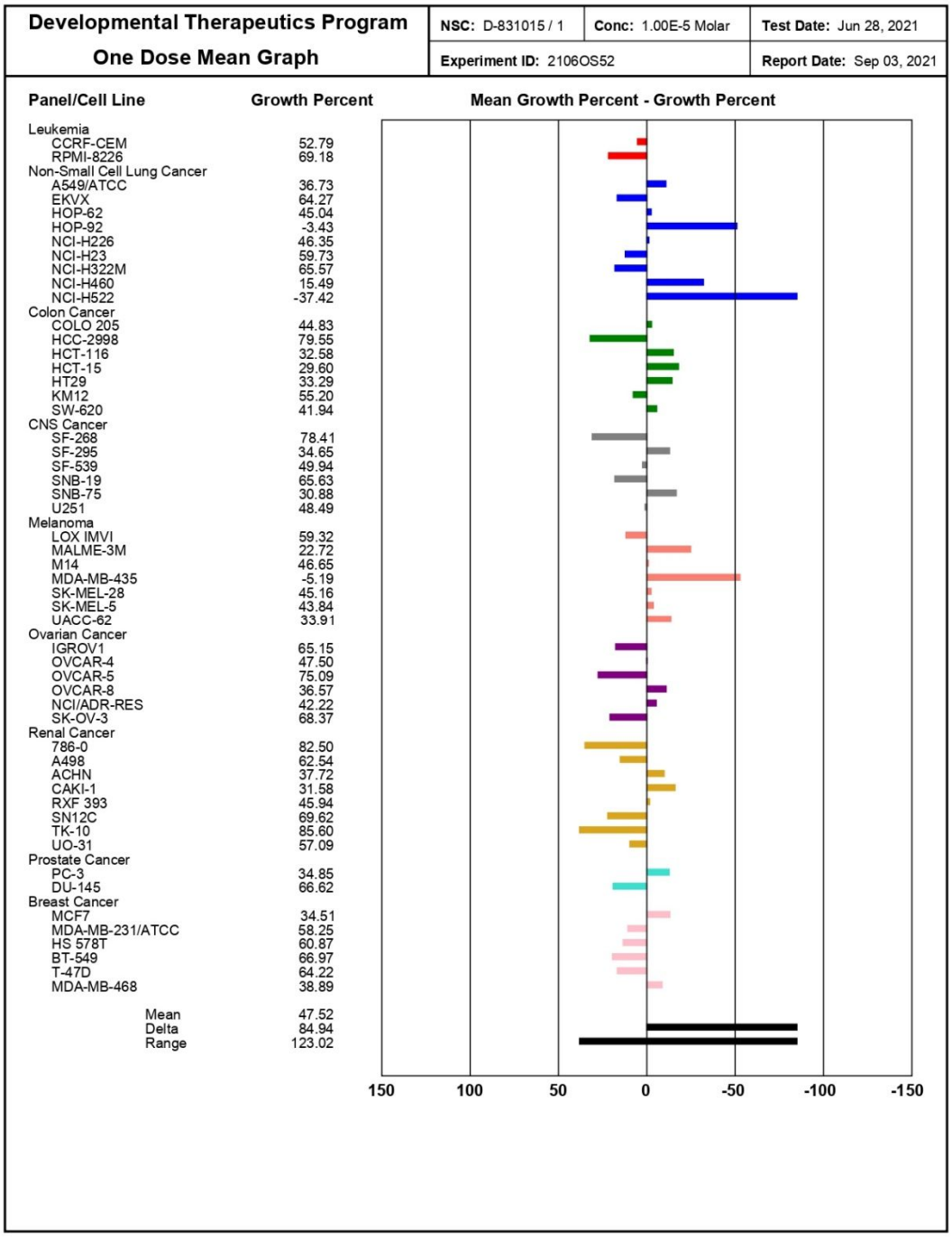

Figure 27 One dose mean graph of **23j** against NCI tumor cells: leukemia (red), non-small cell lung cancer cell (blue), colon cancer cell lines (green), central nervous system cancer cell lines (grey), melanoma cell lines (orange), ovarian cancer cell lines (purple), renal cancer cell lines (yellow), prostate cancer cell lines (light blue) and breast cancer cell lines (pink).

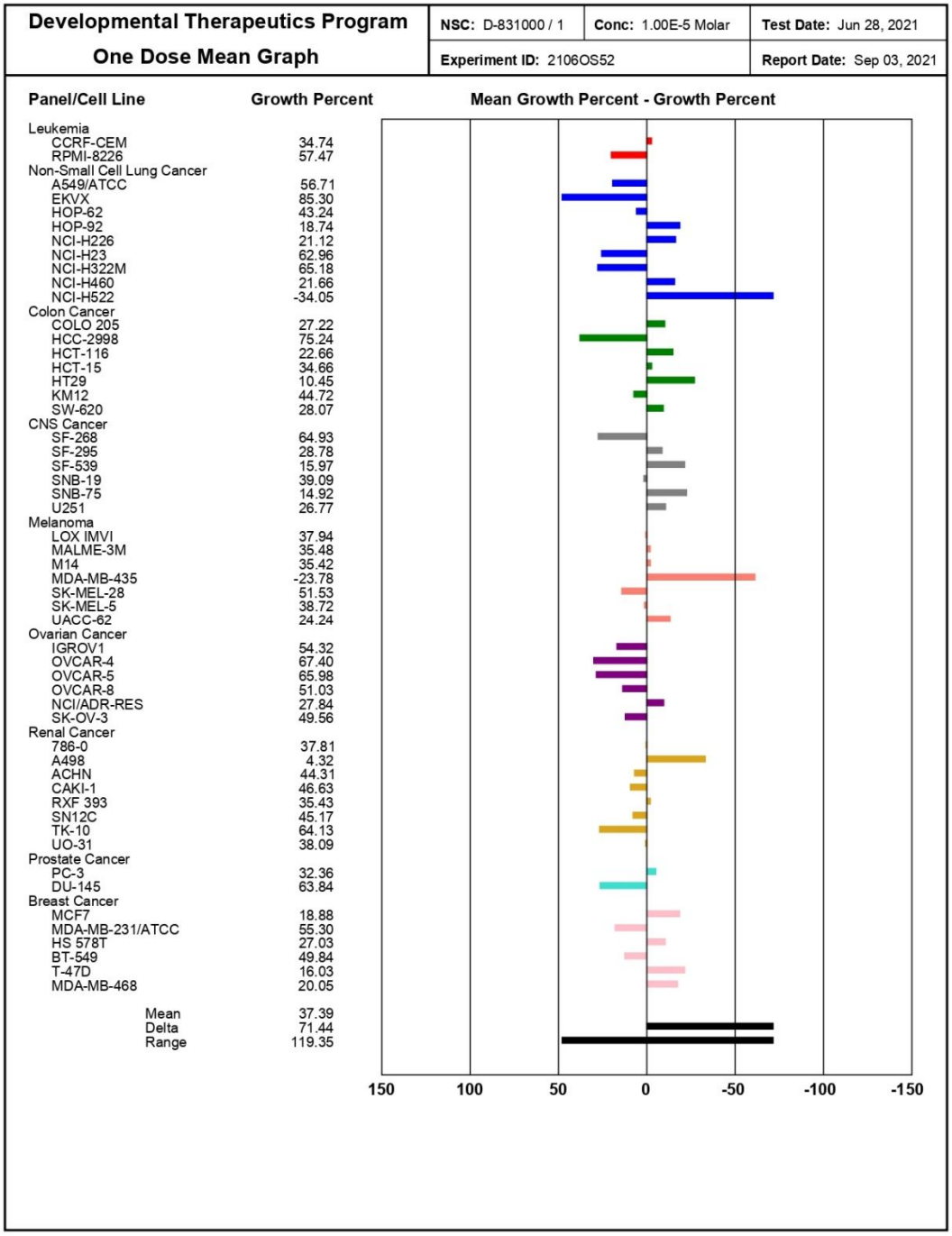

Concerning the anticancer activity of the imidazothiazoles series, compounds **24a, 24b, 24f, 24h, 24j** showed the best results. In particular, compound **24a** bearing unsubstituted indole in position C-3 and phenyl ring in C-6 showed a good anti-proliferative activity against the breast cancer cell line MDA-MB-468 cell (6.49% growth percentage), and against NSCLC cells HOP-92 (-1.71%). Compound **24h** has shown potent cytotoxicity against CNS tumour cell line SNB-75 with a mean value of growth percentage of -7.44. Among tested imidazothiadiazoles, compound **24j** was selected for further antiproliferative investigations in 5-dose assay (10^{-4}-10^{-8} M) in order to determine the IC_{50} values against the full panel of 60 tumour cell lines. As expected compound 5-methoxy-3-(6-phenyl-imidazo[2,1-*b*]thiazol-3-yl)-1*H*-indole **24j**, showed potent antiproliferative activity against the whole NCI-60 panel of tumour cell lines, exhibiting IC_{50} values in the nanomolar range . The highest potency was showed against the melanoma cell line MDA-MB-435 with a GI_{50} value of 71nM, and on Leukemia cell line SR with a GI_{50} of 83.7 nM.

Figure 28. Five doses mean graph of **24j** against NCI tumor cells: leukemia, non-small cell lung cancer cell, colon cancer cell lines, central nervous system cancer cell lines, melanoma cell lines, ovarian cancer cell lines, renal cancer cell lines, prostate cancer cell lines and breast cancer cell lines.

National Cancer Institute Developmental Therapeutics Program
In-Vitro Testing Results

NSC : D - 830957 / 1	Experiment ID : 2108NS67	Test Type : 08	Units : Molar
Report Date : October 25, 2021	Test Date : August 02, 2021	QNS :	MC :
COMI : FS46	Stain Reagent : SRB Dual-Pass Related	SSPL : 0GOB	

Log10 Concentration

Panel/Cell Line	Time Zero	Mean Optical Densities Ctrl	-8.0	-7.0	-6.0	-5.0	-4.0	Percent Growth -8.0	-7.0	-6.0	-5.0	-4.0	GI50	TGI	LC50
Leukemia															
CCRF-CEM	0.458	2.348	2.325	1.647	0.789	0.650	0.612	99	63	18	10	8	1.92E-7	> 1.00E-4	> 1.00E-4
HL-60(TB)	0.409	2.140	1.997	1.977	0.441	0.409	0.426	92	91	2	.	1	2.87E-7	> 1.00E-4	> 1.00E-4
K-562	0.197	2.007	1.983	1.283	0.416	0.318	0.284	99	60	12	7	5	1.62E-7	> 1.00E-4	> 1.00E-4
MOLT-4	0.595	2.870	2.869	2.851	1.166	0.808	0.745	100	99	25	9	7	4.61E-7	> 1.00E-4	> 1.00E-4
RPMI-8226	0.925	2.664	2.637	2.643	1.337	0.770	0.798	98	99	24	-17	-14	4.46E-7	3.85E-6	> 1.00E-4
SR	0.250	1.207	1.124	0.695	0.378	0.322	0.413	91	47	13	7	17	8.37E-8	> 1.00E-4	> 1.00E-4
Non-Small Cell Lung Cancer															
A549/ATCC	0.331	2.086	1.969	1.984	0.987	0.442	0.329	93	94	37	6	.	6.00E-7	7.81E-5	> 1.00E-4
EKVX	0.798	1.806	1.768	1.684	1.242	0.990	0.945	96	88	44	19	15	7.31E-7	> 1.00E-4	> 1.00E-4
HOP-62	0.823	2.025	1.941	1.935	1.265	0.943	0.613	93	92	37	10	-26	5.79E-7	1.91E-5	> 1.00E-4
HOP-92	1.318	1.861	1.741	1.750	1.494	1.156	0.968	78	80	32	-12	-27	4.24E-7	5.30E-6	> 1.00E-4
NCI-H226	0.798	1.706	1.655	1.661	1.252	0.752	0.771	94	95	50	-6	-3	1.00E-6	7.86E-6	> 1.00E-4
NCI-H23	0.575	1.770	1.762	1.680	1.000	0.521	0.629	99	92	36	-9	4	5.57E-7	.	> 1.00E-4
NCI-H322M	0.765	1.930	2.003	1.878	1.217	1.088	0.902	106	95	39	28	12	6.33E-7	> 1.00E-4	> 1.00E-4
NCI-H460	0.247	2.327	2.302	2.319	0.433	0.187	0.175	99	100	9	-24	-29	3.53E-7	1.86E-6	> 1.00E-4
NCI-H522	1.434	3.098	2.946	2.979	1.071	0.629	1.169	91	93	-25	-56	-18	2.30E-7	6.11E-7	.
Colon Cancer															
COLO 205	0.431	1.524	1.567	1.529	0.513	0.217	0.340	104	100	8	-50	-21	3.49E-7	1.35E-6	> 1.00E-4
HCC-2998	0.457	1.542	1.443	1.315	0.892	0.315	0.319	91	79	40	-31	-30	5.55E-7	3.66E-6	> 1.00E-4
HCT-116	0.412	2.912	2.870	2.755	0.987	0.197	0.322	98	94	23	-52	-22	4.15E-7	2.02E-6	.
HCT-15	0.295	1.918	1.832	1.419	0.686	0.319	0.408	95	69	24	1	7	2.66E-7	> 1.00E-4	> 1.00E-4
HT29	0.445	2.637	2.653	2.704	0.501	0.243	0.278	101	103	3	-46	-38	3.37E-7	1.13E-6	> 1.00E-4
KM12	1.700	3.455	3.452	3.436	2.697	1.108	1.860	100	99	57	-35	9	1.19E-6	.	> 1.00E-4
SW-620	0.255	1.691	1.692	1.445	0.512	0.491	0.386	100	83	18	16	9	3.20E-7	> 1.00E-4	> 1.00E-4
CNS Cancer															
SF-268	0.959	2.693	2.529	2.546	1.783	1.103	0.941	91	92	47	8	-2	8.77E-7	6.53E-5	> 1.00E-4
SF-295	0.504	1.959	1.723	1.771	0.791	0.413	0.437	84	87	20	-18	-13	3.55E-7	3.31E-6	> 1.00E-4
SF-539	0.775	2.352	2.277	2.228	0.997	0.348	0.318	95	92	14	-55	-59	3.46E-7	1.60E-6	8.44E-6
SNB-19	0.851	2.377	2.260	2.283	1.507	1.377	0.869	92	94	43	34	1	7.28E-7	> 1.00E-4	> 1.00E-4
SNB-75	1.342	2.413	2.406	2.276	1.200	1.290	0.729	99	87	-11	-4	-46	2.40E-7	7.79E-7	> 1.00E-4
U251	0.303	1.543	1.499	1.474	0.477	0.237	0.264	96	94	14	-22	-13	3.57E-7	2.46E-6	> 1.00E-4
Melanoma															
LOX IMVI	0.258	1.752	1.650	1.616	0.676	0.068	0.223	93	91	28	-74	-14	4.46E-7	1.88E-6	.
MALME-3M	0.774	1.746	1.681	1.680	1.068	1.078	0.542	93	93	30	31	-30	4.85E-7	3.24E-5	> 1.00E-4
M14	0.582	2.049	2.075	1.908	0.510	0.499	0.697	102	90	-12	-14	8	2.47E-7	.	> 1.00E-4
MDA-MB-435	0.553	2.333	2.223	1.307	0.204	0.246	0.324	94	42	-63	-56	-41	7.10E-8	2.52E-7	.
SK-MEL-2	0.908	1.536	1.548	1.535	0.840	0.849	0.678	102	100	-8	-6	-25	2.91E-7	8.51E-7	> 1.00E-4
SK-MEL-28	0.748	2.266	2.356	2.333	1.397	1.358	0.801	106	104	43	40	3	7.63E-7	> 1.00E-4	> 1.00E-4
SK-MEL-5	0.870	3.261	3.123	3.139	1.181	0.740	0.505	94	95	13	-15	-42	3.53E-7	2.91E-6	> 1.00E-4
UACC-257	0.833	2.115	1.997	1.958	1.287	1.352	0.932	91	88	35	40	8	5.25E-7	> 1.00E-4	> 1.00E-4
UACC-62	0.884	3.088	3.087	2.992	1.197	1.105	0.738	100	96	14	10	-17	3.64E-7	2.38E-5	> 1.00E-4
Ovarian Cancer															
IGROV1	0.482	2.103	2.033	1.990	0.956	0.637	0.485	96	93	29	10	.	4.72E-7	> 1.00E-4	> 1.00E-4
OVCAR-4	0.760	1.935	1.864	1.919	1.431	1.024	0.888	94	99	57	22	11	1.60E-6	> 1.00E-4	> 1.00E-4
OVCAR-5	0.573	1.748	1.698	1.737	1.035	0.726	0.580	96	99	39	13	1	6.61E-7	> 1.00E-4	> 1.00E-4
OVCAR-8	0.446	2.086	2.057	2.088	0.898	0.180	0.498	98	100	28	-60	3	4.90E-7	.	.
NCI/ADR-RES	0.684	2.249	2.165	2.040	0.518	0.463	0.628	95	87	-24	-32	-8	2.14E-7	6.04E-7	> 1.00E-4
SK-OV-3	0.930	1.863	1.805	1.838	1.165	1.021	0.705	94	97	25	10	-24	4.52E-7	1.93E-5	> 1.00E-4
Renal Cancer															
786-0	0.820	2.504	2.399	2.498	1.494	0.601	0.380	94	100	40	-27	-54	6.80E-7	3.97E-6	7.28E-5
A498	1.237	1.855	1.775	1.764	1.240	0.791	0.889	87	85	.	-36	-28	2.60E-7	1.03E-6	> 1.00E-4
ACHN	0.369	1.574	1.561	1.585	0.753	0.472	0.238	99	101	32	9	-36	5.46E-7	1.56E-5	> 1.00E-4
CAKI-1	0.686	2.306	2.198	2.101	1.193	0.790	0.443	93	87	31	6	-35	4.64E-7	1.42E-5	> 1.00E-4
RXF 393	0.804	1.667	1.625	1.584	1.115	0.667	0.575	95	90	36	-17	-29	5.53E-7	4.77E-6	> 1.00E-4
SN12C	0.622	2.472	2.361	2.334	1.163	0.631	0.724	94	93	29	.	5	4.70E-7	> 1.00E-4	> 1.00E-4
TK-10	1.229	1.957	1.921	2.244	1.845	1.443	0.889	95	139	85	29	-28	4.24E-6	3.27E-5	> 1.00E-4
UO-31	0.736	2.420	2.286	2.220	1.303	0.961	0.583	92	88	34	13	-21	5.01E-7	2.46E-5	> 1.00E-4
Prostate Cancer															
PC-3	0.535	2.527	2.466	2.092	0.856	0.492	0.583	97	78	16	-8	2	2.84E-7	.	> 1.00E-4
DU-145	0.700	2.678	2.631	2.671	1.344	0.708	0.714	98	100	33	.	1	5.49E-7	> 1.00E-4	> 1.00E-4
Breast Cancer															
MCF7	0.211	1.491	1.379	1.299	0.337	0.280	0.306	91	85	10	5	7	2.92E-7	> 1.00E-4	> 1.00E-4
MDA-MB-231/ATCC	0.488	1.873	1.893	1.552	0.903	0.689	0.553	101	77	30	14	5	3.73E-7	> 1.00E-4	> 1.00E-4
HS 578T	1.419	2.312	2.172	2.164	1.524	1.190	1.084	84	83	12	-16	-24	2.92E-7	2.63E-6	> 1.00E-4
BT-549	1.064	1.739	1.598	1.859	1.023	0.795	0.515	79	118	-4	-25	-52	3.61E-7	9.30E-7	8.70E-5
T-47D	0.747	1.728	1.601	1.636	0.997	0.772	0.777	87	91	25	2	3	4.20E-7	> 1.00E-4	> 1.00E-4
MDA-MB-468	0.822	1.628	1.539	1.569	0.757	0.587	0.696	89	93	-8	-29	-15	2.66E-7	8.33E-7	> 1.00E-4

Furthermore, two other imidazothiazoles **24b** and **24f**, complying with NCI requests, have been selected for five doses assays. Both compounds showed GI%

lower than 50% against all the cell line of the nine tumors subpanel, unfortunately five doses are still in evaluation stage. Therefore, compound **24b** showed wide cytotoxicity activity against wide range of human tumor cell lines, such as NCI-H522 (-42.37%), COLO-205 (-27.03%), HT29 (-17.42%), SK-539 (-29.87%), MDA-MB-435 (-62.39%), NCI/ADR-RES (27.5%) MDA-MB-468 (-38.84%), RXF-393 (-32%).

Figure 29 One dose mean graph of **24b** against NCI tumor cells: leukemia (red), non-small cell lung cancer cell (blue), colon cancer cell lines (green), central nervous system cancer cell lines (grey), melanoma cell lines (orange), ovarian cancer cell lines (purple), renal cancer cell lines (yellow), prostate cancer cell lines (light blue) and breast cancer cell lines (pink).

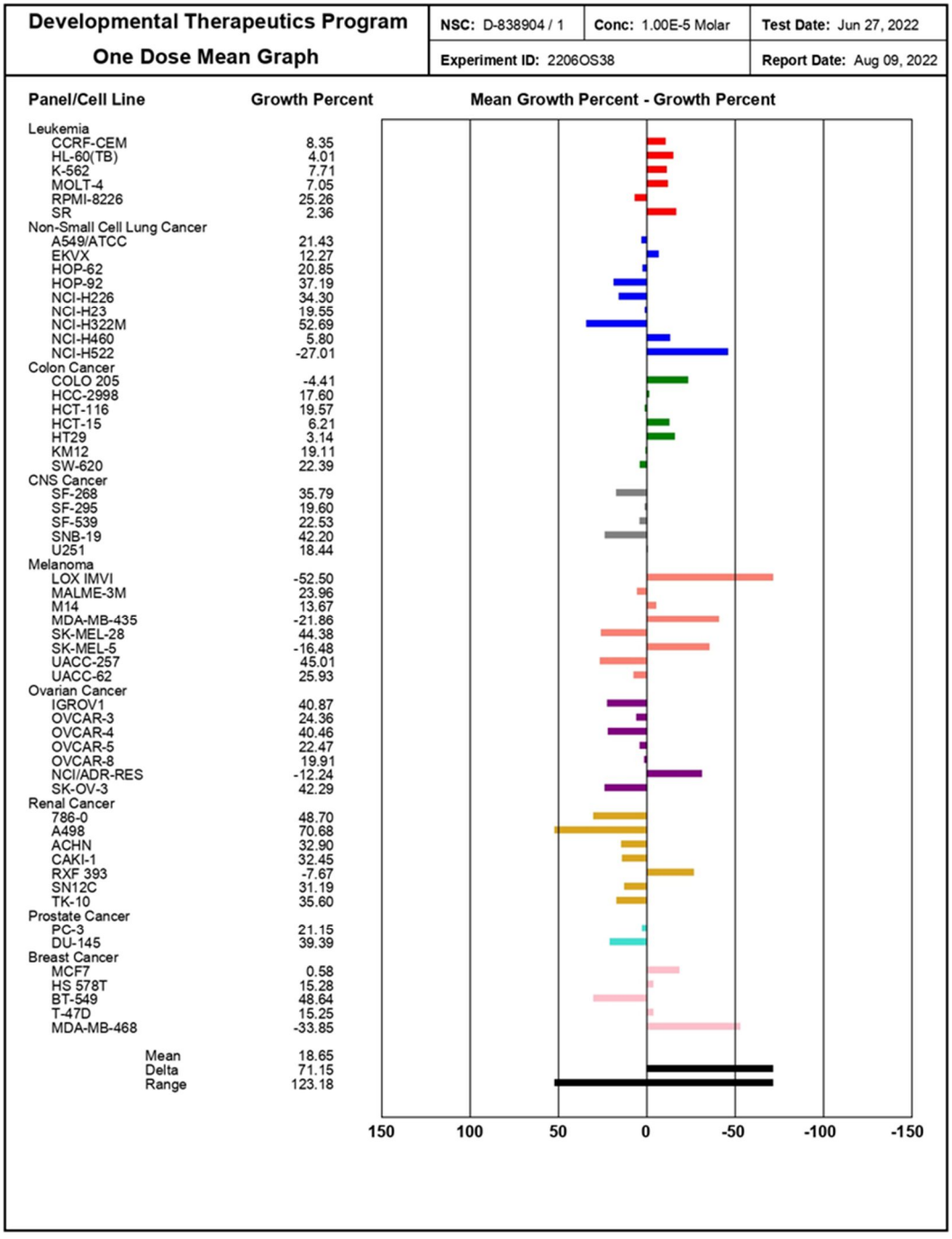

Figure 30. One dose mean graph of **24f** against NCI tumor cells: leukemia (red), non-small cell lung cancer cell (blue), colon cancer cell lines (green), central nervous system cancer cell lines (grey), melanoma cell lines (orange), ovarian cancer cell lines (purple), renal cancer cell lines (yellow), prostate cancer cell lines (light blue) and breast cancer cell lines (pink).

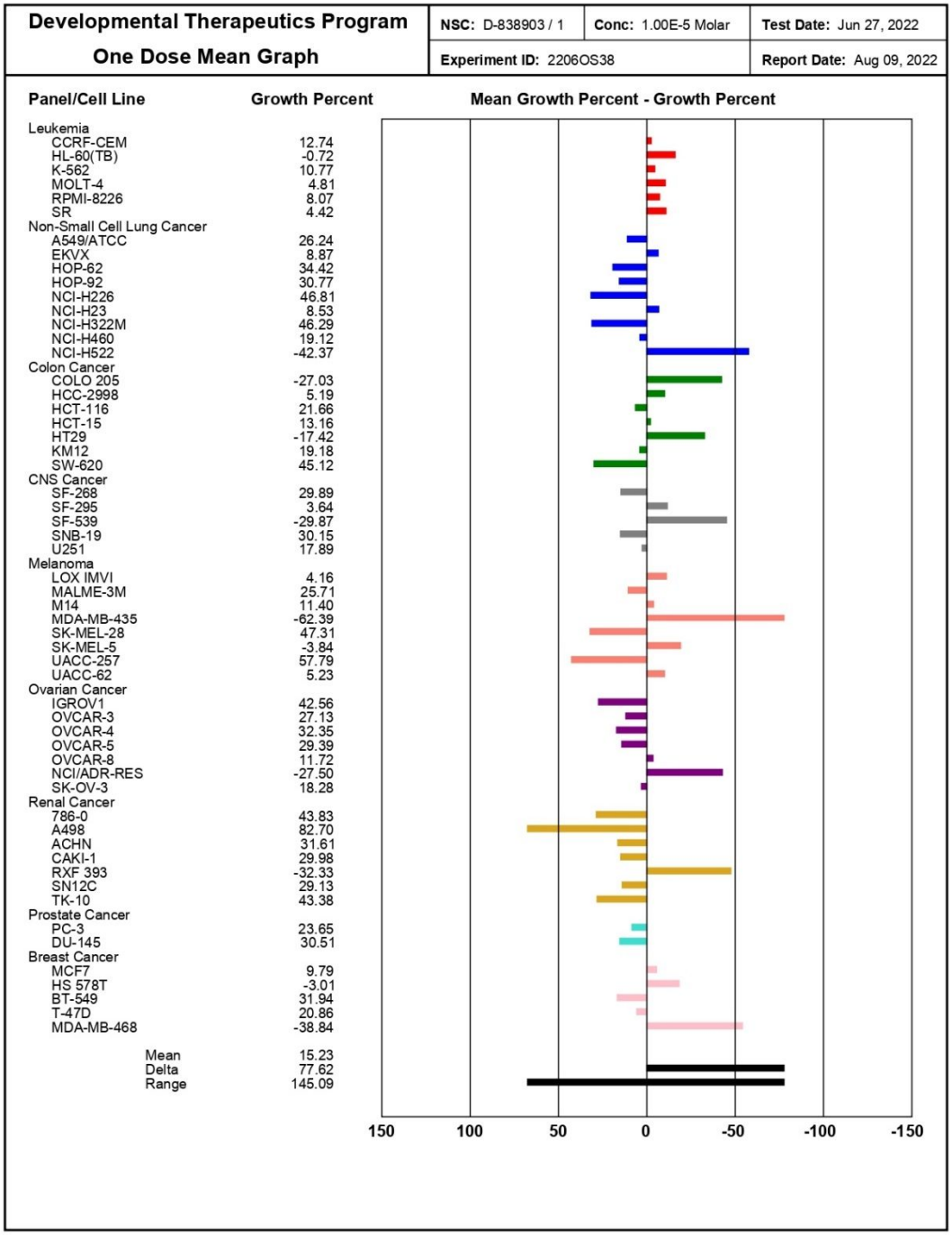

Also compound **24f** showed remarkable antiproliferative activity against the whole panel in particular, against COLO-205 (-4%), NCI-ADR/RES (-12.24%), RFX-393 (-7.07%); NCI-H522 (-27.01), and 3 different cell lines of melanoma, LOX-MVI -52.5, MDB-MA-435 -21.86, SK-MEL-26 -16.48.

Unfortunately, some of imidazo[2,1-*b*]thiazoles and all imidazo[2,1-*b*][1,3,4]thiadiazole derivatives such as **25, 26, 27** synthetized during the last months and sent to NCI are still under evaluation.

Biological assays on Pancreatic Ductal Adenocarcinoma cells

Cells viability assays

The last period of my PhD course was spent at the Cancer Center Amsterdam under the supervision of Prof. Elisa Giovannetti, the novel synthetized compounds **27a-t** were *in vitro* tested in order to evaluate their cytotoxicity against Pancreatic ductal adenocarcinoma cell lines, not included in the NCI panel. The PDAC cell lines used for the assays, including 5 immortalized (BxPC-3, Capan-1, PANC-1, Patu-T, SUIT-2), a Gemcitabine-resistant clone (PANC-1- GR) and a primary culture (PDAC-3). The anti-proliferative activity was evaluated by the Sulforhodamine-B (SRB) assay at 3 different concentration 0.1, 1, 10μM.

Among the PDAC cell lines employed, BxPC-3 (Biopsy xenograft of Pancreatic Carcinoma line-3) does not express KRAS oncogene mutation. KRAS is over expressed in 90-92% of PDAC patients, whereas a small amount of PDAC population 8-10% show other molecular alterations.[242] In the last years KRAS-wild type PDAC may represent a distinct molecular subtype of pancreatic cancer. The genetic hallmarks in this category are different from conventional PDAC, if appropriately selected based on their individual genomic and molecular features, these special PDAC subtypes can be treated with specific therapeutic strategies[243].

Capan-1 are adherent epithelial cell line derived from metastatic PDAC cells from liver.

PANC-1 are human pancreatic epithelioid carcinoma cell line currently used as an *in vitro* model to study pancreatic ductal adenocarcinoma carcinogenesis and

tumour therapies. Specifically, the presence of the SSTR2 receptors and the occurrence of neuroendocrine differentiation make this cell line suitable for pancreatic cancer neuroendocrine chemotherapy and peptide receptor radionuclide therapy evaluation[244]

Panc-1GR cells, a gemcitabine-resistant sub-clone obtained by continuous incubation of Panc-1 with 1 µM of this drug, were achieved as described previously.[245]

Patu-T derive from metastatic site Liver, these cells grew as tumors with a similar morphology and differentiation (grade II) to the primary tumor. [246]

Suit-2 cell line, as Capan-1, are metastatic PDAC cells from liver, this cell line produces and releases at least two tumor markers, carcinoembryonic antigen and carbohydrate antigen 19-9.

PDAC-3 is primary pancreatic ductal adenocarcinoma culture isolated from a patient at Pisa Hospital as described previously.[247]

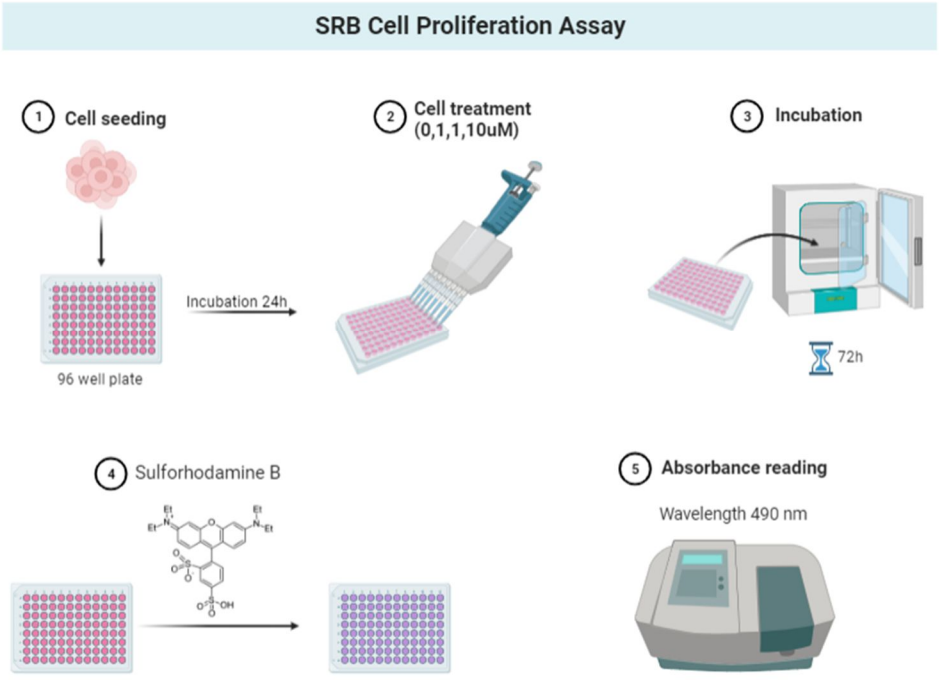

Figure 31. Schematic representation of SRB assay procedure.

All imidazothiadiazoles were initially screened at three different concentration (0.1,1,10μM) on the 5 immortalized cell lines (BxPC-3, Capan-1, PANC-1, Patu-T, Suit-2) in order to detect compounds with most interesting growth inhibition percentage values. Compounds **27a, 27e, 27f, 27s** showed interesting activity between 1μM and 10μM against all tested PDAC cells. Results are reported in the bar charts below as mean growth percent value compared to the untreated control in figure 32.

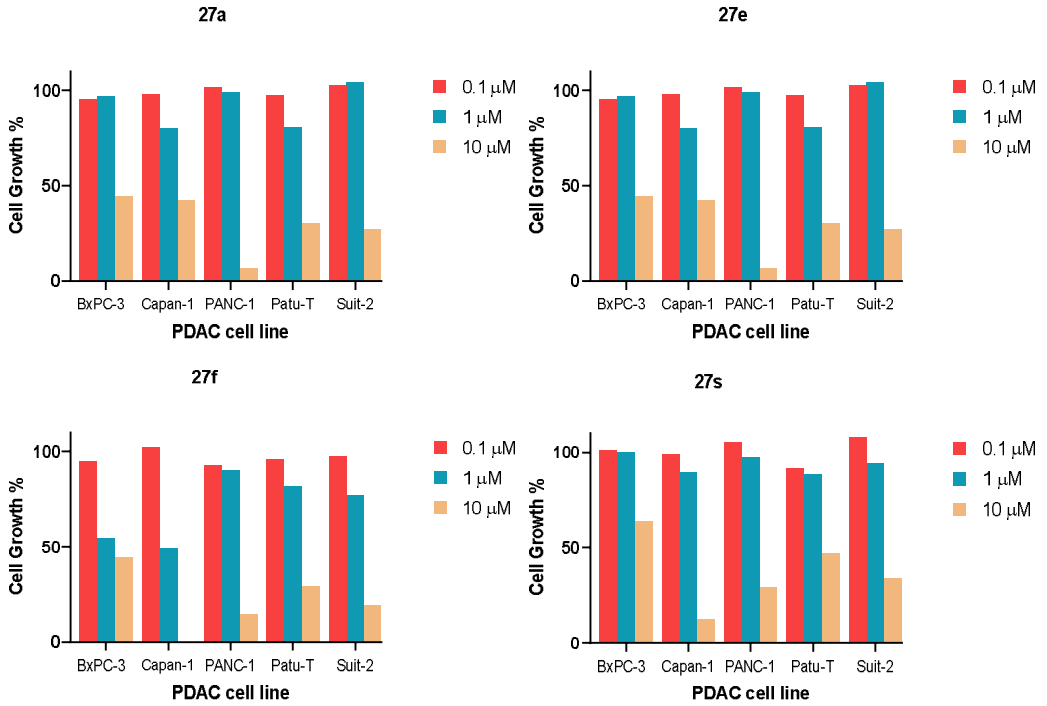

Figure 32. Cell growth data against panel of pancreatic cancer cell lines, measured by the SRB Assay for 72 h exposure and expressed as percentage of cell growth.

Table 9. Antiproliferative activity of compounds **27a, 27e, 27f, 27s** on Pancreatic ductal adenocarcinoma cells.

	IC_{50}[a] (µM)±SEM[b]						
Compound	**Capan-1**	**PANC-1**	**Patu-T**	**SUIT-2**	**BxPC-3**	**PDAC-3**	**PANC-1GR**
27a	2.64±0.06	3.16±0.007	3.73±0.12	2.19±0.17	2.67±0.15	5.54±0.33	6.9±0.05
27e	6.38±0.1	8.65±0.03	12.68±0.7	6.6±0.1	8.83±0.64	12.94±2.7	15.92±2.6
27f	1.54±0.04	1.57±0.08	1.56±0.007	1.7±0.14	1.04±0.08	2.98±0.4	3.44±0.26
27s	4.78±0.01	7.4±0.13	8.43±0.08	10.8±0.12	16.62±0.26	>40	15.49±2.9

[a]Values are means ± SEM of three separate experiments [b] SEM: Standard Error of the Mean

The IC_{50} values were evaluated for all four selected compounds **27a, 27e, 27f, 27s.** The 8 doses assay of compounds on PDAC cell showed the IC_{50} on each cell line tested. Compound **27a** showed good antiproliferative activity, eliciting IC_{50}values ranging from 2.1 to 6.9 µM Compound **27f** showed the highest potency on the PDAC cell lines assayed, exhibiting IC_{50} values in the range 1.04 - 3.4 µM.

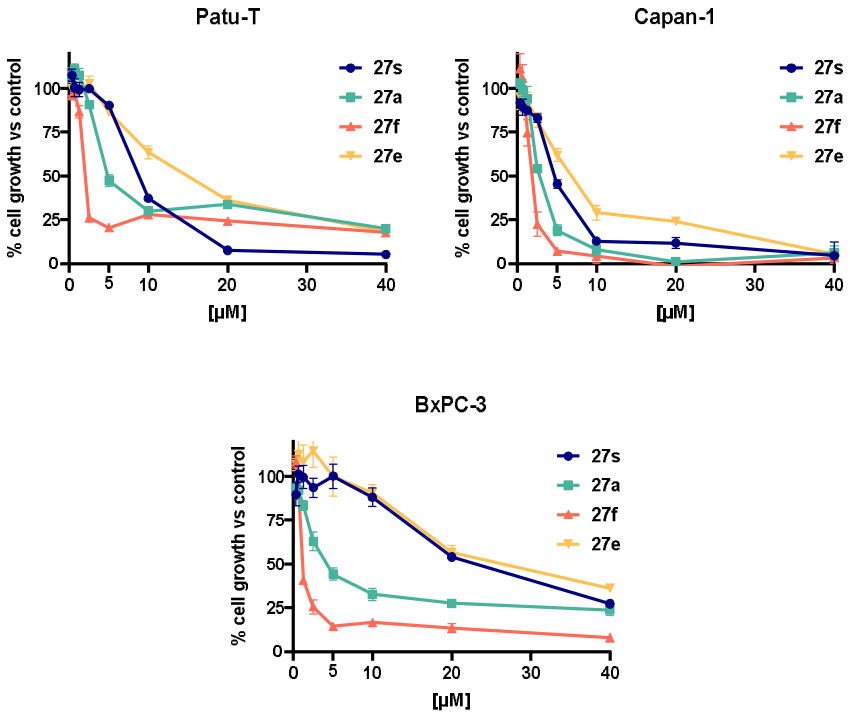

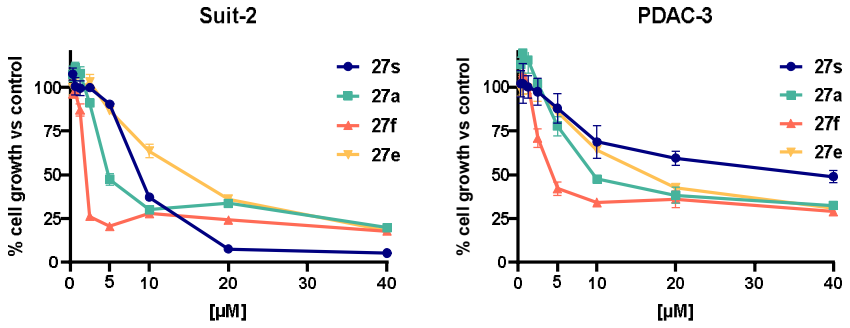

Figure 33. IC_{50} curves of compounds **27a, 27e, 27f, 27s** against four PDAC immortalized cells and a primary cell line (PDAC-3). Error bars report the Standard error of the mean.

Furthermore, in order to expand our study, the selected compounds were tested also against the Gemcitabine resistant (GR) cell line clone PANC-1GR and primary cell line PDAC-3. Noteworthy, analogues **27a-f** elicited interesting antiproliferative activity also against primary PDAC3 with comparable IC_{50} values against the resistant subclone of PANC-1. Compound **27a** showed good anti-proliferative values against resistant cell line PANC-1GR (IC_{50} 6.9 μM) and PDAC-3 (IC_{50} 5.54 μM). Compound **27f** proved to be the most potent derivative also against the resistant tumor cells.

Interestingly, compounds **27a-27f**, as most potent compounds, showed chemical similarity, sharing the unsubstituted NH and N methylated indoles in position C-2 of imidazo[2.1-*b*][1,3,4]thiadiazole nucleus.

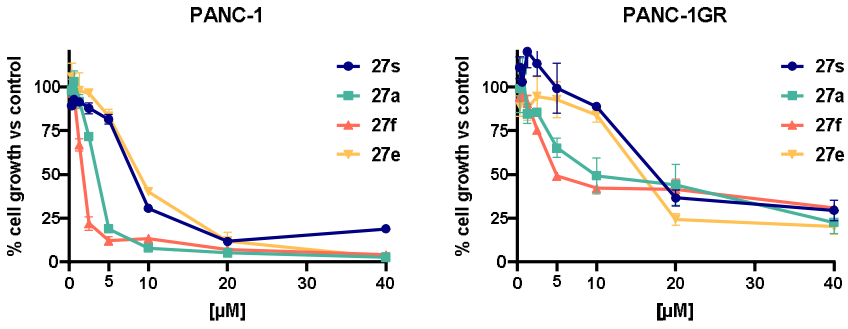

Figure 34. IC_{50} curves of compounds **27a, 27e, 27f, 27s** against cell line (PANC-1) and Epithelial resistant cell clone (PANC-1GR).

Effect on cell cycle

In order to investigate the mechanism of action of these compounds, their effect on the cell cycle was evaluated in pancreatic ductal adenocarcinoma cells (SUIT-2 and PDAC-3) at concentration 4xIC_{50}

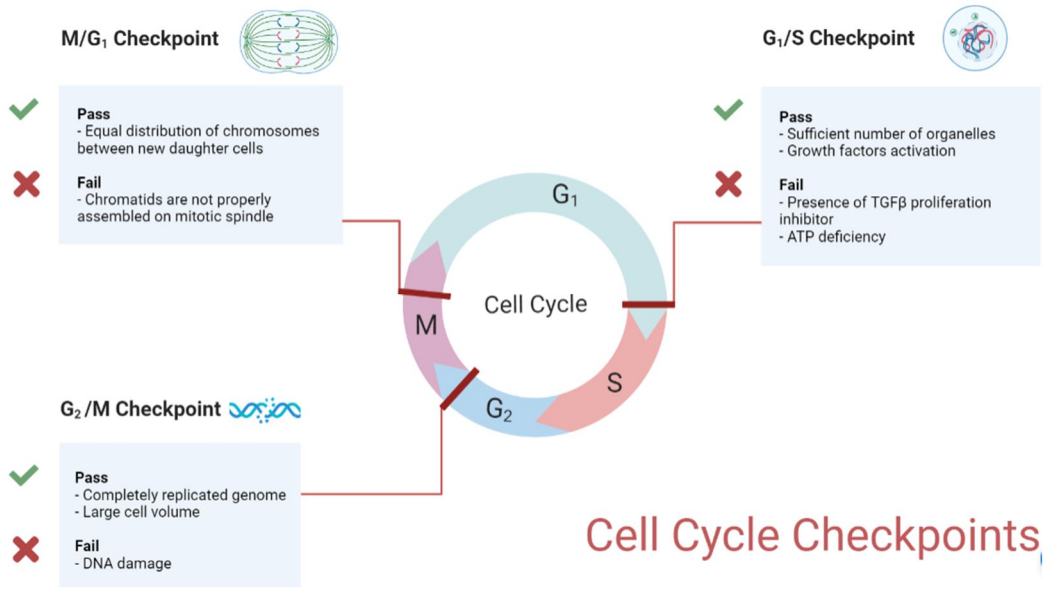

Figure 34. Illustrative effects of targeting cell cycle phase checkpoints

Cell cycle progression was analysed by flow cytofluorimetry, using propidium iodide (3,8-diamino-5-[3-(diethylmethylammonio)propyl]-6phenyl- diiodide, PI) staining solution. PI is an intercalanter that selectively binds nucleic acids. It also acts as a synthetic dye characterized by a low fluorescence (red-orange). The PI is in fact able to establish a stable bond with the DNA, intercalating between two pairs of adjacent bases, with a stoichiometry of one dye per 4–5 base pairs of DNA. Once the dye is bound to nucleic acids, it increases twenty-thirty times, compared to the free dye, its quantum fluorescence efficiency. The PI is therefore an excellent fluorescent "marker" of the double helix nucleic acids, thus providing information on the amount of DNA content in the cells, in relation to the emitted fluorescence intensity. It is known that the DNA content varies according to the phase of the cycle in which a cell is located. In particular, the G2 phase and mitosis (M) have double amount of DNA compared to the G1 phase, while during the DNA synthesis phase (S phase), the cell has a quantity of DNA intermediate

between the content in G1 and G2. This technique allows to analyse the percentage of cells in the various phases of the cell cycle (G0/G1, S and G2/M), as well as to evaluate possible blocks, and to detect the occurrence of apoptotic episodes. Compound **27f** was tested against Suit-2 and PDAC-3 cells at concentration 4xIC_{50}, 6.7µM and 12 µM respectively. On Suit-2 the compound demonstrated potent activity in arresting cell cycle in phase G2/M. (Fig.35)

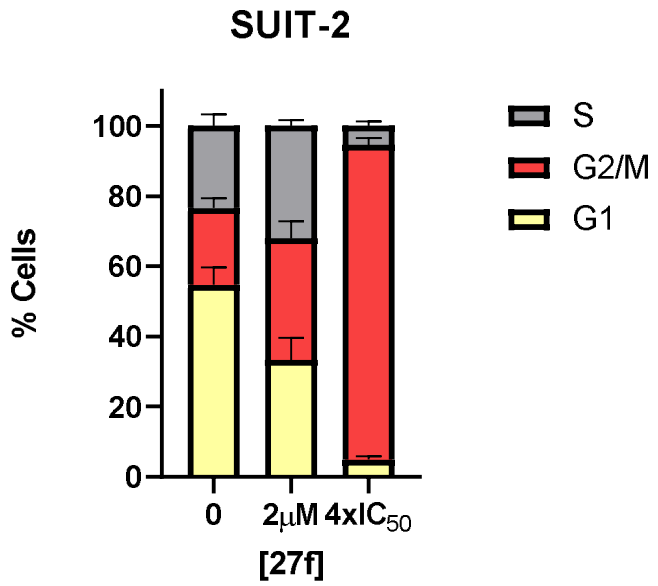

Figure 35. Effect of imidazothiadiazole compound **27f** on cell cycle distribution. SUIT-2 cells were treated with derivative **27f** for 24 hours. Stacked bar graphs showing the percentage of cells at various stages of cell cycle, G1 (pale yellow), S (grey), and G2/M (red) phase, vs untreated control and after treatment with the compounds. Standard deviations are showed. Error bars report standard deviations of three separate experiments.

Compound **27f** tested on PDAC-3 followed a similar trend showing any effect at 2µM compared to the untreated cells; therefore, our derivative showed again potent activity when tested at 4xIC_{50} concentration. Cells incubated for 24h with at 4xIC_{50} showed 70.2% of total cells blocked in phase G2/M.

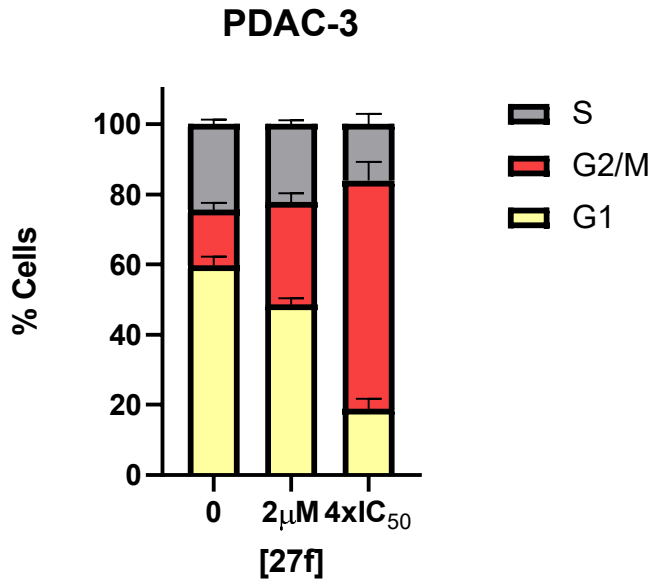

Figure 36. Effect of imidazothiadiazole compound **27f** on cell cycle distribution. PDAC-3 cells were treated with derivative **27f** for 24 hours. Stacked bar graphs showing the percentage of cells at various stages of cell cycle, G1 (pale yellow), S (grey), and G2/M (red) phase, vs untreated control and after treatment with the compounds. Error bars report standard deviations of three separate experiments.

Antimigratory activity

Since early metastasis is a PDAC hallmark, which is responsible of the poor therapeutic response and outcome, it was a priority for our study to investigate antimigratory activity of the new series of imidazothiadiazoles. For this purpose, compounds **27a-27f,** which showed the most potent antiproliferative activity against PDAC cells, were selected in order to investigate their anti-migratory behaviour by scratch wound-healing assays on BxPC-3, Patu-T, SUIT-2, Capan-1, Panc-1, Panc-1GR and PDAC-3 cell lines. Briefly, 5 x 10^4 cells/well were seeded into 96-well flat-bottom plates in a volume of 100 mL and incubated for 24 h to create a monolayer. The scratches in the middle of the wells created a gap, or "wound", between cells by scraping with a specific tool with needles. The cells were then treated with the compounds using 4x IC_{50} concentrations. The wound closure was monitored by phase-contrast microscopy and the pictures were

captured immediately after scratch (T=0), and at 4, 8, 20 and 24 h from the treatment.

As shown in Figure 37, the compounds **27a-27f** induced significant decrease of cell migration percentage compared to the untreated cell. The compounds showed similar antimigratory activity against all cell lines. Imidazothiadiazole analogues **27a** and **27f** showed a distinct reduction of cell migration from 8h were the scratch area (mm^2) was already wider in the treated cells compared to the untreated cells. After 24h, cells treated with compound **27f** had a migration reduction of 2-fold at least against each cell line of our PDAC panel. Statistical analyses revealed that these differences were significant, compared to the respective controls (i.e., untreated cells) in all cell lines.

Compounds **27a-27f** showed potent antimigratory activity in SUIT-2 cells, causing a reduction in cell migration of 31% and 19% respectively; therefore, resistant clone Panc-1GR cells treated with **27a-27f** showed relevant reduction of cells motility, respectively 34% and 26,7% compared to the untreated control. Interestingly compounds inhibited cell motility by 3-folds also in PADC-3 cell lines with percentage of inhibition of 39% for **27a** and 27% for **27f.**

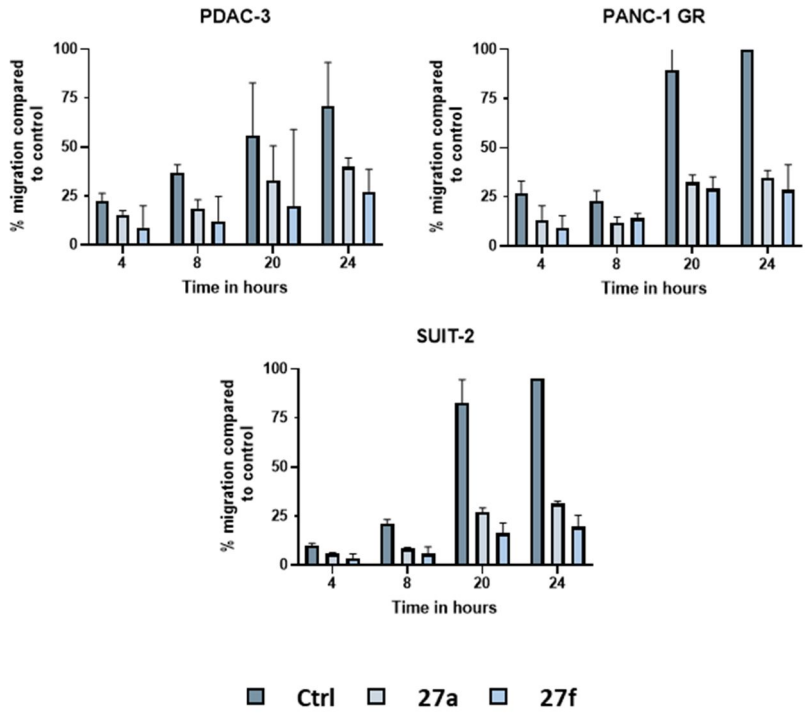

Figure 37. Modulation of the migration rate in PDAC cells. Charts express percentages of migration monitored over time (0, 4, 8, 20 and 24 h) of SUIT-2, PDAC-3, PANC-1GR cells treated with compound **27a-27f** concentration 4x IC_{50}. Points, mean values obtained from the means of at least three different scratch areas. Error bars report Standard deviation values.

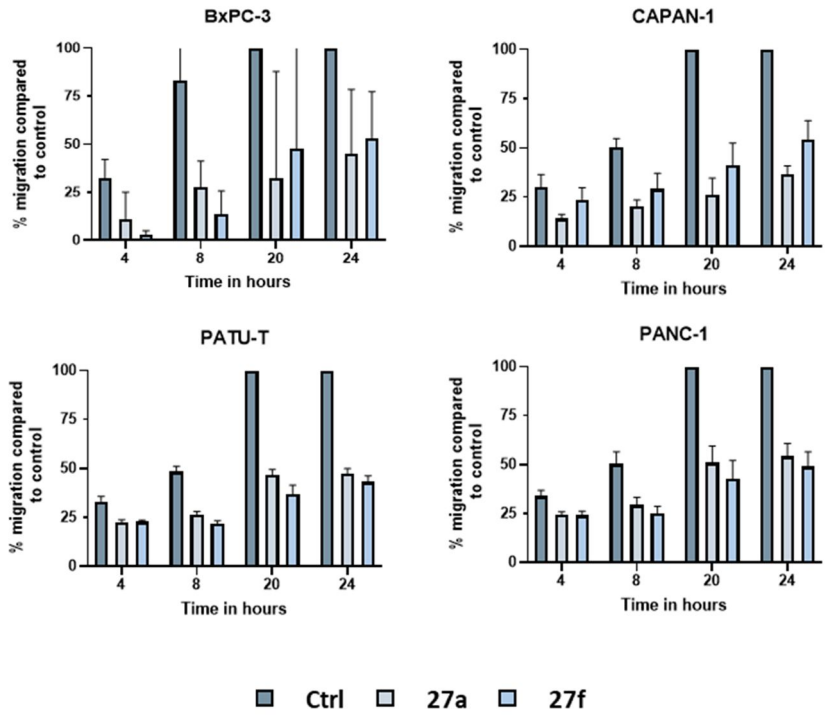

Figure 38. Modulation of the migration rate in PDAC cells. Charts express percentages of migration monitored over time (0, 4, 8, 20 and 24 h) of Panc-1GR (C) PATU-T (D), BxPC-3 and CAPAN-1 cells treated with compound **27a** and **27f** at concentration 4x IC_{50}. Points, mean values obtained from the means of at least three different scratch areas. Error bars report Standard deviation values.

In summary, collected experimental data from the scratch wound-healing assays confirmed the importance of five-membered heterocycle in position C-2 of imidazothiadiazole to hinder the motility in PDAC cell line model.

PamGene Kinases array

Considering the encouraging antiproliferative and antimigratory activities observed against PDAC cell lines assays, a high-throughput analysis with the Pamgene tyrosine kinase peptide substrate array (PamChip) was performed in order to investigate the potential mechanism of action of our compound **27f**. Usually, techniques such as In-gel kinase assays or Western blot-based gel shift, are used to study kinases *in vitro* phosphorylation of protein substrates. However,

these techniques are difficult to standardize for high-throughput applications and do not allow easy identification of upstream kinases. In contrast, real-time measurement of cellular kinase activities via peptide-based array technology, through “on chip” pharmacology, provides many advantages for high-throughput applications to study signal transduction. Furthermore, this method facilitates discriminating specificity and magnitude of kinase activity changes in different experimental settings, in cell lysates of cell lines or biopsies of clinical patient samples.[248] The peptide microarray, called PamChip® array, wherein each array (PamChip®) is probed with either serine threonine kinase (STK)- specific or protein tyrosine kinase (PTK)-specific conserved peptides of phosphomotifs (13–24 amino acid length) on a porous Al_2O_2 carrier. The peptides are covalently attached to a porous matrix via a spacer. [249]

Then, Pancreatic ductal adenocarcinoma cell lines chosen SUIT-2 and PDAC-3, were incubated with **27f** ($5xIC_{50}$) for 2h and then cell lysates containing activated or inactivated kinases are pumped up and down through the porous array in the presence of ATP to facilitate the phosphorylation of peptides by the protein kinases in the lysates. The assay mixture of both STK/PTK arrays contains fluorescein isothiocyanate (FITC)-labelled antibody, which allows us to quantify the peptide phosphorylation during incubation. Real-time recording of reaction kinetics is measured by taking images (fluorescent signal intensity) via a charge-coupled device camera which captures the kinetic images for every 6 s for the entire length of program 45–90 min embedded in the PamStation® Bionavigation software).

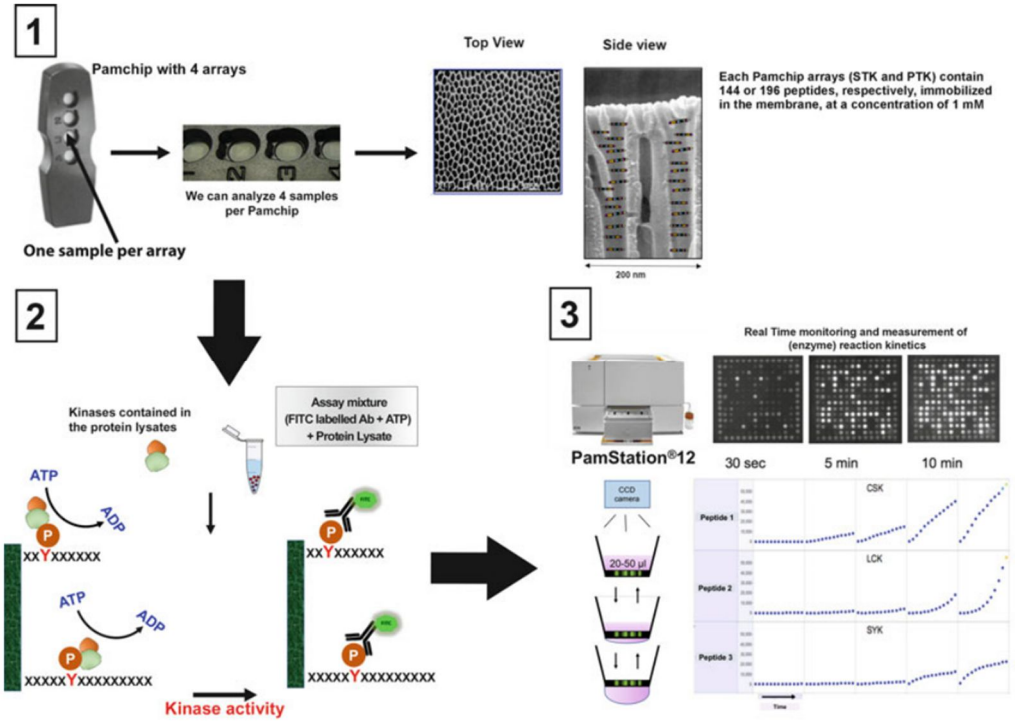

Figure 38 Principle of Pamgene Peptide array 1) Pamchip runs 4 samples at one time, targetable phosphopeptides residue of kinase are immobilized on solid support (Al_2O_3) 2) Substrate peptides are incubated with cell lysate, during the incubation reaction mix is pumped through the array 3) fluorescent imaging of each array is performed A FITC-conjugated PY20 antibody, present in the reaction mix is used to detect the phosphorylation signal by a 12-bit CCD camera in the Pamstation.

Compound **27f** showed wide inhibition, blocking the phosphorylation of 49 protein kinases peptide substrates in SUIT-2 cells with inhibition scores from 66% to 27% compared to untreated control; while in primary cells PDAC-3 compound **27f** was able to inhibit 53 different peptide substrates with inhibition % scores from 26% to 71% compared to the control cells. In figure 40 the kinases with a higher inhibition than 50% are shown. Compound **27f** showed wide inhibition activity, exhibiting a high selectivity against Focal adhesion kinase 1 and 2 (PTK2 and PTK2B) in both cell lines, with an inhibition percentage of 66% and 71%, respectively.

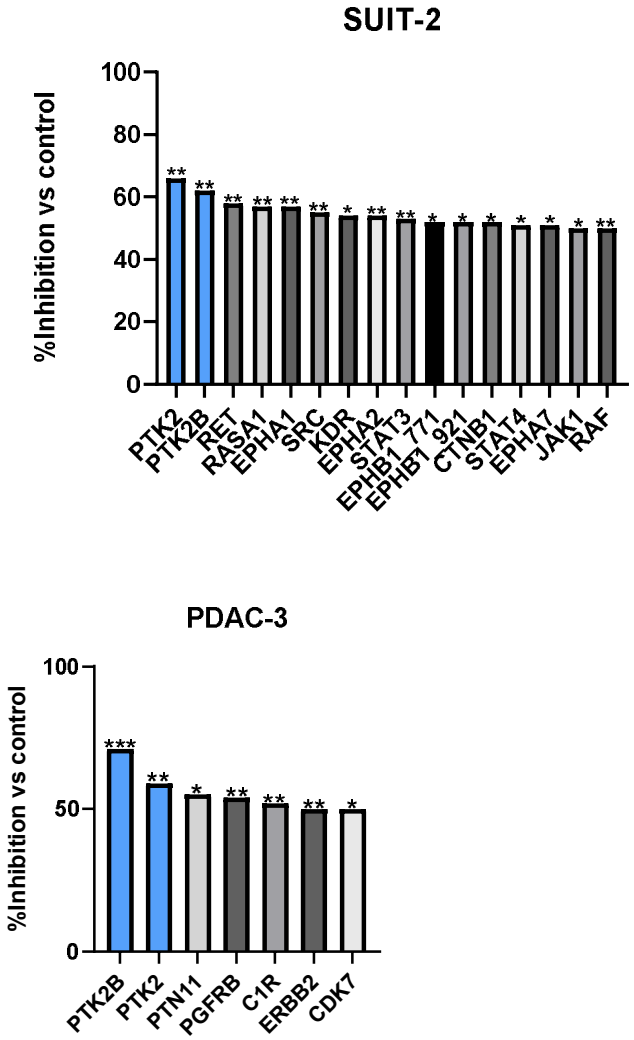

Figure 40. Protein kinases significantly inhibited in SUIT-2 and PDAC-3 by **27f**. Bar charts report protein kinase with inhibition percentage higher than 50% compared to untread cells. FAK family had highest inhibition percentage in both cell lines. P values were calculated with Student's t-test. ***p < 0.001, **p < 0.01, *p < 0.05.

Finally, additional SRB experiments were performed to evaluate the *in vitro* cytotoxicity of compound **27f** against the normal fibroblasts Hs27. The result of these experiments displayed that imidazothiadiazole **27f** have any effect on the Hs27 at the highest concentration (40μM) tested, confirming the safety of this compound on non tumour cells.

Anti-biofilm activity

Considering the interesting anti-biofilm activity described for the lead compounds, all pyrimidinone derivatives were tested in order to evaluate their antibiofilm activity against relevant Gram-positive and Gram-negative pathogens. Firstly compounds **23** were tested against the planktonic form of different bacterial strains, including the Gram-positive *S. aureus 25923, S. aureus 6538, Enterococcus faecalis* and the Gram-negative *P. aeruginosa 15442* and *E. coli 25922.*

Currently the main strategies to counteract biofilms essentially belong to two different approaches: i) the prevention of their formation by interfering with the bacterial adhesion on the host surface or ii) the dispersing of mature biofilm by interfering with the matrix components leading to the disruption of biofilm architecture.

Many targets are identified in order to develop compounds able to modulate biofilm life cycle, such as the quorum sensing (QS) system, which is the bacterial cell-to-cell signalling responsible for the coordination of many virulence factors, the nucleotide second messenger signalling systems, and Toxin-antitoxin system.[193]

Almost all the new compounds **23** showed no effect against the planktonic form of the tested strains eliciting MIC values higher than 100 µg/mL. Only derivatives **23k, 23l, 23o, 23p** and **23v** showed low antibacterial activity exhibiting MIC values ranging from 25 to 75 µg/mL.

Table 10. Antibacterial activity of compounds **23** expressed as MIC values (μg/mL) against the planktonic form of *S. aureus* and *E. faecalis*.

Compound	MIC (μg/mL)
23k	50 (S.a.)
23l	50 (S.a.),25 (E.f.)
23m	n.s.
23n	n.s.
23o	50 (E.f.)
23p	75 (S.a.)
23q	n.s.
23r	n.s.
23s	n.s.
23t	n.s.
23u	n.s.
23v	50 (S.a.)

The anti-biofilm activity of compounds **23** was also evaluated against the same strains, in terms of inhibition of biofilm formation and disruption of mature biofilm. Interestingly, this new class of compounds showed a different behaviour towards biofilm life cycle respect the series previously described. Pyrimidinone analogues, in fact, showed a marked reduction in the inhibition of biofilm formation in comparison with imidazotiadiazole analogues. Only compounds **23k, 23l, 23o, 23p** proved to be able to inhibit biofilm formation in at least one bacterial strain, showing BIC_{50} values in the range 6.1-21.1 μg/mL (Table 11)

Table 11. Inhibition of biofilm formation.

Compound	BIC_{50} (µg/mL)
23k	14.5 (P.a.)
23l	21.1 (S.a.)
23m	n.s.
23n	n.s
23o	6.3 (S.a.), 14.4 (P.a.), 6.1 (E.c.)
23p	7.6 (S.a.)
23q	n.s
23r	n.s
23s	n.s
23t	10.4 (P.a.)
23u	n.s
23v	18.2 (S.a.)

Interestingly, all the new derivatives showed dispersal activity in a dose dependent manner, eliciting at the screening concentration of 100 µg/mL a percentage of inhibition against mature biofilm ranging from 51 to 79%. In particular, **23v** showed the highest potency against the 24h preformed biofilm of all the tested strains showing IC_{50} values ranging from 17 to 27 µg/mL In order to extend the anti-biofilm evaluation against other pathogens biofilm-forming, the dispersal activity of compound **23v** was also evaluate against *M. Hominis, P.Acnes, C. Albicans* and the results are reported in the table.

Table 12. IC_{50} of Preformed bacterial biofilm (µg/mL)

Compounds	***P. Aeruginosa***	***S. Aureus***	***E. Coli***	***M. Hominis***	***P. Acnes***	***C. Albicans.***
23v	21	27	17	39	36	40

EXPERIMENTAL SECTION

Chemistry

The dry solvents used for organic synthesis (acetonitrile, dimethylformammide and diethyl ether) and the reagents were purchased from Sigma-Aldrich Co, Alfa Aesar, VWR International and Acros Organics. Other solvents were purified and dried using standard method: toluene was distilled from calcium hydride, ethanol and methanol from iodine and magnesium. All dry solvents were stored over 4 Å molecular sieves. All air- or moisture-sensitive reactions were performed using oven-dried glassware under an inert dry nitrogen atmosphere. Analytical thin layer chromatography (TLC) was performed on silica gel 60 F254 plates (0.25 mm thickness) and the developed plates were examined under ultraviolet (UV) light. All melting points were taken on a Buchi-Tottoly capillary apparatus and were uncorrected. IR spectra were determined in bromoform with a Shimadzu FT / IR 8400S spectrophotometer and peaks were reported in wavenumber (cm^{-1}). 1H and ^{13}C NMR spectra were measured at 200 and 50 MHz, respectively, on DMSO-d6 or $CDCl_3$ solution, using a Bruker Avance II series 200 MHz spectrometer. Chemical shifts were described in parts per million (δ), coupling constants (J) are expressed in Hertz (Hz), and splitting patterns were reported as singlet (s), doublet (d), triplet (t), quartet (q), multiplet (m), doublet of doublets (dd) and triplet of doublets (td). Chromatography column was performed with MERK silica gel 230-400 mesh ASTM or FLASH40i Biotage chromatography or with Buchi Sepacore chromatography module (prepacked cartridge reference).

General procedure for the synthesis of 1*H*-indole-3-carbonitriles 41a-e

A solution of the suitable indole **40a** (5.10 mmol) in anhydrous acetonitrile (4.5 mL) was treated dropwise with chlorosulfonyl isocyanate (CSI) (0.44 mL, 5.10 mmol). The reaction mixture was maintained at 0 °C under stirring for 2 h, then, anhydrous dimethylformamide (DMF) (2.8 mL, 36.39 mmol) was slowly added and the mixture was stirred at 0 °C for 1.5 h. The resulting solution was poured into crushed ice. The solid obtained was filtered and dried (yields 98-100%).

Analytical and spectroscopic data for compounds **41a-e** are in agreement with those previously reported.[209]

General procedure for the synthesis of 1-methylindole-3-carbonitrile 42a-e

To a solution of the suitable 3-cyanoindole **41a** (7.03 mmol) in anhydrous DMF (10 mL) 3.61 mmol of K_2CO_3 and dimethyl carbonate (1.8 mL, 21.4 mmol) were added and the mixture was heated at 130 C for 3.5 h. After cooling (0-5 °C), water and ice (25 mL) was slowly added under stirring. The oily suspension obtained was extracted with diethyl ether (3x 10 mL), the organic phase was washed with water and brine, dried over Na2SO4 and the solvent evaporated at reduced pressure to obtain the 3-cyano-1- methylindoles **42a** in excellent yields

Analytical and spectroscopic data for compounds **42a-e** are in agreement with those previously reported.[209]

General procedure for the synthesis of 5-(1*H*-Indol-3-yl)-1,3,4-thiadiazol-2-amines 43a-j

A mixture of the suitable indole-3-carbonitrile **40a-e** or **41a-e** (5 mmol), thiosemicarbazide (5 mmol) and trifluoroacetic acid (5 mL) was heated under stirring at 60 C for 3.5 h. The reaction mixture was then poured into ice and neutralized with $NaHCO_3$ saturated solution. The solid obtained was filtered off, washed with water, cyclohexane and diethyl ether to give 5-(1*H*-indol-3-yl)-1,3,4-thiadiazol-2-amines **43a-j** in excellent yields.

Analytical and spectroscopic data for the derivatives **43a-j** are in accordance to those reported in literature.[209]

General procedure for the synthesis of 3-Oxo-3-thiophen-3-yl-propionic acid ethyl ester 45

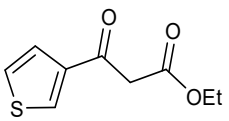

A three necks-round bottom flask, equipped with addition funnel, nitrogen inlet and temperature probe was charged with anhydrous THF and NaH (60%

dispersion in mineral oil,). The suspension was stirred at room temperature for 10 min and then a THF solution of 3-acetylthiophene **44** (25 mmol, 1 equiv. c = 0.62 M) was added dropwise over a period of 20 min. A slight increase of the temperature (4-5°C) was observed during the addition, and then the reaction mixture was warmed to 35°C and stirred for 30 min. A THF solution of diethyl carbonate (50 mmol, 2 equiv) was added over a period of 1 hour. After one additional hour, the reaction mixture was cooled down to -10 °C and quenched with slow addition of water (5-10 ml). Glacial acetic acid (3 ml) was added and the mixture was stirred for 20 min and then warmed to room temperature. The organic layer was separated and the aqueous layer was extracted with ethyl acetate (3x 50 ml). The combined organic layers were washed with brine, dried with anhydrous Na_2SO_4 and concentrated under reduced pressure. Purification was done by column chromatography using silica gel column and a mixture of hexanes and ethyl acetate as eluent. Cyclohexane (100%) was used to elute the excess of diethyl carbonate, and the amount of ethyl acetate was progressively increased from 20% to 50% to elute the title compound **45**.

Analytical and spectroscopic data for the derivative **45** are in accordance to those reported in literature.[250]

General procedure for the synthesis of -[1,3,4]thiadiazolo[3,2-a]pyrimidin-5-one 23

A mixture of 5-(1*H*-indol-3-yl)-1,3,4-thiadiazol-2-amine **43a-j** (0.92 mmol) and the suitable β-ketoesters (0.92 mmol) in polyphosphoric acid (PPA) was stirred at 130°C for 2h. After cooling at room temperature the reaction was quenched with ice cold water. The product was neutralized with $NaHCO_3$, and the crude was purified by column chromatography.

2-(1H-Indol-3-yl)-7-phenyl-5H-[1,3,4]thiadiazolo[3,2-a]pyrimidin-5-one (23a)

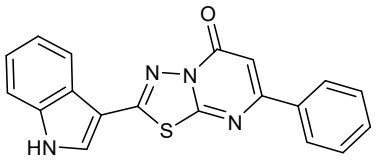

Yield: 55%; white solid; m.p.: 321°C; IR (cm^{-1}): 3142 (NH);1653 (CO) ^{1}H NMR (200 MHz, DMSO) δ 7.03 (1H, d, J= 2 Hz, Ar); 7,32 (2H, dd, J=2.6, 3.1 Hz, Ar), 7.32-7.57 (4H, m, Ar), 8.13 (2H, dd, J=1.3, 2.7 Hz , Ar); 8.24 (1H, dd, J=2.4, 3.3 Hz, Ar); 8,41 (1H, d, J = 2.3 Hz, Ar)**,** 12.27 (1H, s, NH). Anal. Calculated for $C_{19}H_{12}N_4OS$ (MW: 344.39)

2-(5-Methoxy-1H-indol-3-yl)-7-phenyl-5H-[1,3,4]thiadiazolo[3,2-a]pyrimidin-5-one (23b)

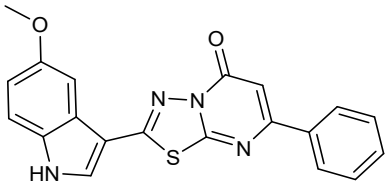

Yield: 41 %; brown solid; m.p.: 328 °C; IR (cm^{-1}): 3207 (NH); 1662 (CO) ^{1}H NMR (200 MHz, DMSO) δ: 3.85 (3H, s, CH_3), 6.69 (1H, d, J=8.9 Hz, Ar), 7.02 (1H, s, Ar), 7.47 (1H, d, J=9,1 Hz, Ar), 7.49-7.53 (3H, m, Ar), 7.73 (1H, s, Ar), 8.14 (2H, dd, J= 1.7, 3.3 Hz, Ar), 8.35 (1H, s , Ar), 12.17 (1H, s , NH).^{13}C NMR (50 MHz, DMSO) δ: 55.94 (q), 100.62 (s), 103.57 (d), 103.94 (d), 105.63 (s), 113.34 (d), 113.88 (d), 124.98 (s), 127.61 (d), 129.29 (s), 129.4 (d), 131.17 (d), 132.24 (s), 135.6 (s), 142.89 (d), 155.91 (s), 156.98 (s), 157.13 (d), 158.95 (s). Anal. Calculated for $C_{20}H_{14}N_4O_2S$ (MW: 374.41).

2-(5-Bromo-1H-indol-3-yl)-7-phenyl-5H-[1,3,4]thiadiazolo[3,2-a]pyrimidin-5-one (23c)

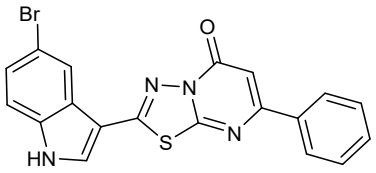

Yield: 48 %; yellow solid; m.p.: 348 °C; IR (cm^{-1}): 3170 (NH); 1660 (CO) ^1H NMR (200 MHz, DMSO) δ: 7.04 (1H, s, Ar), 7.44 (1H, d, J = 8.3 Hz, Ar), 7.52 (4H, m, Ar), 8.13 (2H, d, J = 2.8 Hz, Ar), 8.36 (1H, s, Ar), 8.47 (1H, s, Ar), 12.46 (1H, s, NH). Anal. Calculated for $C_{19}H_{11}BrN_4OS$ (MW: 423.28)

2-(5-Chloro-1H-indol-3-yl)-7-phenyl-5H-[1,3,4]thiadiazolo[3,2-a]pyrimidin-5-one (23d)

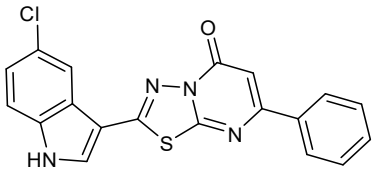

Yield: 36 %; beige solid; m.p.: 320 °C; IR (cm^{-1}): 3134 (NH); 1663 (CO) ^1H NMR (200 MHz, DMSO) δ 7.02 (1H, s, Ar), 7.32 (1H, d J= 4.3Hz, Ar),7.51-7.57 (4H, m, Ar), 8.11 (2H, m, Ar); 8.19 (1H, d J=3.8 Hz, Ar), 8.46 (1H, s, Ar), 12,42 (1H, s, NH). Anal. Calculated for $C_{19}H_{11}ClN_4OS$ (MW: 378.83).

2-(5-Fluoro-1H-indol-3-yl)-7-phenyl-5H-[1,3,4]thiadiazolo[3,2-a]pyrimidin-5-one (23e)

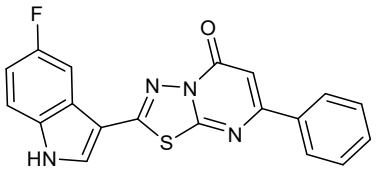

Yield: 42 %; pale yellow solid; m.p.: >350 °C; IR (cm^{-1}): 3230 (NH); 1678 (CO); ^1H NMR (200 MHz, DMSO) δ 7.04 (1H, d, J = 3 Hz, Ar), 7.19 (1H, d, J = 1.3, Ar), 7.41-7.64 (4H, m, Ar), 7.94 (1H, d, J = 3.2, Ar), 8.14 (2H, dd, J = 1.2, 15.5 Hz, Ar), 8.48 (1H, d, J = 1.5 Hz, Ar), 12.38 (1H, s, NH).^{13}C NMR (50 MHz, DMSO) δ: 103.96 (d), 109.59 (s), 112.07 (d), 123.40 (s), 127.53 (d), 129.30 (d), 129.69 (d), 131.20 (d), 133.91 (d), 134.24 (s), 135.97 (d), 137.13 (s), 148.97 (d), 153.88 (d), 157.02(d), 159.11 (d), 159.53 (s), 161.34 (s), 170.41 (s). Anal. Calculated for $C_{19}H_{11}FN_4OS$ (MW: 362.38).

2-(1-Methyl-1H-indol-3-yl)-7-phenyl-5H-[1,3,4]thiadiazolo[3,2-a]pyrimidin-5-one (23f)

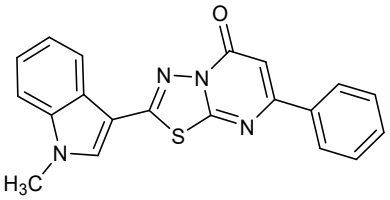

Yield: 46 %; light brown solid; m.p.: 265°C; IR (cm^{-1}): 3329 (NH);1678 (CO) ^{1}H NMR (200 MHz, DMSO) δ 3.9 (3H, s, CH_3), 6.99 (1H, s, Ar), 7.34-7.51 (5H, m, Ar), 7.6 (1H, d, J = 4.6 Hz, Ar), 8.09 (1H, s, Ar), 8.22 (2H, dd, J=3.4, 3.3 Hz, Ar), 8.37 (1H, s, Ar).^{13}C NMR (50 MHz, DMSO) δ: 33.72 (q), 103.95 (d), 104.77 (s), 111.57 (d), 121.29 (d), 122.63 (d), 123.93 (d), 124.53 (s), 127.5 (d), 129.26 (d), 131.15 (d), 135.29 (d), 135.97 (s), 137.81 (s), 153.54 (s), 156.96 (s), 158.96 (s), 161.42 (s). Anal. Calculated for $C_{20}H_{14}N_4OS$ (MW: 358.41).

2-(5-Methoxy-1-methyl-1H-indol-3-yl)-7-phenyl-5H-[1,3,4]thiadiazolo[3,2-a]pyrimidin-5-one (23g)

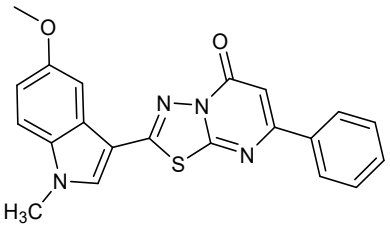

Yield: 30%; beige solid; m.p.: 335°C; IR (cm^{-1}): 1678 (CO). ^{1}H NMR (200 MHz, DMSO) δ: 3.87 (3H, s, CH_3), 3.90 (3H, s, CH_3), 6.29 (1H, s, Ar), 7.16 (1H, td, J = 9.2, 2.5 Hz, Ar), 7.24 (1H, td, J = 9.9, 2.7 Hz, Ar), 7.58 (1H, dd, J = 8.9, 4.4 Hz, Ar), 7.67 (1H, dd, J = 9.1, 4.4 Hz, Ar), 7.93 – 7.83 (2H, m, Ar), 8.21 (1H, s, Ar), 8.45 (1H, s, Ar). ^{13}C NMR (50 MHz, DMSO) δ: 33.93 (q), 56.01 (q), 103.71 (d), 103.98 (d), 104.35 (s), 112.57 (d), 113.22 (d), 125.30 (s), 127.52 (d), 129.31 (d), 131.19 (d), 133.00 (d), 135.47 (s), 136.00 (s), 153.60 (s), 156.20 (s), 156.97 (s), 158.93 (s). Anal. Calculated for $C_{21}H_{16}N_4O_2S$ (MW: 388.44).

2-(5-Bromo-1-methyl-1H-indol-3-yl)-7-phenyl-[1,3,4]thiadiazolo[3,2-a]pyrimidin-5-one (23h)

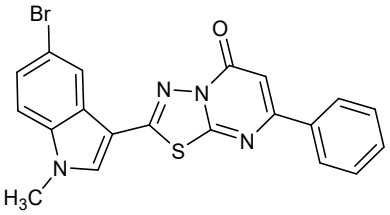

Yield: 32 %; off-white solid; m.p.: 318 °C; IR (cm^{-1}): 1663 (CO) ^{1}H NMR (200 MHz, DMSO) δ: 3.9 (3H, s, CH_3), 7.03 (1H, s, Ar), 7.53-7.65 (3H, m, Ar), 7.64 (1H, d, J = 8.6 Hz, Ar), 8.13 (2H, dd, J = 1.8, 3.5 Hz, Ar), 8.34 (1H, s , Ar), 8,47 (1H, s, Ar).^{13}C NMR (50 MHz, DMSO) δ: 34.01 (s), 104.04 (d), 104.39 (s), 113.95 (d), 115.41 (s), 116.46 (s), 123.42 (d), 123.45 (d), 126.61 (d), 127.56 (d), 127.58 (d), 129.32 (d), 130.05 (d), 134.67 (s), 135.82 (d), 136.76 (s), 142.57 (s), 151.95 (s), 155.56 (s) ,171.17(s). Anal. Calculated for $C_{20}H_{13}BrN_4OS$ (MW: 437.31).

2-(5-Chloro-1-methyl-1H-indol-3-yl)-7-phenyl-5H-[1,3,4]thiadiazolo[3,2-a]pyrimidin-5-one (23i)

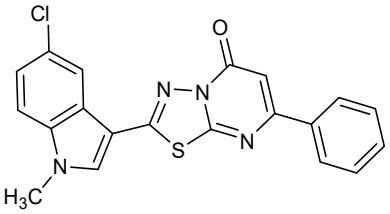

Yield: 39%; off-white solid; m.p.: 312 °C; IR (cm^{-1}): 1676 (CO) ^{1}H NMR (200 MHz, DMSO) δ 3.91 (3H, s, CH_3), 7.02 (1H, s, Ar), 7.39 (1H, d, J=8.7 Hz, Ar), 7.47 (3H, m, Ar), 7.67 (1H, d, J= 6.7 Hz, Ar), 8.14 (2H, dd, J= 2.4, 3.3 Hz, Ar), 8.2 (1H, s, Ar), 8.46 (1H, s, Ar). ^{13}C NMR (50 MHz, DMSO) δ 33.44 (q), 104.03 (d), 105.28 (s), 112.63 (d), 116.16 (s), 120.60 (d), 122.96 (d), 125.87 (s), 125.97 (d), 127.43 (s), 127.56 (d), 128.44 (d), 128.92 (d), 129.32 (d), 129.38 (d), 131.62 (s), 135.96 (s), 136.49 (s), 168.11 (s), 188.07 (s). Anal. Calculated for $C_{20}H_{13}ClN_4OS$ (MW 392.86).

2-(5-Fluoro-1-methyl-1H-indol-3-yl)-7-phenyl-5H-[1,3,4]thiadiazolo[3,2-a]pyrimidin-5-one (23j)

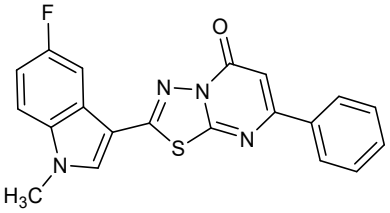

Yield: 45%; pale yellow solid; m.p.: 299 °C; IR (cm^{-1}): 1681 (CO) ^{1}H NMR (200 MHz, DMSO) δ 3.89 (3H, s, CH_3), 6.98 (1H, s, Ar), 7.2-7.57 (4H, m, Ar); 7.61 (1H, d, J= 2.7 Hz ,Ar), 7.87 (2H, dd, J=2.3, 8.8, Ar); 8.43(1H, s, Ar).^{13}C NMR (75MHz, DMSO) δ: 34.08 (q), 103.97 (d), 104.75 (s), 106.08 (d), 106.41 (d), 112.01 (d), 112.35 (d), 113.31 (d), 124.82 (s), 127.52 (d), 129.29 (d), 131.2 (d), 134.56 (s), 135.93 (s), 136.82 (d), 153.37 (s), 156.98 (s), 157.63 (s), 159.05 (s), 160.75 (s). Anal. Calculated for $C_{20}H_{13}FN_4OS$ (MW: 376.41).

2-(1H-Indol-3-yl)-7-methyl-5H-[1,3,4]thiadiazolo[3,2-a]pyrimidin-5-one (23k)

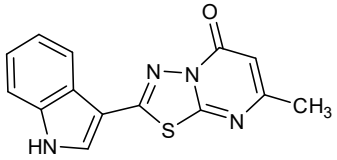

Yield: 30%; off-white solid; m.p.: 271 °C; IR (cm^{-1}): 3360 (NH), 1674 (CO); ^{1}H NMR (200 MHz, DMSO) δ 2.29 (3H, s, CH_3), 6.29 (1H, s, Ar), 7.11-7.33 (4H, m, Ar), 7.48 (1H, dd, J= 1.7, 6.5 Hz, Ar), 7.54 (1H, d, J=7.2 Hz, Ar), 8.19 (2H, dd, J=3.4, 3.3 Hz ,Ar), 8.36 (1H, s, Ar), 12.23 (1H, s, NH). ^{13}C NMR (50 MHz, DMSO) δ: 23.73 (q), 105.82 (s), 107.19 (d), 113.08 (d), 121.18 (d), 122.30 (d), 123.93 (d), 124.23 (d), 124.80 (s), 131.87 (d), 137.25 (s), 156.51 (s), 162.93 (s), 168.83 (s). Anal. Calculated for $C_{14}H_{10}N_4OS$ (MW: 282.32).

7-Methyl-2-(1-methyl-1H-indol-3-yl)-5H-[1,3,4]thiadiazolo[3,2-a]pyrimidin-5-one (23l)

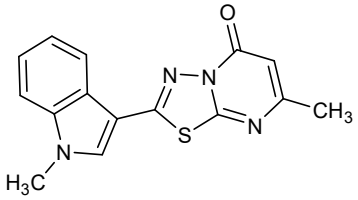

Yield: 28%; brown solid; m.p.: 260 °C; IR (cm^{-1}): 1674 (CO); ^{1}H NMR (200 MHz, DMSO) δ 3.1 (3H, d, J=2.6 Hz, CH_3), 3.87(3H, s, CH_3), 6.28 (1H, d, J = 2.5

Hz, Ar), 7.34 (2H, m, Ar), 7.62 (1H, dd, J= 2.4, 4.1 Hz, Ar), 8.19 (1H, dd, J= 2, 3.9 Hz, Ar), 8.36 (1H, s, Ar). ^{13}C NMR (50 MHz, DMSO) δ: 23.75 (q), 33.75 (q), 104.72 (s), 107.24 (d), 111.63 (d), 121.28 (d), 122.63 (d), 123.96 (d), 124.57 (s), 131.89 (d), 135.26 (d), 137.85 (s), 153.24 (s), 156.48 (s), 162.90 (s), 168.85 (s). Anal. Calculated for $C_{15}H_{12}N_4OS$ (MW: MW 296.35).

2-(1H-Indol-3-yl)-7-thiophen-3-yl-[1,3,4]thiadiazolo[3,2-a]pyrimidin-5-one (23m)

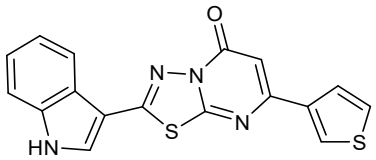

Yield: 36 %; beige solid; m.p.: 337 °C; IR (cm^{-1}): 3301(NH), 1668(CO) ^{1}H NMR (200 MHz, DMSO) δ 6.93 (1H, s, Ar), 7.31 (2H, m, Ar),7.55 (1H, d, J = 3.6 Hz, Ar), 7.69 (1H, d, J = 1.4 Hz, Ar), 7.76 (1H, d, J= 0.8 Hz, Ar), 8.23 (1H, m, Ar) 8.35 (1H, s, Ar), 8.38 (1H, s, Ar), 12.23 (1H, s, NH).^{13}C NMR (50 MHz, DMSO) δ: 103.46 (d), 105.92 (s), 113.11 (d), 121.21 (d), 122.32 (d), 123.94 (d), 124.26 (d), 126.81 (s), 128.16 (d), 130.05 (d), 131.93 (d), 137.29 (s), 139.38 (s), 153.76 (s), 155.27 (s), 157.15 (s), 161.61 (s). Anal. Calculated $C_{17}H_{10}N_4OS_2$ (MW.: 350.42).

2-(5-Methoxy-1H-indol-3-yl)-7-thiophen-3-yl-[1,3,4]thiadiazolo[3,2-a]pyrimidin-5-one (23n)

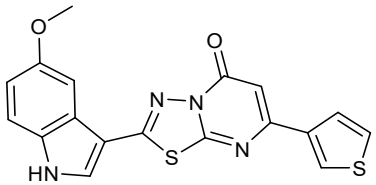

Yield: 25 %; brown solid; m.p.: 340 °C; IR (cm^{-1}): 3101 (NH); 1670 (CO) ^{1}H NMR (200 MHz, DMSO) δ 3.85 (3H, s, CH_3), 6.93 (1H, s, Ar), 6.97 (1H, dd, J = 2.1, 3.3 Hz, Ar), 7.47 (1H, d, J = 8.7 Hz, 1H), 7.78 (1H, d, J = 5.1 Hz, Ar), 8.32 (1H, d, J = 3 Hz, Ar), 8.35 (1H, d, J = 3.6 Hz, Ar), 12.14 (1H, s, NH). ^{13}C NMR (50 MHz, DMSO) δ 56.00 (q), 103.48 (d), 103.59 (d), 105.65 (s), 113.41 (d), 113.89 (d), 125.01 (s), 126.81 (d), 128.09 (d), 128.12 (d), 128.73 (s), 132.07 (d), 132.28 (s), 139.41 (s), 155.24 (s), 155.91 (s), 157.09 (s), 167.45 (s). Anal. Calculated for $C_{18}H_{12}N_4O_2S_2$ (MW: 380.44).

2-(5-Bromo-1H-indol-3-yl)-7-thiophen-3-yl-[1,3,4]thiadiazolo[3,2-a]pyrimidin-5-one (23o)

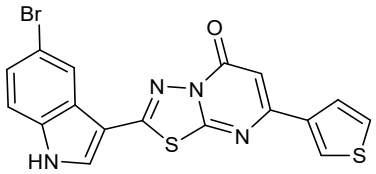

Yield: 29 %; grey solid; m.p.: 326 °C; IR (cm^{-1}): 3437 (NH); 1674 (CO) ^{1}H NMR (200 MHz, DMSO) δ 6.97 (1H, s, Ar), 7.45 (1H, d, J = 8.9 Hz, Ar), 7.55 (1H, d, J = 8.6 Hz, Ar), 7.70 (1H, d, J = 2.3 Hz, Ar), 7.78 (1H, d, J = 3.2 Hz, Ar), 8.27 (1H, s, Ar), 8.37 (1H, s, Ar), 8.48 (1H, s, Ar), 11.93 (1H, s, NH).^{13}C NMR (50 MHz, DMSO) δ: 103.48 (d), 105.53 (s), 114.93 (s), 115.21 (d), 123.35 (d), 125.87 (s), 126.59 (d), 126.81 (d), 128.15 (d), 128.20 (d), 133.28 (d), 136.10 (s), 139.34 (s), 153.42 (s), 155.35 (s), 157.12 (s), 161.51 (s). Anal. Calculated for $C_{17}H_9BrN_4OS_2$ (MW: 429.31).

2-(5-Chloro-1H-indol-3-yl)-7-thiophen-3-yl-[1,3,4]thiadiazolo[3,2-a]pyrimidin-5-one (23p)

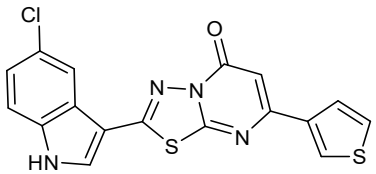

Yield: 27 %; light brow solid; m.p.: >350 °C; IR (cm^{-1}): 3101 (NH); 1668 (CO) ^{1}H NMR (200 MHz, DMSO) δ: 7.07 (1H, d, J = 3.3 Hz, Ar), 7.44 (1H, d, J=8.7 Hz, 1H), 7.70-8.92 (3H, m, Ar), 8.34 (1H, d, J = 3 Hz, Ar), 8.43 (1H, d, J = 3.6 Hz, Ar), 12.52 (1H, s, NH).^{13}C NMR (50 MHz, DMSO) δ: 103.52 (d), 114.85 (d), 115.90 (s), 120.39 (d), 120.98 (s), 124.09 (d), 125.33 (s), 126.86 (d), 127.02 (s), 128.20 (d), 128.24 (d), 129.05 (s), 133.46 (d), 135.90 (s), 139.40 (s), 155.40 (s), 157.18 (s). Anal. Calculated for $C_{17}H_9ClN_4OS_2$ (MW: 384.86).

2-(5-Fluoro-1H-indol-3-yl)-7-thiophen-3-yl-[1,3,4]thiadiazolo[3,2-a]pyrimidin-5-one (23q)

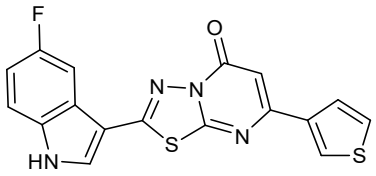

Yield: 31 %; beige solid; m.p.: >350 °C; IR (cm^{-1}): 3226 (NH), 1670 (CO) ^{1}H NMR (200 MHz, DMSO) δ 6.69 (1H, s, Ar), 7.18 (1H, t, J = 8 Hz, Ar), 7.57 (1H, m, Ar), 7.70 (1H, d, J = 1.1 Hz, Ar), 7.78 (1H, d, J = 3.4 Hz, Ar), 7.91 (1H, d, J = 10.1 Hz, Ar), 7.36 (1H, s, Ar), 8.48 (1H, d, J = 0.8 Hz, Ar), 12.38 (1H, s, NH Anal. Calculated for $C_{17}H_9FN_4OS_2$ (MW: 368.41).

2-(1H-Indol-3-yl)-7-thiophen-3-yl-[1,3,4]thiadiazolo[3,2-a]pyrimidin-5-one (23r)

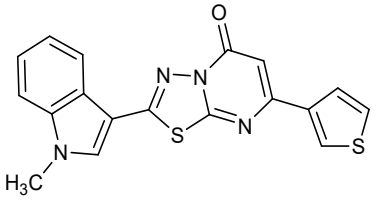

Yield: 33 %; grey solid; m.p.: 340 °C; IR (cm^{-1}): 1678(CO) ^{1}H NMR (200 MHz, DMSO) δ 3.90 (3H, s, CH_3), 6.93 (1H, s, Ar), 7.42 – 7.29 (2H, m, Ar), 7.62 (1H, d, J = 7.1 Hz, Ar), 7.69 (1H, s, Ar), 7.76 (1H, d, J = 3.9 Hz, Ar), 8.22 (1H, d, J = 5.9 Hz, Ar), 8.34 (1H, s, Ar).). ^{13}C NMR (50 MHz, DMSO) δ: 33.73 (q), 103.44 (d), 104.79 (s), 110.82 (d), 111.58 (d), 121.29 (d), 122.63 (d), 123.96 (d), 124.54 (s), 126.78 (d), 128.13 (d), 135.20 (d), 137.84 (d), 139.34 (s), 153.27 (s), 155.24 (s), 157.12 (s), 161.45 (s). Anal. Calculated for $C_{18}H_{12}N_4OS_2$ (MW: 357.37)

2-(5-Methoxy-1-methyl-1H-indol-3-yl)-7-thiophen-3-yl-[1,3,4]thiadiazolo[3,2-a]pyrimidin-5-one (23s)

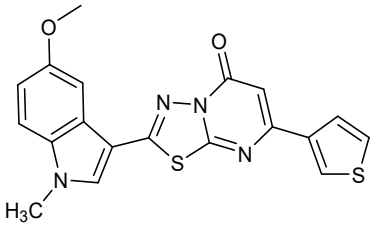

Yield: 23 %; brown solid; m.p.: 323°C; IR (cm^{-1}): 1676 (CO) ^{1}H NMR (200 MHz, DMSO) δ 3.85(3H, s, CH_3), 3.87 (3H, s, CH_3), 6.90 (1H, s, Ar), 7.01 (1H, m, Ar), 7,53 (1H, dd, J = 1.7, 0.9 Hz, Ar), 7.69 (2H, m, Ar), 7.76 (1H, s, Ar), 8.30 (1H, s, Ar) 8.30 (1H, s, Ar), 8.32 (1H, d, J = 2.2 Hz, Ar). ^{13}C NMR (50 MHz, DMSO) δ: 33.89 (q), 56.03 (q), 103.48 (d), 103.74 (d), 104.37 (s), 112.48 (d), 113.24 (d), 116.28 (s), 125.31 (s), 126.80 (d), 128.10 (d), 133.00 (s), 135.32 (d), 139.38 (s), 153.25 (s), 153.43 (s), 154.92 (s), 155.18 (s),156.20 (s), 157.04 (s). Anal. Calculated for $C_{19}H_{14}N_4O_2S_2$ (MW: 394.47).

2-(5-Bromo-1-methyl-1H-indol-3-yl)-7-thiophen-3-yl-[1,3,4]thiadiazolo[3,2-a]pyrimidin-5-one (23t)

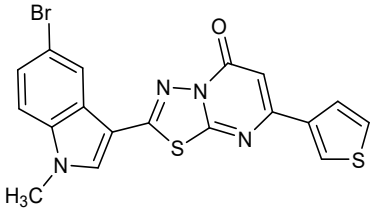

Yield: 25 %; brown solid; m.p.: 320 °C; IR (cm^{-1}): 1647 (CO) ^{1}H NMR (200 MHz, DMSO) δ 3.92 (3H, s, CH_3), 6.97 (1H, s, Ar), 7.52 (1H, d, J = 9.0 Hz, Ar), 7.64 (1H, d, J = 8.8 Hz, Ar), 7.71 (1H, s, Ar), 7.78 (1H, s, Ar), 8.36 (1H, s, Ar), 8.47 (1H, s, Ar).^{13}C NMR (50 MHz, DMSO) δ: 33.99 (q), 103.51 (d), 104.38 (s), 113.89 (d), 115.39 (s), 123.42 (d), 126.03 (s), 126.57 (d), 126.81 (d), 128.18 (d), 128.23 (d), 136.57 (s), 136.72 (s), 139.32 (s), 148.86 (s), 155.31 (s), 157.12 (s), 165.18 (s). Anal. Calculated for $C_{18}H_{11}BrN_4OS_2$ (MW: 443.34).

2-(5-Chloro-1-methyl-1H-indol-3-yl)-7-thiophen-3-yl-[1,3,4]thiadiazolo[3,2-a]pyrimidin-5-one (23u)

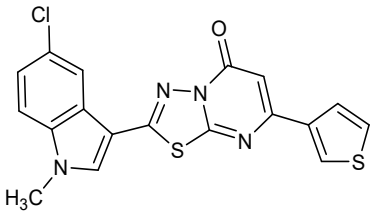

Yield: 23%; brown solid; m.p.: >350°C; IR (cm^{-1}): 1668 (CO); ^{1}H NMR (200 MHz, DMSO) δ: 3.90 (3H, s, CH_3), 6.92 (1H, s, Ar), 7.39 (1H, d, J = 8.2 Hz, Ar), 7.65 (2H, m, Ar), 7.75 (1H, dd, J = 1, 1.1 Hz, Ar), 8.18 (1H, s, Ar) 8.33 (1H, s,

Ar), 8.43 (1H, d, J = 4.6 Hz, Ar). ^{13}C NMR (50 MHz, DMSO) δ 33.98 (q), 103.49 (d), 112.10 (s), 113.44 (d), 115.38 (s), 120.39 (d), 123.40 (d), 123.97 (d), 125.44 (s), 126.79 (d), 127.38 (s), 128.19 (d), 136.44 (s), 136.66 (d), 139.31 (s), 155.30 (s), 157.08 (s). Anal. Calculated for $C_{18}H_{11}ClN_4OS_2$ (MW: 398.89)

2-(5-Fluoro-1-methyl-1H-indol-3-yl)-7-thiophen-3-yl-[1,3,4]thiadiazolo[3,2-a]pyrimidin-5-one (23v)

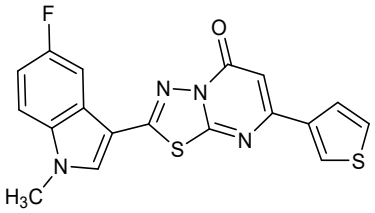

Yield: 32%; grey solid; m.p.: >350 °C; IR (cm^{-1}): 1656 (CO) ^{1}H NMR (200 MHz, DMSO) δ 3.92 (3H, s, CH_3), 6.93 (1H, s, Ar), 7.24 (1H, dd, J = 4.3, 1.8 Hz, Ar), 7.69 (2H, m, Ar), 7.77 (1H, d, J = 1.3 Hz, Ar), 7.89 (1H, d, J = 4.6 Hz, Ar), 8.34 (1H, s, Ar), 8.45 (1H, s, Ar). ^{13}C NMR (50 MHz, DMSO) δ 34.05 (q), 103.47 (d), 104.78 (s), 105.53 (s), 106.09 (d), 111.98 (d), 112.33 (d), 113.13 (d), 124.98 (s) 126.78 (d), 128.14 (d), 134.57 (s), 136.70 (d), 139.32 (s), 153.01 (s), 155.26 (s), 157.05 (s), 160.74 (s). Anal. Calculated for $C_{18}H_{11}FN_4OS_2$ (MW: 382.43).

General procedure for the synthesis of 1-(5-substututed -1H-indol-3-yl)-2-chloroethanone (47a-b)

To stirred ice-cooled suspension of $AlCl_3$ (2.0 eq.,) in dichloromethane (30 mL) chloroacetyl chloride (1.2 eq.) was slowly added under a nitrogen atmosphere, followed by a solution of indole derivatives **46a-b** (20.4 mmol) in dichloromethane (35 mL). The resulting mixture was stirred at 0 °C for 10 min and at room temperature for 4 h. The mixture was poured into stirred ice and water and extracted with ethyl acetate (2×). the combined organics were washed with brine (2×), dried over Na_2SO_4, and concentrated in vacuum.

.

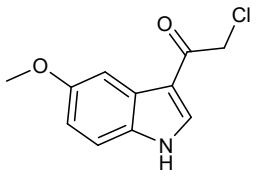

The residue was purified by column chromatography using DCM as eluent obtaining 1-(5-Methoxy-1H-indol-3-yl)-2-chloroethanone **47a** (55% yield) as brown solid.

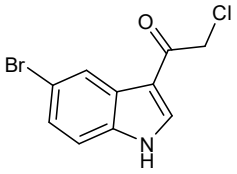

The residue was triturated with ethyl acetate/hexanes to give 1-(5-bromo-1H-indol-3-yl)-2-chloroethanone **47b** (61% yield) as an off-white solid.

Analytical and spectroscopic data for the derivatives **47a-b** are in accordance to those reported in literature.[251]

General synthesis of 3-bromoacetylindoles (49)

Bromine (0.1mL, d=3.12g mL^{-1}, 1.9mmol) was added dropwise to a cold suspension of the appropriate 3-acetylindole **48** (1.9mmol) in anhydrous MeOH (3mL). The mixture was heated at reflux for 2h. After cooling the solvent was evaporated under reduced pressure. The residue was treated with H_2O (20mL),

treated with $NaHCO_3$, (150mg) and extracted with EtOAc (3×50mL). The organic phase was dried, evaporated under reduced pressure, and purified by column chromatography using DCM as eluent.

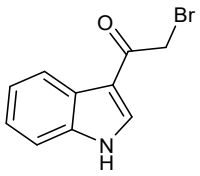

Analytical and spectroscopic data for the derivatives **49** are in accordance to those reported in literature[252]

General synthesis of 4-(1H-Indol-3-yl)-thiazol-2-ylamine derivatives (50a-c)

The mixture of indole analogues **48a-b** or **49** (17.8 mmol) and 2-thiourea (1.25 mL, 23.1 mmol) in EtOH was heated at 80 °C for 3 hr, and the resulting solution was concentrated under reduced pressure. To the residue was added water (15 mL) and saturated aqueous $NaHCO_3$ (4 mL), and the mixture was extracted with EtOAc (3 × 20 mL). The organic solution was combined, washed with water (15 mL), brine (10 mL) and dried over Na_2SO_4. Crude compounds were triturated with cyclohexane.

4-(1H-Indol-3-yl)-thiazol-2-ylamine derivatives (50a)

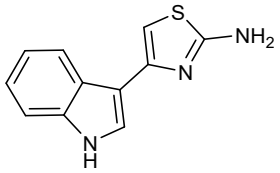

Yield: 65%, light yellow solid; IR (cm^{-1}): 3419, 3385 (NH_2); 3275 (NH). Analytical and spectroscopic data for the derivatives **50a** are in accordance to those reported in literature[253]

4-(5-Methoxy-1H-indol-3-yl)-thiazol-2-ylamine (50b)

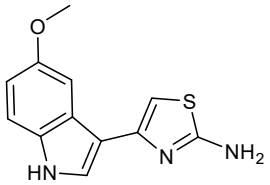

Yield: 59%; light brown solid; IR (cm^{-1}): 3396, 3404 (NH_2); 3290 (NH). ^1H NMR (200 MHz, DMSO-d6) δ: 3.81 (3H, s ,CH_3), 6.67 (1H, s, Ar), 6.78 (1H , dd, J = 8.8, 2.4 Hz, Ar), 6.90 (2H, s, NH_2), 7.30 (1H, d, J = 8.8 Hz, Ar), 7.44 (1H, d, J = 2.3 Hz, Ar), 7.58 (1H, d, J = 2.6 Hz, Ar), 11.02 (1H, s, NH). Anal. Calculated for $C_{12}H_{11}N_3OS$ (MW: 245.30).

4-(5-Bromo-1H-indol-3-yl)-thiazol-2-ylamine (50c)

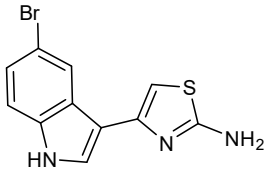

Yield: 70%; brown solid; IR (cm^{-1}) :3414, 3388 (NH_2), 3460 (NH); ^1H NMR (200 MHz, DMSO-d6) δ: 6.73 (1H, s, Ar), 6.98 (2H, s, NH_2), 7.24 (1H, d, J = 9.2 Hz, Ar), 7.37 (1H, d, J = 8.5 Hz, Ar), 7.71 (1H, s, Ar), 8.22 (1H, s, Ar), 11.41 (1H, s, NH).

General procedure for the synthesis of 3 -(6-substituted-imidazo[2,1-*b*]thiazol-3-yl)-1H-indole (24a-l)

A mixture of 4-(-1H-indol-3-yl)-thiazol-2-ylamine derivatives **50a-c** (0.92 mmol) and the suitable α-bromoacetyl derivative (0.92 mmol) in 30 mL of anhydrous ethanol was stirred at reflux for 24-48 h. After cooling at room temperature, solvent was removed under vacuum, the crude compound was neutralized with sat. sol. $NaHCO_3$, and purified by column chromatography to afford desired compounds **24.**

3 -(6-Phenyl-imidazo[2,1-b]thiazol-3-yl)-1H-indole (24a)

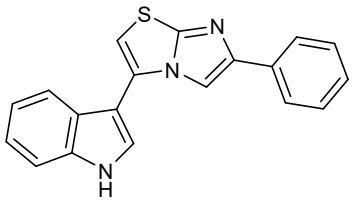

Yield: 17%; off-white solid; m.p.: 249 °C; IR (cm^{-1}): 3446 (NH); ^{1}H NMR (200 MHz, DMSO-d6) δ: 7.30 – 7.17 (4H, m, Ar), 7.47 – 7.36 (4H, m, Ar), 7.56 (1H, d, J = 8.0 Hz, Ar), 7.90 (1H, d, J = 7.8 Hz, Ar), 8.01 – 7.94 (2H, m, Ar), 7.96 (1H, s, Ar), 7.98 (1H, d, J = 1.0 Hz, Ar), 8.24 (1H, d, J = 2.7 Hz, Ar), 8.59 (1H, s, Ar), 11.86 (1H, s, NH). ^{13}C NMR (50 MHz, DMSO-d6) δ:104.71 (s), 105.57 (d), 109.81 (d), 112.71 (d), 119.63 (d), 120.88 (d), 122.95 (d), 125.09 (s), 125.40 (d), 127.48 (d), 127.57 (s), 128.99 (d), 130.04 (d), 134.82 (s), 136.86 (s), 146.89 (s), 149.10 (s). Anal. Calculated for $C_{19}H_{13}N_3S$ (MW 315.39).

3-(6-Thiophen-3-yl-imidazo[2,1-b]thiazol-3-yl)-1H-indole (24b)

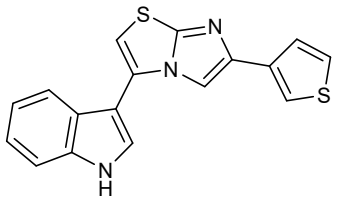

Yield: 15%; yellow solid; m.p.: 248 °C; IR (cm^{-1}): 3448 (NH); ^{1}H NMR (200 MHz, DMSO-d6) δ:7.28-7.37 (2H, m, Ar), 7.45 (1H, s, Ar), 7.64 (1H, d, J = 7.6 Hz, Ar), 7.68 (1H, dd, J = 3.1, 7.5 Hz, Ar), 7.87 (1H, s, Ar), 7.95 (1H, d, J = 7.9, Ar), 8.24 (1H, s, Ar), 8.5 (1H, s, Ar), 11.89 (1H, s, NH). ^{13}C NMR (50 MHz, DMSO-d6) δ: 55.56 (q), 104.44 (s), 106.48 (d), 110.03 (d), 110.65 (d), 113.27 (d), 113.63 (s), 114.71 (d), 117.86 (d), 121.82 (d), 125.62 (d), 126.69 (s), 126.83 (s), 126.87 (d), 130.04 (d), 135.57 (s), 136.20 (s), 146.79 (s), 148.97 (s), 160.08 (s). Anal. Calculated for $C_{17}H_{11}N_3OS_2$ (MW:321.42).

3-[6-(2,5-Dimethoxy-phenyl)-imidazo[2,1-b]thiazol-3-yl]-1H-indole (24c)

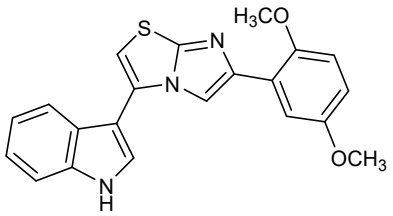

Yield: 20 %; beige solid; m.p.: 284°C; IR (cm^{-1}):3354(NH); ^{1}H NMR (200 MHz, DMSO-d6) δ: 3.78 (3H, s, CH_3), 3.84 (3H, s, CH_3), 6.83(1H, dd, J = 8.9, 2.7 Hz, Ar)), 7.03 (1H, d, J=8.9 Hz, Ar), 7.23 (2H, dt, J=7.1 ,7.5 ,7.9 Hz, Ar), 7.32 (1H, s, Ar), 7.56 (1H, d, J = 8 Hz, Ar), 7.77 (1H, s, Ar), 7.75 (1H, d, J = 2.6 Hz, Ar), 7.79 (1H, d, J = 7.8 Hz, Ar) 8.06 (1H, d, J = 1.2 Hz, Ar), 8.23 (1H, s, Ar), 11.78 (1H, s, NH). ^{13}C NMR (50 MHz, DMSO-d6) δ: 55.9 (q), 56.52 (q), 104.82 (s), 106.3 (d), 112.87 (d), 113.28 (d), 113.61 (d), 119.62 (d), 120.78 (d), 122.99 (d), 123.75 (s), 125.23 (s), 125.52 (d), 127.52 (s), 136.86 (s), 142.41 (s), 150.63 (s), 153.82 (s). Anal. Calculated for $C_{21}H_{17}N_3O_2S$ (MW: 375.44).

3-[6-(4-Fluoro-phenyl)-imidazo[2,1-b]thiazol-3-yl]-1H-indole (24d)

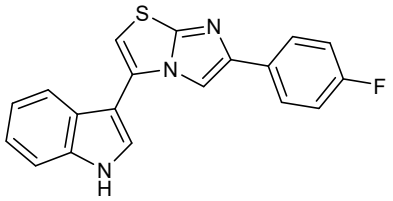

Yield:22 %;off-white solid; m.p.: 242°C; IR (cm^{-1}):3446 (NH); ^{1}H NMR (200 MHz, DMSO-d6) δ: 7.18-7.3 (4H, m, Ar), 7.41 (1H, s, Ar), 7.56 (1H, d, J = 8, Ar), 7.89 (1H, d, J = 7.8, Ar), 8.00 (2H, dd, J = 2.2, 5.9 Hz, Ar), 8.23 (1H, d, J = 2.2, Ar), 11.87 (1H, s, NH). ^{13}C NMR (50 MHz, DMSO-d6) δ: 112.72 (d), 115.68 (d), 115.97 (d), 119.63 (d), 120.89 (d), 122.26 (d), 122.95 (d), 125.06 (d), 127.22 (d), 127.32 (d), 127.56 (s), 128.83 (s), 131.38 (s), 131.98 (d), 134.94 (s), 135.01 (s), 136.85 (s), 145.72 (d), 145.97 (s). Anal. Calculated for $C_{19}H_{12}FN_3S$ (MW:333.38).

5-Bromo-3-(6-phenyl-imidazo[2,1-b]thiazol-3-yl)-1H-indole (24e)

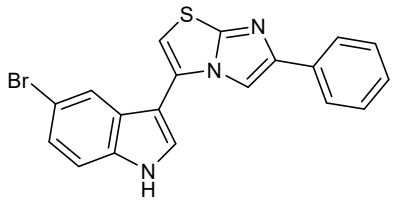

Yield: 16 %; light brown solid; m.p.: 253 °C; IR (cm^{-1}): 3438 (NH); ^{1}H NMR (200 MHz, DMSO-d6) δ: 7.27 (1H, t, J = 7.1, 7.3 Hz, Ar), 7.32 (1H, s, Ar), 7.56 (1H, d, J = 8.6 Hz, Ar), 7.97 (2H, d, J = 7.5 Hz, Ar), 8.06 (1H, s, Ar), 8.23 (1H, s, Ar), 11.78 (1H, s, NH). ^{13}C NMR (50 MHz, DMSO-d6) δ: 104.45 (s), 106.41 (d), 109.77 (d), 113.63 (s), 114.72 (d), 121.82 (s), 125. 19 (d), 125.62 (d), 126.71 (s), 126.83 (d), 126.86 (d), 127.51 (d), 129.01 (d), 134.79 (s), 135.57 (s), 146.93 (s), 149.07 (s), 151.09 (d). Anal. Calculated for $C_{19}H_{12}BrN_3OS$ (MW:392.99).

5-Bromo-3-(6-thiophen-3-yl-imidazo[2,1-b]thiazol-3-yl)-1H-indole (24f)

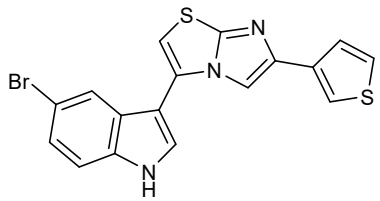

Yield: 13 %; off-white solid; m.p.: 280°C; IR (cm^{-1}): 3441(NH); ^{1}H NMR (200 MHz, DMSO-d6) δ: 7.39 (1H, dd, J = 8.7, 1.7 Hz, Ar), 7.46 (1H, s, Ar), 7.52 (1H, d, J = 8.6 Hz, Ar), 7.63 – 7.56 (2H, m, Ar), 7.79 (1H, dd, J = 2.6, 1.3 Hz, Ar), 8.02 (1H, d, J = 1.4 Hz, Ar), 8.22 (1H, d, J = 2.7 Hz, Ar) , 8.43 (1H, s, Ar), 12.04 (1H, s, NH). ^{13}C NMR (50 MHz, DMSO-d6) 104.51 (s), 106.31 (d), 109.59 (d), 113.62 (s), 114.72 (d), 120.05 (d), 121.82 (d), 125.63 (s), 126.39 (d), 126.65 (s), 126.72 (d), 126.91 (d), 135.56 (s), 136.79 (s), 143.66 (s), 148.80 (s). Anal. Calculated for $C_{17}H_{10}BrN_3OS_2$ (MW: 400.32).

5-Bromo-3-[6-(2,5-dimethoxy-phenyl)-imidazo[2,1-b]thiazol-3-yl]-1H-indole (24g)

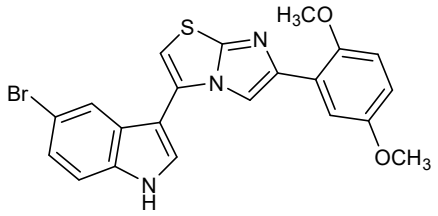

Yield: 15 %; pale yellow solid; m.p.: 247°C; IR (cm^{-1}): 3122 (NH); ^{1}H NMR (200 MHz, DMSO-d6) δ: 3.77 (3H, s, CH_3), 3.85 (3H, s, CH_3), 6.83(1H, dd, J = 5.7; 3 Hz, Ar), 7.03(1H, d, J = 9.1 Hz, Ar), 7.39 (2H, d, J = 9.1 Hz, Ar), 7.53 (1H, d, J = 8.6 Hz, Ar), 7.73 (1H, d, J = 2.7 Hz, Ar), 7.94 (1H, s, Ar), 8.13 (1H, s, Ar), 8.21 (1H, s, Ar), 11.99 (1H, s, NH). ^{13}C NMR (50 MHz, DMSO-d6 31.16 (q), 55.82 (q), 56.45 (q), 104.44 (s), 107.1 (d), 112.72 (d), 113.17 (d), 113.42 (s), 113.61 (d), 114.87 (d), 121.7 (d), 123.49 (s), 125.57 (d), 126.66 (s), 126.91 (s), 127.08 (d), 135.53 (s), 142.29 (s), 150.55 (s), 153.72 (s).Anal. Calculated for $C_{22}H_{19}N_3O_3S$ (MW: 405.47).

5-Bromo-3-[6-(4-fluoro-phenyl)-imidazo[2,1-b]thiazol-3-yl]-1H-indole (24h)

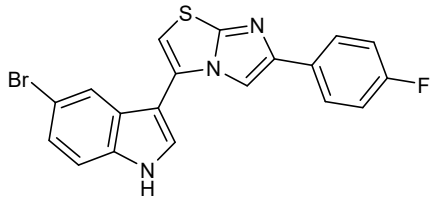

Yield: 20%;beige solid; m.p.: 267 °C; IR (cm^{-1}): 3442 (NH); ^{1}H NMR (200 MHz, DMSO-d6) δ: 7.25 (2H, t, J = 8.5 Hz, Ar), 7.39 (1H, d, J = 8.6 Hz, Ar), 7.56 – 7.48 (2H , m, Ar), 8.01 (3H, dd, J = 13.0, 7.1 Hz, Ar), 8.28 (1H, s, Ar), 8.58 (1H, s, Ar), 12.06 (1H, s, NH). ^{13}C NMR (50 MHz, DMSO-d6) δ:104.44 (s), 106.47 (d), 109.62 (d), 113.63 (s),114.70 (d), 115.70 (d), 115.98 (d), 121.81 (d), 125.63 (d), 126.71 (s), 126.79 (d), 126.86 (s), 127.22 (d), 127.32 (d), 131.33 (s), 131.37 (s), 135.57 (s), 146.02 (s), 149.13 (s), 160.28 (s). Anal. Calculated for $C_{19}H_{11}BrFN_3S$ (MW:412.28).

5-Bromo-3-[6-(3-methoxy-phenyl)-imidazo[2,1-b]thiazol-3-yl]-1H-indole (24i)

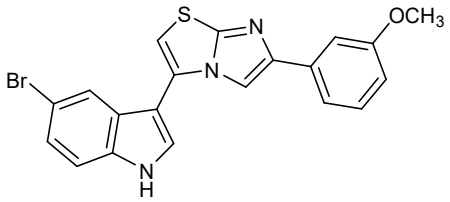

Yield: 10 %; light brown solid; m.p.: 214°C; IR (cm^{-1}): 3446 (NH); ^{1}H NMR (200 MHz, DMSO-d6) δ: 6.84 (1H, d, J = 8.2 Hz, Ar), 7.32 (1H, td, J = 2.9, 8.1, 10.7 Hz, Ar), 7.37-7.41 (1H, dd, J= 1.2, 8.3 Hz, Ar), 8.04 (1H, s, Ar), 8.29 (1H, s, Ar), 8.59 (1H, d, J = 3.1, Ar), 12.05 (1H, s, NH). ^{13}C NMR (50 MHz, DMSO-d6) δ: 55.56 (q), 104.44 (s), 106.49 (d), 110.03 (d), 110.65 (d), 113.27 (d), 113.63 (s), 114.71 (d), 117.86 (d), 121.82 (d), 125.62 (d), 126.69 (s), 126.83 (d), 126.87 (s), 130.04 (d), 135.57 (s), 136.20 (s), 146.79 (s), 148.97 (s), 160.08 (s). Anal. Calculated for $C_{20}H_{14}BrN_3OS$ (MW:424.31).

5-Methoxy-3-(6-phenyl-imidazo[2,1-b]thiazol-3-yl)-1H-indole (24j)

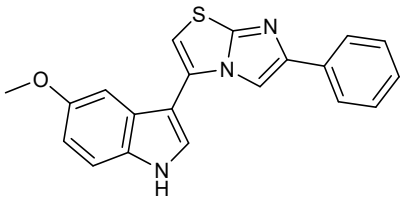

Yield: 16 %; pale yellow solid; m.p.: 222°C; IR (cm^{-1}): 3362(NH); ^{1}H NMR (200 MHz, $CDCl_3$) δ: 4.32 (3H, s, CH_3), 7.48 (1H, dd, J = 8.8, 2.3 Hz, Ar), 7.61 (1H, d, J = 2.0 Hz, Ar), 7.93 – 7.72 (5H, m, Ar), 8.06 (1H, d, J = 2.6 Hz, Ar), 8.32 (3H, m, Ar), 9.30 (1H, s, Ar). ^{13}C NMR (50 MHz, $CDCl_3$) δ: 55.94 (q), 101.06 (d), 106.37 (s), 106.53 (d), 107.89 (d), 112.75 (d), 113.13 (s), 113.96 (d), 121.04 (s), 124.16 (d), 125.24 (d), 127.23 (s), 127.40 (d), 128.72 (d), 129.18 (s), 129.97 (s), 150.29 (s), 155.21 (s). Anal. Calculated for $C_{20}H_{15}N_3OS$ (MW: 345.42).

5-Methoxy-3-(6-thiophen-3-yl-imidazo[2,1-b]thiazol-3-yl)-1H-indole (24k)

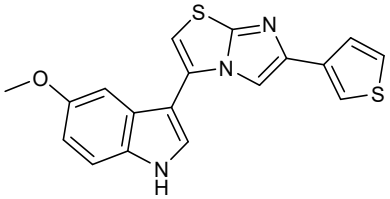

Yield: 13%; light brown solid; m.p.: 266 °C; IR (cm^{-1}): 3446 (NH); ^{1}H NMR (200 MHz, DMSO-d6) δ: 3.84 (3H, s, CH_3), 6.93(1H, s, Ar), 7.55 (5H, m, Ar), 7.85 (1H, s, Ar), 8.12 (1H, s, Ar), 8.45 (1H, s, Ar), 11.73 (1H, s, NH). ^{13}C NMR (50 MHz, DMSO-d6) δ: 55.92 (q), 101.44 (d), 104.54 (s), 105.11 (d), 109.67 (d), 113.13 (d), 113.45 (d), 120 (d), 125.5 (s), 125.66 (d), 126.42 (d), 126.9 (d), 127.61 (s), 131.8 (s), 136.83 (s), 143.58 (s), 148.79 (s), 154.91 (s). Anal. Calculated for $C_{18}H_{13}N_3OS_2$ (MW: 351.45).

3-[6-(4-Fluoro-phenyl)-imidazo[2,1-b]thiazol-3-yl]-5-methoxy-1H-indole (24l)

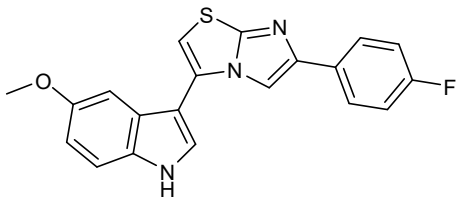

Yield: 15 %; beige solid; m.p.: 277 °C; IR (cm^{-1}): 3439 (NH); ^{1}H NMR (200 MHz, DMSO-d6) δ: 3.82 (3H, s, CH_3), 6.92 (1H, d, J = 7.7 Hz, Ar), 7.27 (2H, d J = 8,1 Hz, Ar), 7.32 (1H, s, Ar), 7.45 (2H, d, J = 9.3 Hz, Ar), 8.01 (2H, m, Ar), 8.17 (1H, s, Ar), 8.58 (1H, s, Ar), 11.87 (1H, s, NH). ^{13}C NMR (50 MHz, DMSO-d6) δ: 55.94 (q), 101.47 (d), 104.48 (s), 105.24 (d), 109.72 (d), 113.11 (d), 113.44 (d), 115.71 (d), 115.99 (d), 125.5, 125.74 (d), 127.2 (d), 127.31 (d), 127.66 (s), 131.43 (s), 131.81 (s), 134.26 (s), 145.94 (s), 154.94 (s), 163.48 (s). Anal. Calculated for $C_{20}H_{14}FN_3OS$ (MW:363.41).

3-[6-(2,5-Dimethoxy-phenyl)-imidazo[2,1-b]thiazol-3-yl]-5-methoxy-1H-indole (24m)

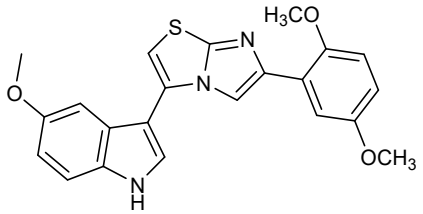

Yield: 18%; beige solid; m.p.: 212°C; IR (cm^{-1}) : 3458(NH); ^{1}H NMR (200 MHz, DMSO-d6) δ: 3.78 (3H, s, CH_3), 3.80 (3H, s, CH_3), 3.82 (3H, s, CH_3), 6.83 (1H, dd, J = 8.9, 3.2 Hz, Ar), 6.93 – 6.89 (1H, m, Ar), 7.02 (1H, d, J = 9.0 Hz, Ar), 7.22 (1H, d, J = 2.0 Hz, Ar), 7.31 (1H, s, Ar), 7.45 (1H, d, J = 8.8 Hz, Ar), 7.75 (1H, d, J = 3.1 Hz, Ar), 7.97 (1H, d, J = 2.6 Hz, Ar), 8.22 (1H, s, Ar), 11.60 (1H,s, Ar) ^{13}C NMR (50 MHz, DMSO-d6)δ: Anal. Calculated for $C_{20}H_{14}FN_3OS$ (MW:363.41).

General procedure for the synthesis of 1H-pyrrolo[2,3-b]pyridine-3-carbaldehyde derivatives (56)

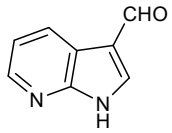

To a solution of commercial available starting material **55** (61.2 mmol) in acetic acid (20 mL) and water (40 mL) was added HMTA (67.3 mmol). The reaction mixture was stirred at 120 °C for 6 h. After cooling, the resulting precipitate was collected and dried to afford desired compounds **56a-b**, (Yield: 75%) as a yellow solid; Analytical and spectroscopic data for the derivatives **56** are in accordance to those reported in literature.[254]

General procedure for the synthesis of 1H-Pyrrolo[2,3-b]pyridine-3-carbaldehyde oxime analogues (57)

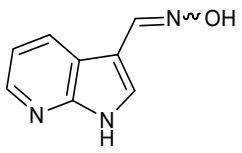

To a solution of 7-azaindole-3-carboxaldehydes **56** (2.2 mmol) in EtOH (25 mL) was added a solution of $NH_2OH{\cdot}HCl$ (7.8 mmol) and Na_2CO_3 (4.0 mmol) in

water (10 mL) and the mixture was refluxed for 2 h at 95 °C. After concentrating the reaction mixture under reduced pressure, the resulting precipitate was filtered off, washed with ice-cold water, and air-dried to yield **57**.

Yield: 90%, white solid; Analytical and spectroscopic data for the derivatives **57** are in accordance to those reported in literature[254]

General procedure for the synthesis of 1H-Pyrrolo[2,3-b]pyridine-3-carbonitrile analogues (58)

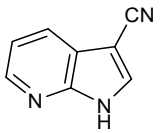

mixture of 1H-pyrrolo[2,3-*b*]pyridine-3-carbaldehyde oxime **57** (6.21 mmol) and acetic anhydride (53 mmol) was heated under reflux for 4 h. The reaction mixture was cooled to room temperature and poured into ice-cold water. The solid obtained was filtered and washed with excess of ice-cold water. The white solid was suspended in water (20 mL) and the aqueous suspension was heated under reflux for 3 h. The reaction mixture was cooled to room temperature and poured into ice-cold water. The white solid obtained was filtered, washed with excess of ice-cold water and used without further purification (yield: 80%).

Analytical and spectroscopic data for the derivatives **58** are in accordance to those reported in literature[255]

General procedure for the synthesis of 1-methyl-Pyrrolo[2,3-b]pyridine-3-carbonitrile (59)

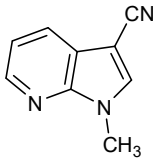

To a cold solution of 1H-pyrrolo[2,3-*b*]pyridine-3-carbonitrile **58** (2.5 mmol) in anhydrous toluene (25 mL), tBuOK (0.38 g, 3.4 mmol) and TDA-1 (1 or 2 drops) were added at 0 °C. The reaction mixture was stirred at room temperature for 3 h and then methyl iodide (2.5 mmol, 0.2 mL) was added at 0 °C. TLC analysis (ethyl acetate) revealed that methylation was complete after 1 h. The solvent was

evaporated under reduced pressure. The residue was treated with water, extracted with DCM (3 × 20 mL), dried (Na_2SO_4), evaporated and purified by column chromatography using DCM/ethyl acetate (9/1) as eluent, to give the desired product as white solid (yield: 80%)

Analytical and spectroscopic data for the derivatives **59** are in accordance to those reported in literature.[256]

General procedure for the synthesis of 5-(1H-Pyrrolo[2,3-b]pyridin-3-yl)-[1,3,4]thiadiazol-2-ylamine (60a-b)

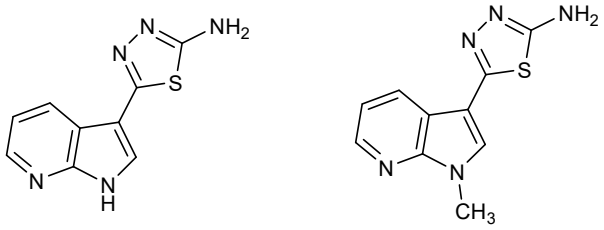

A mixture of the suitable 1H-pyrrolo[2,3-*b*]pyridine-3-carbonitrile (5 mmol), thiosemicarbazide (5 mmol) and trifluoroacetic acid (5 mL) was heated under stirring at 60 °C for 2.5 h. The reaction mixture was then poured into ice and neutralized with $NaHCO_3$ saturated solution. The solid, obtained as white solid, was filtered off, washed with water, cyclohexane and diethyl ether to give **60a-b** in excellent yields (75-90%).

Analytical and spectroscopic data for the derivatives **60a-b** are in accordance to those reported in literature.[257]

General procedure for the synthesis of 2-Bromo-1-pyridin-4-yl-ethanone or 2-Bromo-1-pyridin-3-yl-ethanone (63,64)

Bromine(108 mmol) was added drop wise to a cold (0°C) solution of 3- acetyl-pyridine (99 mmol) in acetic acid containing 33% of HBr (165 mL) under vigourous stirring. The vigorously stirred mixture was warmed to 40°C for 2h and then to 75°C. After 2h at 75°C, the mixture was cooled and diluted with ether (400 mL) to precipitate the product, which was recovered by filtration and washed with diethyl ether to give white crystals. (yield 90%)

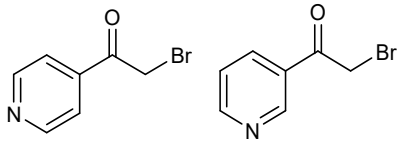

Analytical and spectroscopic data for the derivatives **63, 64** are in accordance to those reported in literature.[258]

General procedure for the synthesis of 2-Bromo-1-(2,3-dihydro-benzo[1,4]dioxin-6-yl)-ethanone (66)

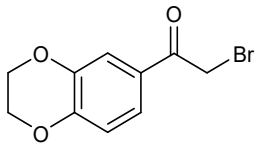

Pyridinium tribromide (3.1 mmol, 1 g) in 15 mL MeOH was added dropwise over 30 min to a stirred solution of 3′,4′-(ethylenedioxy)-acetophone (3.1 mmol) in 10 mL dichloromethane. The mixture was reacted at room temperature for about 10 h. After completion of the reaction, the solvent is removed in vacuum, the product is dissolved with 100 mL dichloromethane and washed with water and saturated sodium chloride solution, then the organic phase was dried by anhydrous sodium sulfate and concentrated in vacuum. The crude product can be purified by crystallization from ethyl acetate (68%).

Analytical and spectroscopic data for the derivatives **66** are in accordance to those reported in literature.[141]

General procedure for the synthesis of 2-Bromo-1-furan-2-yl-ethanone (68)

Bromine (20.0 mmol) was added to a solution of the 2-Acetylfuran **67** (20.0 mmol) in Et_2O (30 mL). The solution was stirred for 6-12 h. The reaction progress was monitored by TLC. When the starting material disappeared, the reaction was quenched with water (20 mL), and extracted with Et_2O (2 × 20 mL). The combined organic phases were washed with saturated aqueous $NaHCO_3$ solution (30 mL), saturated aqueous $Na_2S_2O_3$ solution (30 mL), brine (30 mL), and dried over Na_2SO_4. After being filtered and concentrated, the residue was purified by flash chromatography to give α-bromoketone with yields of **68**, as brown solid in good yield (65%).

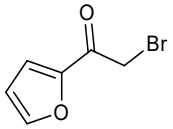

Analytical and spectroscopic data for the derivatives **68** are in accordance to those reported inliterature.[250]

General procedure for the synthesis of 3-(6-Phenyl-imidazo[2,1-b][1,3,4]thiadi azol-2-yl)-1H-pyrrolo[2,3-b]pyridine derivatives 25

A mixture of 5-(1H-pyrrolo[2,3-b]pyridin-3-yl)-[1,3,4]thiadiazol-2-ylamine **60** (0.92 mmol) and the suitable α-bromoacetyl derivative (0.92 mmol) in 30 mL of anhydrous ethanol was stirred at reflux for 24 h. After cooling at room temperature the desired product **25** was filtered off and washed with cold ethanol.

3-(6-Phenyl-imidazo[2,1-b][1,3,4]thiadiazol-2-yl)-1H-pyrrolo[2,3-b]pyridine (25a)

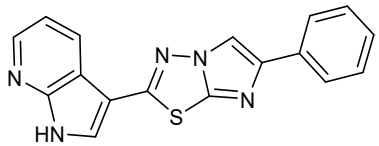

Yield: 42 %; off-white solid; m.p.: 254 °C; IR (cm^{-1}): 3290 (NH);^{1}H NMR (200 MHz, DMSO) δ 7.36 – 7.24 (2H, m, Ar), 7.42 (2H, t, J = 7.6 Hz, Ar), 7.88 (1H, s, Ar), 7.91 (1H, s, Ar), 8.43 – 8.39 (1H, m, Ar), 8.53 – 8.46 (2H, m, Ar), 8.70 (1H, s, Ar), 12.66 (1H, s, NH).^{13}C NMR (50 MHz, DMSO) δ 105.9 (s), 110.99 (d), 116.74 (s), 118.23 (d), 124.98 (s), 125.01 (d), 127.61 (d), 129.11 (s), 129.13 (d), 129.30 (d), 130.22 (d), 134.50 (s), 145.20 (d), 145.50 (s), 149.32 (s). Anal. Calculated for $C_{17}H_{11}N_5S$ (MW: 317.37)

3-[6-(4-Fluoro-phenyl)-imidazo[2,1-b][1,3,4]thiadiazol-2-yl]-1H-pyrrolo[2,3-b]pyridine (25b)

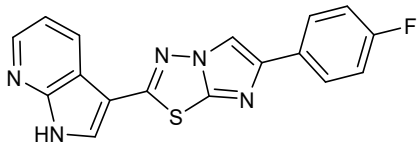

Yield: 40 %; pale yellow solid; m.p.: 243 °C; IR (cm^{-1}): 3396 (NH) ^{1}H NMR (200 MHz, DMSO) δ 7.25 (2H, td, J = 3, 2, 1.8Hz, Ar), 7.35 – 7.31 (1H, m, Ar), 7.91 (2H, td, J = 3, 3.4, 4.6 Hz, Ar), 8.40 (1H, dd, J = 4.7, 1.6 Hz, Ar), 8.48 (2H, dd, J = 8.0, 1.7 Hz, Ar), 8.67 (1H, s, Ar), 12.64 (1H, s, NH).Anal. Calculated for $C_{17}H_{10}FN_5S$ (MW: 335.36).

3-[6-(2,5-Dimethoxy-phenyl)-imidazo[2,1-b][1,3,4]thiadiazol-2-yl]-1H-pyrrolo[2,3-b]pyridine (25c)

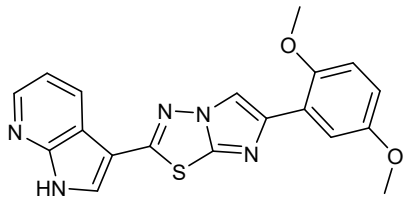

Yield: 27 %; off-white solid; m.p.: 264 °C; IR (cm^{-1}): 3335 (NH).^{1}H NMR (200 MHz, DMSO) δ 3.77 (3H, s, CH_3), 3.92 (3H, s, CH_3), 6.84 (1H, dd, J=9, 3.1 Hz, Ar), 7.04 (1H, d, J= 9 Hz, Ar), 7.33 (1H, dd, J= 3.2, 4.7 Hz, Ar), 7.73 (1H, d, J=3.2 Hz, Ar), 8.41 (1H, dd, J=1.6, 3 Hz, Ar), 8.47 (1H, d, J=2.4, Hz, Ar), 8.48 (1H, s, Ar), 8.52(1H, dd, J=1.6, 6.4 Hz, Ar), 12.63 (1H, s, NH).Anal. Calculated for $C_{19}H_{15}N_5O_2S$ (MW: 377.42).

3-[6-(3-Methoxy-phenyl)-imidazo[2,1-b][1,3,4]thiadiazol-2-yl]-1H-pyrrolo[2,3-b]pyridine (25d)

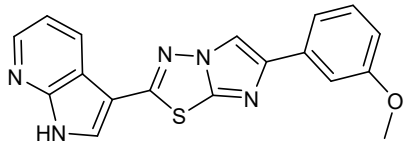

Yield: 36 %; pale yellow solid; m.p.: 244 °C; IR (cm^{-1}): 3290 (NH) ^{1}H NMR (200 MHz, DMSO) δ 3.82 (3H, s, CH_3), 6.85 (1H, d, *J* = 8.2 Hz, Ar), 7.38 – 7.29 (2H, m, Ar), 7.46 (2H, s, Ar), 8.41 (1H, d, J = 4.6 Hz, Ar), 8.53 – 8.45 (2H, m, Ar), 8.73 (1H, s, Ar), 12.68 (1H, s, NH).^{13}C NMR (50 MHz, DMSO) δ 55.53 (q), 105.89 (s), 110.28 (d), 111.28 (d), 113.31 (d), 116.74 (s), 117.43 (d), 118.23 (d), 129.29 (d), 130.19 (d), 135.89 (s), 143.51 (s), 145.19 (s), 145.33 (s), 149.31 (s), 157.02 (d), 157.15 (s), 160.09 (s). Anal. Calculated for $C_{18}H_{13}N_5OS$ (MW: 347.08).

3-(6-Thiophen-3-yl-imidazo[2,1-b][1,3,4]thiadiazol-2-yl)-1H-pyrrolo[2,3-b]pyridine (25e)

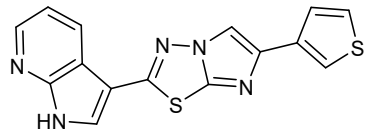

Yield: 25 %; off-white solid; m.p.: 255 °C; IR (cm^{-1}): 3298 (NH); ^{1}H NMR (200 MHz, DMSO) δ 7.22 (1H, t, J = 3.9 Hz, Ar), 7.33 (1H, dd, J = 7.9, 4.7 Hz, Ar), 7.54 (1H, dd, J = 5.0, 1.1 Hz, Ar), 7.61 (1H, dd, J = 5.0, 2.9 Hz, Ar), 7.77 (1H, dd, J = 2.9, 1.0 Hz, Ar), 8.41 (1H, dd, J = 4.7, 1.4 Hz, Ar), 8.52 – 8.47 (2H, m, Ar), 8.54 (1H, s, Ar), 12.66 (1H, s, NH). Anal. Calculated for $C_{15}H_9N_5S_2$ (MW: 323.03).

3-(6-Pyridin-3-yl-imidazo[2,1-b][1,3,4]thiadiazol-2-yl)-1H-pyrrolo[2,3-b]pyridine (25f)

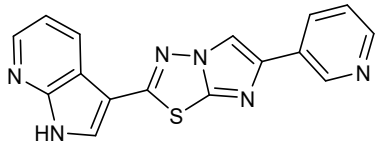

Yield: 31 %; grey solid; m.p.: 267 °C; IR (cm^{-1}): 3320 (NH);^{1}H NMR (200 MHz, DMSO) δ 7.34 (1H, dd, J = 7.9, 4.7 Hz, Ar), 7.98 (1H, dd, J = 8.1, 5.5 Hz, Ar), 8.41 (1H, dd, J = 4.7, 1.6 Hz, Ar), 8.49 (1H, dd, J = 7.9, 1.6 Hz, Ar), 8.54 (1H, s, Ar), 8.74 (1H, dd, J = 5.5, 1.1 Hz, Ar), 8.82 – 8.78 (1H, m, Ar), 9.02 (1H, s, Ar), 9.27 (1H, d, J = 1.8 Hz, Ar), 12.71 (1H, s, NH). ^{13}C NMR (50 MHz, DMSO) δ 105.64 (s), 113.73 (d), 116.73 (s), 118.36 (d), 127.08 (d), 129.35 (d), 129.97 (s), 130.84 (d), 133.05 (s), 138.76 (d), 139.85 (s), 139.95 (d), 142.13 (d), 145.00 (s), 145.25 (d), 149.28 (s),158.43(s). Anal. Calculated for $C_{16}H_{10}N_6S$ (MW: 318.36).

3-[6-(2,3-Dihydro-benzo[1,4]dioxin-6-yl)-imidazo[2,1-b][1,3,4]thiadiazol-2-yl]-1H-pyrrolo[2,3-b]pyridine (25g)

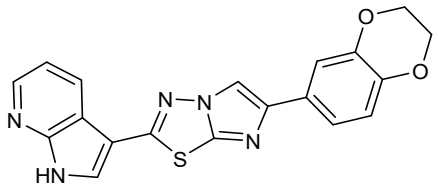

Yield: 39 %;off-white solid; m.p.: 231 °C; IR (cm^{-1}): 3332 (NH); ^{1}H NMR (200 MHz, DMSO) δ 4.29 – 4.24 (4H, m, CH_2), 6.90 – 6.86 (1H, m, Ar), 7.32 – 7.29 (1H, m, Ar), 7.34 (1H, d, *J* = 1.8 Hz, Ar), 7.36 (1H, dd, *J* = 3.7, 2.0 Hz, Ar), 8.40 (1H, dd, *J* = 4.7, 1.6 Hz, Ar), 8.45 (1H, s, Ar), 8.47 (1H, dd, *J* = 7.9, 1.6 Hz, Ar), 8.55 (1H, s, Ar), 12.61 (1H, s, NH). Anal. Calculated for $C_{19}H_{13}N_5O_2S$ (MW: 375.4).

1-Methyl-3-(6-phenyl-imidazo[2,1-b][1,3,4]thiadiazol-2-yl)-1H-pyrrolo[2,3-b]pyridine (25h)

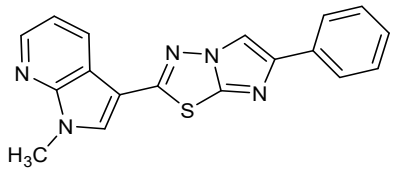

Yield: 24 %; off-white solid; m.p.: 221 °C; ^{1}H NMR (200 MHz, DMSO) δ 3.92 (3H, s, CH_3), 7.28 (1H, t, J = 7.3 Hz, Ar), 7.40 (3H, dt, J = 7.9, 6.2 Hz, Ar), 7.89 (2H, d, J = 7.7 Hz, Ar), 8.48 (2H, t, J = 5.8 Hz, Ar), 8.54 (1H, s, Ar), 8.69 (1H, s, Ar). ^{13}C NMR (50 MHz, DMSO) δ 31.96 (q), 104.58 (s), 111.04 (d), 117.01 (s), 118.44 (d), 125.01 (d), 127.65 (d), 129.13 (d), 129.52 (d), 133.46 (d), 134.38 (s), 145.00 (d), 145.40 (s), 148.22 (s), 156.76 (s). Anal. Calculated for $C_{18}H_{13}N_5S$ (MW: 331.39).

3-[6-(2,5-Dimethoxy-phenyl)-imidazo[2,1-b][1,3,4]thiadiazol-2-yl]-1-methyl-1H-pyrrolo[2,3-b]pyridine (25i)

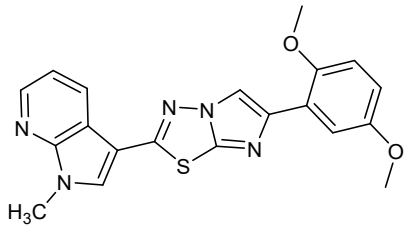

Yield: 37 %; beige solid; m.p.: 245 °C; ^{1}H NMR (200 MHz, DMSO) δ 3.77 (3H, s, CH_3), 3.90 (3H, *s*, CH_3), 3.92 (3H, *s*, CH_3), 6.87 (1H, dd, *J* = 8.9, 2.8 Hz, Ar), 7.03 (1H, t, *J* = 7.8 Hz, Ar), 7.38 (1H, dd, *J* = 7.7, 4.9 Hz, Ar), 8.52 (1H, d, J = 1.1 Hz, Ar), 8.47 (2H, d, J = 7.4 Hz, Ar), 8.58 (2H, s, Ar). Anal. Calculated for $C_{20}H_{17}N_5O_2S$ (MW: 391.45).

1-Methyl-3-(6-thiophen-3-yl-imidazo[2,1-b][1,3,4]thiadiazol-2-yl)-1H-pyrrolo[2,3-b]pyridine (25j)

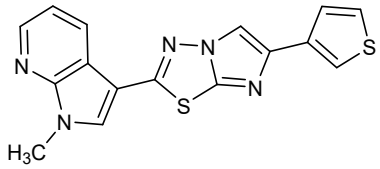

Yield: 21%; light brown solid; m.p.: 270 °C; ^{1}H NMR (200 MHz, DMSO) δ 3.90 (3H, s, CH_3), 7.37 – 7.34 (1H, m, Ar), 7.53 (1H, dd, *J* = 5.0, 1.2 Hz, Ar), 7.60 (1H, dt, J = 5.0, 2.5 Hz, Ar), 7.69 – 7.64 (1H, m, Ar), 7.77 (1H, dd, *J* = 2.9, 1.2 Hz, Ar), 8.45 (1H, dt, *J* = 3.3, 1.7 Hz, Ar), 8.52 (1H, d, *J* = 1.1 Hz, Ar). Anal. Calculated for $C_{16}H_{11}N_5S_2$ (MW: 337.42)

1-Methyl-3-(6-pyridin-3-yl-imidazo[2,1-b][1,3,4]thiadiazol-2-yl)-1H-pyrrolo[2,3-b]pyridine (25p)

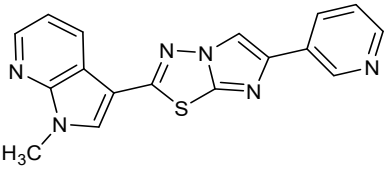

Yield: 25 %; yellow solid; m.p.: 243°C; ^{1}H NMR (200 MHz, DMSO) δ 3.89 (3H, s, CH_3), 7.43 – 7.31 (1H, m, Ar), 7.93 (1H, dd, *J* = 7.6, 4.5 Hz, Ar), 8.44 (2H, d, *J*

= 5.1 Hz, Ar), 8.54 (1H, s, Ar), 8.71 (2H, d, *J* = 4.8 Hz, Ar), 8.96 (1H, s, Ar), 9.21 (1H, s, Ar). ^{13}C NMR (50 MHz, DMSO) δ 31.97 (q), 104.30 (s), 113.64 (d), 116.88 (d), 118.53 (s), 124.95 (d), 126.93 (d), 129.48 (s), 132.86 (s), 133.89 (d), 138.42 (d), 139.85 (s), 140.01 (d), 142.24 (d), 145.03 (d),148.16 (s),157.94 (s). Anal. Calculated for $C_{17}H_{12}N_6S$ (MW: 332.38)

1-Methyl-3-(6-pyridin-4-yl-imidazo[2,1-b][1,3,4]thiadiazol-2-yl)-1H-pyrrolo[2,3-b]pyridine (25l)

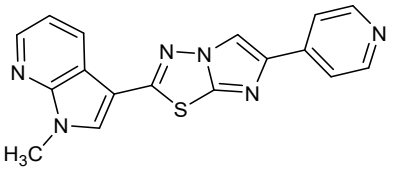

Yield: 40 %; off-white solid; m.p.: 233°C; ^{1}H NMR (200 MHz, DMSO) δ 3.93(3H, s, CH_3), 7.39 (1H, dd J= 3.7, 4.7Hz, Ar), 7.89 (1H, dd J=5, 6.4 Hz, Ar). 8.48 (2H, m, Ar), 8.6 (1H, s, Ar), 8.69 (1H, s, Ar), 8.7 (1H, d, J=1.2, Ar), 8.99 (1H, d, J=1.4, Ar), 9.93 (1H, s, Ar). Anal. Calculated for $C_{17}H_{12}N_6S$ (MW: 332.38).

3-[6-(2,3-Dihydro-benzo[1,4]dioxin-6-yl)-imidazo[2,1-b][1,3,4]thiadiazol-2-yl]-1-methyl-1H-pyrrolo[2,3-b]pyridine(25m)

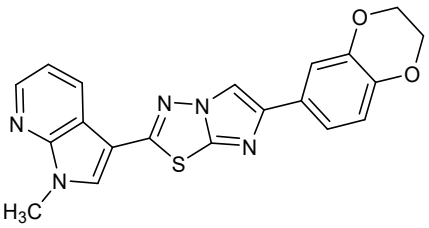

Yield: 28 %; white solid; m.p.: 257 °C; ^{1}H NMR (200 MHz, DMSO) δ 3.94 (3H, s, CH_3), 4.31 (4H, d, J = 4.3 Hz, CH_2), 5.87 (1H, s, Ar), 7.43 – 7.29 (3H, m, Ar), 8.50 – 8.40 (2H, m, Ar), 8.55 (1H, s, Ar), 8.60 (1H, s, Ar). ^{13}C NMR (50 MHz, DMSO) δ 31.99 (q), 64.62 (t), 104.54 (s), 110.32 (d), 113.74 (d), 117.04 (s), 117.76 (d), 118.26 (d), 118.45(d), 119.71 (d), 127.46 (s), 129.55 (d), 133.46 (d), 143.40 (s), 144.01 (s), 144.72 (s), 144.97 (d), 148.20 (s), 156.70 (s). Anal. Calculated for $C_{20}H_{15}N_5O_2S$ (MW: 389.43).

3-(6-Furan-2-yl-imidazo[2,1-b][1,3,4]thiadiazol-2-yl)-1-methyl-1H-pyrrolo[2,3-b]pyridine (25n)

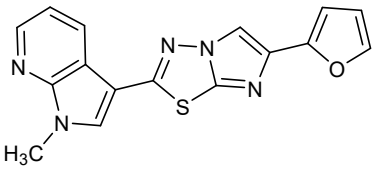

Yield: 45 %; brown solid; m.p.: 221 °C; ^{1}H NMR (200 MHz, DMSO) δ 3.91 (3H, s, CH_3), 6.59 (1H, dd, J = 3.2, 1.8 Hz, Ar), 6.70 (1H, d, J = 3.2 Hz, Ar), 7.37 (1H, dd, J = 7.8, 4.7 Hz, Ar), 7.70 (1H, d, J = 0.8 Hz, Ar), 8.40 (1H, s, Ar), 8.47 (2H, dd, J = 9.7, 2.1 Hz, Ar), 8.55 (1H, s, Ar). Anal. Calculated for $C_{16}H_{11}N_5OS$ (MW: 321.36).

3-[6-(3-Methoxy-phenyl)-imidazo[2,1-b][1,3,4]thiadiazol-2-yl]-1-methyl-1H-pyrrolo[2,3-b]pyridine (25o)

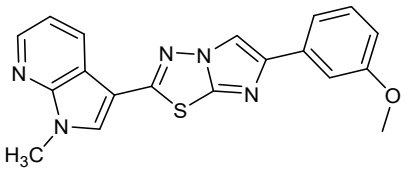

Yield: 30 %; off-white solid; m.p.: 249 °C; ^{1}H NMR (200 MHz, DMSO) δ 3.81 (3H, s, CH_3), 3.90 (3H, s, CH_3), 6.87 (1H, d, J = 8.0 Hz, Ar), 7.40 – 7.27 (2H, m, Ar), 7.43 (2H, m, Ar), 8.46 (2H, d, *J* = 6.9 Hz, Ar), 8.54 (1H, s, Ar), 8.72 (1H, s, Ar). Anal. Calculated for $C_{19}H_{15}N_5OS$(MW: 361.42).

General procedure for the synthesis of 5-Thiazol-4-yl-[1,3,4]thiadiazol-2-ylamine(70)

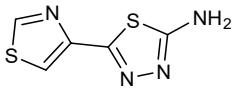

A mixture of commercial 1,3-thiazole-4-carboxylic acid 4 (25mmol) and thiosemicarbazone (25mmol) in $POCl_3$(7ml) was stirred vigorously at 75°C for 0.5h. After addition of H_2O (30ml), the reaction mixture was heated under reflux for 4h and basified to pH 8 by 50% NaOH solution. The mixture was filtered and the filter cake was purified by column chromatography (PE/EA 9:1)

Analytical and spectroscopic data for the derivative **70** are in accordance to those reported in literature.[259]

General procedure for the synthesis of 6-Phenyl-2-thiazol-4-yl-imidazo[2,1-b][1,3,4]thiadiazole 26

A mixture of 5-Thiazol-4-yl-[1,3,4]thiadiazol-2-ylamine(70) (0.92 mmol) and the suitable α-bromoacetyl derivatives (0.92 mmol) in 30 mL of anhydrous ethanol was stirred at reflux for 24 h. After cooling at room temperature, the desired products **26** were filtered off and washed with cold ethanol.

6-(4-Fluoro-phenyl)-2-thiazol-4-yl-imidazo[2,1-b][1,3,4]thiadiazole (26a)

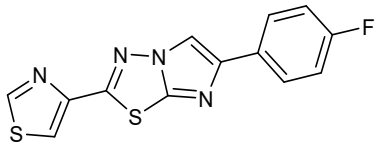

Yield: 40 %; yellow solid; m.p.: 290 °C; ^{1}H NMR (200 MHz, DMSO-d6) δ: 7.25 (2H, d, J = 7.0 Hz, Ar), 7.92 (2H, d, J = 5.4 Hz, Ar), 8.63 (1H, s, Ar), 8.73 (1H, d, J = 1.1 Hz, Ar), 9.35 (1H, s, Ar). ^{13}C NMR (50 MHz, DMSO-d6) 110.87 (d), 113.14 (s), 115.94 (d), 116.22 (d), 119.65 (s), 121.05 (d), 126.41 (s), 127.09 (d), 127.19 (d), 130.82 (s), 131.46 (s), 145.24 (s). Anal. Calculated for $C_{13}H_7FN_4S_2$ (MW 302.35).

6-(2,5-Dimethoxy-phenyl)-2-thiazol-4-yl-imidazo[2,1-b][1,3,4]thiadiazole (26b)

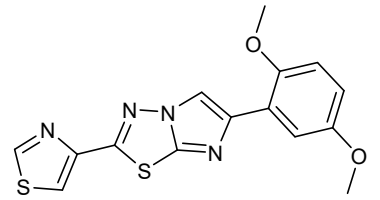

Yield: 33 %; grey solid; m.p.: 220 °C; ^{1}H NMR (200 MHz, DMSO-d6) δ: 3.76 (3H, s, CH_3), 3.91 (3H, s, CH_3), 6.85 (1H, dd, J = 8.9, 3.0 Hz, Ar), 7.04 (1H, d, J = 9.0 Hz, Ar), 7.73 (1H, d, *J* = 3.0 Hz, Ar), 8.50 (1H, s, Ar), 8.50 (1H, s, Ar), 9.35 (1H, s, Ar). Anal. Calculated for $C_{15}H_{12}N_4O_2S_2$ (MW 344.41)

6-(3-Methoxy-phenyl)-2-thiazol-4-yl-imidazo[2,1-b][1,3,4]thiadiazole (26c)

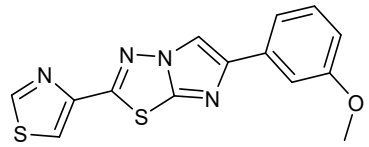

Yield 34: %; light brown solid; m.p.: 236°C; ^{1}H NMR (200 MHz, DMSO-d6) δ: 3.85 (3H, s, CH_3), 6.90 (1H, d, J = 6.7 Hz, Ar), 7.36 (1H, d, J = 8.2 Hz, Ar), 7.36 (1H, d, J = 8.2 Hz, Ar), 7.51 (1H, m, Ar), 8.66 (1H, s, 1 Ar), 8.79 (1H, s, Ar), 9.38 (1H, s, Ar). ^{13}C NMR (50 MHz, DMSO-d6) δ :55.58 (q), 110.52 (d), 111.29 (d), 113.59 (d), 117.64 (d), 121.05 (d), 130.28 (d), 135.67 (s), 137.19 (d), 145.01 (s), 145.50 (s), 146.00 (s), 160.14 (s), 187.51 (s). Anal. Calculated for $C_{14}H_{10}N_4OS_2$ (MW 314.39)

2-Thiazol-4-yl-6-thiophen-3-yl-imidazo[2,1-b][1,3,4]thiadiazole (26d)

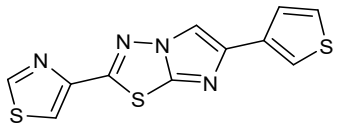

Yield: 40 %; brown solid; m.p.: 249°C; ^{1}H NMR (200 MHz, DMSO-d6) δ: 7.55 (1H, d, J = 5.0 Hz, Ar), 7.61 (1H, dd, J = 4.6, 3.1 Hz, Ar), 7.79 (1H, d, J = 2.7 Hz, Ar), 8.56 (1H, s, Ar), 8.60 (1H, s, Ar), 9.34 (1H, s, Ar).^{13}C NMR (50 MHz, DMSO-d6) δ: 110.69 (d), 120.47(s), 120.52 (d), 120.92 (d), 123.53 (s), 126.08 (d), 127.32 (d), 136.22(s), 142.25 (d), 142.90 (s), 145.51 (s). Anal. Calculated for $C_{11}H_6N_4S_3$ (MW 290.39).

2-Thiazol-4-yl-6-(4-trifluoromethyl-phenyl)-imidazo[2,1-b][1,3,4]thiadiazole (26e)

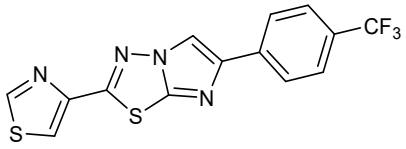

Yield: 52%; pale yellow solid; m.p.: 288 °C; ^{1}H NMR (200 MHz, DMSO-d6) δ: 7.81 (2H, d, J = 4.1 Hz, Ar), 8.13 (2H, d, J = 5.4 Hz, Ar), 8.67 (1H, s, Ar), 8. 95 (1H, s, Ar), 9.37 (1H, s, Ar). ^{13}C NMR (50 MHz, DMSO-d6) δ: 108.51 (s), 114.34 (d), 121.35 (s), 121.47 (d), 125.59 (s), 126.11 (s), 126.55 (d), 132.76 (d), 133.77

(d), 136.87 (d), 139.53 (s), 141.03 (s). Anal. Calculated for $C_{14}H_7N_4S_2$ (MW 352.36).

General procedure for the synthesis of 3-(6-Aryl-2-yl-imidazo[2,1-b][1,3,4]thiadiazol-2-yl)-1H-indole 27

A mixture of 5-(1H-Indol-3-yl)-[1,3,4]thiadiazol-2-ylamine (0.92 mmol) and the suitable α-bromoacetyl derivatives **66** or **68** (0.92 mmol) in 30 mL of anhydrous ethanol was stirred at reflux for 24 h. After cooling at room temperature, the desired products **27a-t** were filtered off and washed with cold ethanol.

3-(6-Furan-2-yl-imidazo[2,1-b][1,3,4]thiadiazol-2-yl)-1H-indole (27a)

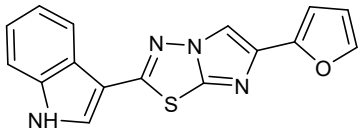

Yield: 22 %; white solid; m.p.: 218 °C; IR (cm^{-1}) 3152; ^1H NMR (200 MHz, DMSO-d6) δ: 6.59 (1H, d, J = 1.3 Hz, Ar), 6.71 (1H, d, J = 3.4 Hz, Ar), 7.34 – 7.25 (2H, m, Ar), 7.55 (1H, dd, J = 6.8, 2.7 Hz, Ar), 7.70 (1H, d, *J* = 2.1 Hz, Ar), 8.18 (1H, dd, *J* = 4.9, 2.6 Hz, Ar), 8.33 (1H, d, *J* = 2.8 Hz, Ar), 8.41 (1H, d, *J* = 4.3 Hz, Ar), 12.14 (1H, s,NH). ^{13}C NMR (50 MHz, DMSO-d6) δ: 105.62 (d), 106.99 (s), 110.22 (d), 112.07 (d), 113.05 (d), 120.86 (d), 121.98 (d), 123.70 (d), 124.24 (s), 129.97 (d), 137.19 (s), 137.61 (s), 142.38 (d), 143.84 (s), 149.73 (s), 157.84 (s). Anal. Calculated for $C_{16}H_{10}N_4OS$ (MW: 306.34).

3-(6-Furan-2-yl-imidazo[2,1-b][1,3,4]thiadiazol-2-yl)-5-methoxy-1H-indole (27b)

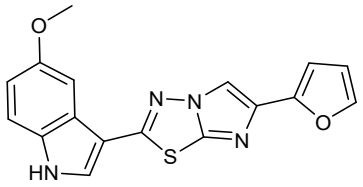

Yield: 20 %; yellow solid; m.p.: 252 °C; IR (cm^{-1}) 3147; ^1H NMR (200 MHz, DMSO-d6) δ: 6.58 (1H, dd, *J* = 3.2, 1.7 Hz, Ar), 6.69 (1H, d, *J* = 3.2 Hz, Ar), 6.94 (1H, dd, J = 8.8, 2.4 Hz, Ar), 7.44 (1,H, d, *J* = 8.8 Hz, Ar), 7.64 (1H, d, *J* = 2.3 Hz, Ar), 7.69 (1H, d, *J* = 0.7 Hz, Ar), 8.24 (1H, d, J = 3.0 Hz, Ar), 8.40 (1H, s,

Ar), 11.99 (1H, s, NH). ^{13}C NMR (50 MHz, DMSO-d6) δ: 55.99 (q), 103.01 (d), 105.57 (d), 106.78 (s), 110.27 (d), 112.03 (d), 113.48 (d), 113.80 (d), 124.89 (s), 130.21 (d), 132.19 (s), 137.57 (s), 142.35 (d), 143.75 (s), 149.79 (s), 155.68 (s). Anal. Calculated for $C_{17}H_{12}N_4O_2S$ (MW: 336.37)

5-Bromo-3-(6-furan-2-yl-imidazo[2,1-b][1,3,4]thiadiazol-2-yl)-1H-indole (27c)

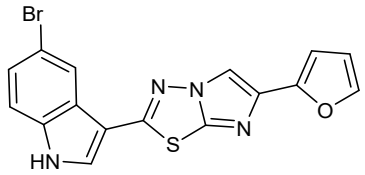

Yield: 35 %; brown solid; m.p.: 285 °C; IR (cm^{-1}) 3147; ^{1}H NMR (200 MHz, DMSO-d6) δ: 6.59 (1H, d, *J* = 1.4 Hz,Ar), 6.69 (1H, d, J = 3.0 Hz, Ar), 7.42 (1H,d, *J* = 7.6 Hz, 1 Ar), 7.52 (1H, dd, *J* = 8.6, 3.2 Hz, Ar), 7.70 (1H, s, Ar), 8.32 (1H, s, Ar), 8.39 (1H, d, *J* = 3.0 Hz, Ar), 8.48 (1H, d, *J* = 3.6 Hz, Ar), 12.31 (1H, s, NH). ^{13}C NMR (50 MHz, DMSO-d6) δ: 105.65 (d), 106.64 (s), 110.42 (d), 112.06 (d), 114.58 (s), 115.11 (d), 123.09 (d), 125.87 (s), 126.33 (d), 130.04 (d), 131.36 (d), 135.97 (s), 137.68 (s), 142.42 (s), 143.75 (s), 149.72 (s), 157.34 (s). Anal. Calculated for $C_{16}H_9BrN_4OS$ (MW: 385.24)

***5-Chloro-3-(6-furan-2-yl-imidazo[2,1-b][1,3,4]thiadiazol-2-yl)-1H-indole* (27d)**

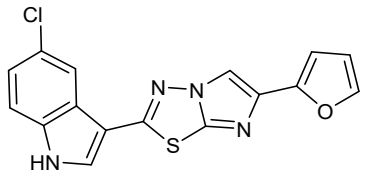

Yield: 28 %; yellow solid; m.p.: 248 °C; IR (cm^{-1}) 3150 (NH); ^{1}H NMR (200 MHz, DMSO-d6) δ: 6.58 (1H, dd, *J* = 3.2, 1.7 Hz, Ar), 6.69 (1H, d, *J* = 3.1 Hz, Ar), 7.31 (1H,dd, J = 8.6, 2.0 Hz, Ar), 7.57 (1H, d, *J* = 8.7 Hz, Ar), 7.57 (1H, d, *J* = 8.7 Hz, Ar), 7.70 (1H, s, Ar), 8.17 (1H, d, *J* = 1.7 Hz, Ar), 8.40 (1H, d, *J* = 3.0 Hz, Ar), 8.46 (1H,d, *J* = 3.5 Hz, Ar), 12.31 (1H,s, Ar). ^{13}C NMR (50 MHz, DMSO-d6) δ: 105.68 (d), 106.76 (s), 107.80 (d), 110.39 (d), 114.59 (s), 114.70 (d), 120.07 (d), 123.77 (d), 125.27 (s), 126.33 (s), 126.62 (s), 131.47 (d), 135.73 (s), 137.67 (s),143.72 (d), 149.70 (s). Anal. Calculated for $C_{16}H_9ClN_4OS$ (MW: 340.79)

5-Fluoro-3-(6-furan-2-yl-imidazo[2,1-b][1,3,4]thiadiazol-2-yl)-1H-indole (27e)

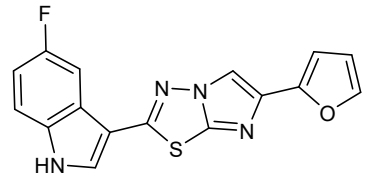

Yield: 40 %; off-white solid; m.p.: 265 °C; IR (cm^{-1}) 3153;^{1}H NMR (200 MHz, DMSO-d6) δ: 6.58 (1H, d, *J* = 1.3 Hz, Ar), 6.69 (1H, d, J = 2.9 Hz, Ar), 7.17 – 7.11 (1H, m, Ar), 7.58 – 7.53 (1H, m, Ar), 7.70 (1H, s, Ar), 7.86 (1H, dd, *J* = 9.5, 1.7 Hz, Ar), 8.39 (1H, d, *J* = 2.8 Hz, Ar), 8.41 (1H, s, Ar), 12.22 (1H, s, NH). ^{13}C NMR (50 MHz, DMSO-d6) δ: 105.64 (d), 105.96 (d), 107.15 (s), 110.29 (d), 111.82 (d), 112.10 (d), 112.71 (s), 114.37 (d), 124.68 (s), 131.59 (d), 133.84 (s), 137.67 (s), 142.39 (d), 149.74 (s), 157.17 (s), 157.50 (s), 160.30 (s), 166.91(s). Anal. Calculated for $C_{16}H_9FN_4OS$ (MW:324.33).

3-(6-Furan-2-yl-imidazo[2,1-b][1,3,4]thiadiazol-2-yl)-1-methyl-1H-indole (27f)

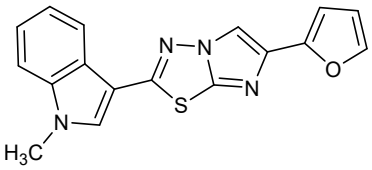

Yield: 36 %; yellow solid; m.p.: 188 °C; ^{1}H NMR (200 MHz, DMSO-d6) δ: 3.90 (3H, s, CH_3), 6.59 (1H, s, Ar), 6.70 (1H, s, Ar), 7.44 – 7.26 (2H, m, Ar), 7.62 (1H, d, J = 7.3 Hz, Ar), 7.71 (1H, s, Ar), 8.18 (1H, d, J = 6.3 Hz, Ar), 8.34 (1H, s, Ar), 8.40 (1H, s, Ar). ^{13}C NMR (50 MHz, DMSO-d6) δ: 33.61 (q), 105.62 (d), 105.93 (s), 110.23 (d), 111.52 (d), 112.07 (d), 121.00 (d), 122.27 (d), 123.74 (d), 124.55 (d), 133.48 (s), 137.70 (s), 142.38 (s), 143.72 (s), 149.75 (s), 157.37 (s). Anal. Calculated for $C_{17}H_{12}N_4OS$ (MW: 320.07)

3-(6-Furan-2-yl-imidazo[2,1-b][1,3,4]thiadiazol-2-yl)-5-methoxy-1-methyl-1H-indole (27g)

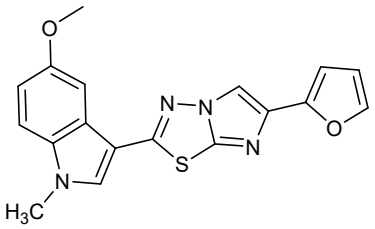

Yield: 38 % ; brown solid; m.p.: 167 °C; ^{1}H NMR (200 MHz, DMSO-d6) δ: 3.86 (6H, s, CH_3), 6.59 (1H, s, Ar), 6.69 (1H, s, Ar), 7.00 (1H, d, *J* = 8.8 Hz, Ar), 7.53 (1H, d, *J* = 9.0 Hz, Ar), 7.64 (1H, s, Ar), 7.70 (1H, s, Ar), 8.26 (1H, s, Ar), 8.39 (1H, s, Ar). ^{13}C NMR (50 MHz, DMSO-d6) δ: 33.76 (q), 56.04 (q), 102.16 (s), 103.21 (d), 105.58 (d), 110.28 (d), 112.04 (d), 112.37 (d), 113.35 (d), 125.20 (s), 132.90 (s), 133.64 (d), 137.55 (s), 141.58 (s), 142.36 (d), 149.76 (s), 155.98 (s), 157.49 (s). Anal. Calculated for $C_{18}H_{14}N_4O_2S$ (MW: 350.39)

5-Bromo-3-(6-furan-2-yl-imidazo[2,1-b][1,3,4]thiadiazol-2-yl)-1-methyl-1H-indole (27h)

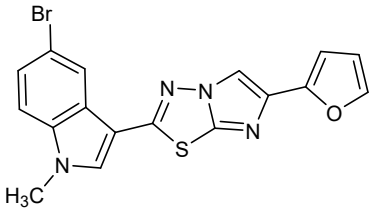

Yield: 35 %; pale yellow solid; m.p.: 245 °C; ^{1}H NMR (200 MHz, DMSO-d6) δ: 3.89 (3H, s, Ar), 6.58 (1H, dd, *J* = 3.0, 1.6 Hz, Ar), 6.69 (1H, d, *J* = 3.1 Hz, Ar), 7.48 (1H, dd, J = 8.7, 1.5 Hz, Ar), 7.60 (1H, d, J = 8.8 Hz, Ar) 7.69 (1H, s, Ar), 8.30 (1H, s, Ar), 8.37 (1H, s, Ar), 8.44 (1H, s, Ar). Anal. Calculated for $C_{17}H_{11}BrN_4OS$ (MW: 399.26).

5-Chloro-3-(6-furan-2-yl-imidazo[2,1-b][1,3,4]thiadiazol-2-yl)-1-methyl-1H-indole (27i)

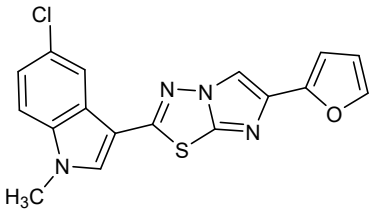

Yield: 38 %; white solid; m.p.: 253 °C; 1H NMR (200 MHz, DMSO-d6) δ: 3.90 (3H, s, CH_3), 6.58 (1H, dd, *J* = 3.0, 1.7 Hz, Ar), 6.69 (1H, d, *J* = 3.0 Hz, Ar), 7. .49 (1H, dd, J = 8.7, 1.5 Hz, Ar),7.65 – 7.56 (1H, m, Ar), 7.68 (1H, d, *J* = 3.4 Hz, Ar), 8.31 (1H, s, Ar), 8.37 (1H, d, J = 4.9 Hz, Ar), 8.42 (1H, d, J = 3.5 Hz, Ar). Anal. Calculated for $C_{17}H_{11}ClN_4OS$ (MW: 354.81).

5-Fluoro-3-(6-furan-2-yl-imidazo[2,1-b][1,3,4]thiadiazol-2-yl)-1-methyl-1H-indole (27j)

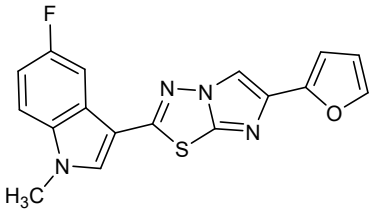

Yield: 45%; off-white solid; m.p.: 246 °C; ^{1}H NMR (200 MHz, DMSO-d6) δ: 6.58 (1H, s, Ar), 6.69 (1H, d, J = 3.0 Hz, Ar), 7.22 (1H, td, *J* = 9.1, 2.0 Hz, Ar), 7.64 (1H, dd, *J* = 9.0, 4.4 Hz, Ar), 7.69 (1H, s, Ar), 7.85 (1H, dd, *J* = 9.7, 2.0 Hz, Ar), 8.37 (1H, s, Ar), 8.44 (1H, s, Ar). ^{13}C NMR (50 MHz, DMSO-d6) δ: 33.92 (q), 105.64 (d), 105.81 (d), 105.93 (s), 106.14 (d), 110.29 (d), 111.77 (d),112.08 (d), 113.04 (d), 134.48 (s), 134.96 (d), 137.67 (s), 142.39 (d), 149.73 (s), 157.03 (s), 157.45 (s), 160.57 (s). Anal. Calculated for $C_{17}H_{11}FN_4OS$ (MW: 338.36).

3-[6-(2,3-Dihydro-benzo[1,4]dioxin-6-yl)-imidazo[2,1-b][1,3,4]thiadiazol-2-yl]-1H-indole (27k)

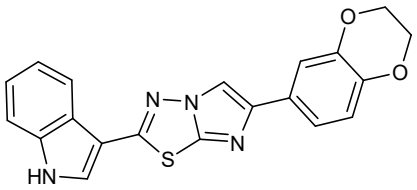

Yield: 40 %; yellow solid; m.p.: 230 °C (dec); IR (cm^{-1}): 3020 (NH); ^{1}H NMR (200 MHz, DMSO-d6) δ: 4.28 (4H, s, CH_2), 6.94 (1H, d, J = 8.2 Hz, Ar), 7.30 (2H, dd, J = 9.3, 5.6 Hz, Ar), 7.37 (1H, d, J = 6.6 Hz, Ar), 7.55 (1H, d, J = 6.4 Hz, Ar), 8.15 (1H, d, J = 5.4 Hz, Ar), 8.40 (1H, s, Ar), 8.71 (1H, s, Ar), 12.21 (1H, s, NH).^{13}C NMR (50MHz,DMSO-d6)δ: 64.61 (t), 64.66 (t), 106.63 (s), 106.87 (s), 110.53 (d), 113.10 (d), 113.88 (d), 115.12 (d), 117.74 (d), 118.37 (d), 119.70 (d), 120.78 (d), 122.11 (d), 123.77 (d), 124.25 (d), 126.13 (s), 126.70 (s), 130.25 (d), 130.35 (d), 137.21 (s), 142.95 (s), 143.74 (s), 144.08 (s). Anal. Calculated for $C_{20}H_{14}N_4OS$ (MW 374.42)

3-[6-(2,3-Dihydro-benzo[1,4]dioxin-6-yl)-imidazo[2,1-b][1,3,4]thiadiazol-2-yl]-5-methoxy-1H-indole (27l)

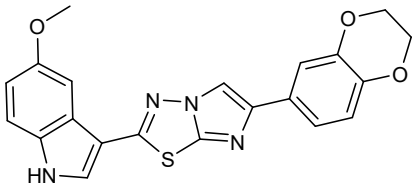

Yield: 47 %; off-white solid; m.p.: 265 °C (dec); IR (cm^{-1}): 3197 (NH); ^{1}H NMR (200 MHz, DMSO-d6) δ: 3.85 (3H, d, *J* = 2.6 Hz, CH_3), 4.27 (4H, s, CH_2), 6.98 – 6.86 (2H, m, Ar), 7.35 (2h, dd, *J* = 7.7, 2.5 Hz, Ar), 7.44 (1H, dd, *J* = 8.8, 2.5 Hz, Ar), 7.63 (1H, s, Ar), 8.23 (1H, s, Ar), 8.59 (1H, d, *J* = 2.7 Hz, Ar), 11.98 (1H, s, Ar). ^{13}C NMR (50 MHz, DMSO-d6) δ: 55.90 (2xq) ,64.59 (2xt), 102.77 (d), 106.85 (s), 110.23 (d), 113.54 (d), 113.60 (d), 113.80 (d), 117.71 (d), 118.12 (d), 124.86 (s), 128.04 (s), 130.04 (d), 132.14 (s), 143.04 (s), 143.18 (s), 143.96 (s), 144.87 (s), 155.62 (s), 157.50 (s).Anal. Calculated for $C_{21}H_{16}N_4O_3S$ (MW 404.44).

5-Bromo-3-[6-(2,3-dihydro-benzo[1,4]dioxin-6-yl)-imidazo[2,1-b][1,3,4]thiadiazol-2-yl]-1H-indole (27m)

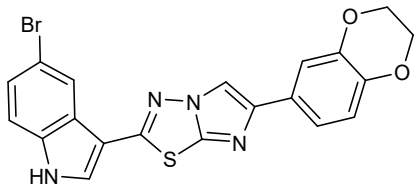

Yield: 31 %; light brown solid; m.p.: 327 °C (dec); IR (cm^{-1}): 3142 (NH);^{1}H NMR (200 MHz, DMSO-d6) δ: 4.27 (4H, s, CH_2), 6.89 (1H, d, J = 8.0 Hz, Ar), 7.32 (1H, s, Ar), 7.35 (1H, s, Ar), 7.42 (1H, d, J = 8.6 Hz, Ar), 7.51 (1H, d, J = 8.6 Hz,Ar), 8.32 (1H, s, Ar), 8.37 (1H, d, J = 1.3 Hz, Ar), 8.64 (1H, s, Ar), 12.21 (1H, s, NH). ^{13}C NMR (50 MHz, DMSO-d6) δ: 64.5 2(2xt), 106.74 (s), 110.30 (d), 113.58 (s), 114.51 (s),115.08 (d), 117.72 (d), 118.10 (d), 123.11 (d), 125.47 (s), 126.26 (d), 128.08 (s), 131.09 (d), 135.95 (s), 143.20 (s), 143.97 (s), 145.16 (s), 156.78 (s). Anal. Calculated for $C_{20}H_{13}BrN_4OS$ (MW 351.99).

5-Chloro-3-[6-(2,3-dihydro-benzo[1,4]dioxin-6-yl)-imidazo[2,1-b][1,3,4]thiadiazol-2-yl]-1H-indole (27n)

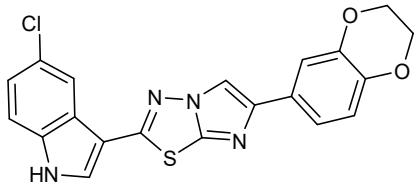

Yield: 44 %; yellow solid; m.p.: 340 °C (dec); IR (cm^{-1}): 3136 (NH);^{1}H NMR (200 MHz, DMSO-d6) δ: 4.28 (4H, s, CH_2), 6.91 (1H, d, J = 7.5 Hz, Ar), 7.43 – 7.27 (3H, m, Ar), 7.57 (1H, d, J = 7.6 Hz,Ar), 8.17 (1H, s, Ar), 8.40 (1H, s, Ar), 8.65 (1H, s, Ar), 12.30 (1H, s, NH). ^{13}C NMR (50 MHz, DMSO-d6) δ: 31.96 (t), 104.51 (s), 110.91 (d), 115.72 (d), 116.15 (d), 117.00 (s), 118.43 (d), 126.87 (s), 126.97 (d), 129.54 (d), 130.79 (s), 133.49 (d), 143.43 (s), 144.28 (s), 144.93 (d), 148.14 (s), 156.84 (s), 160.31 (s), 163.54 (s). Anal. Calculated for $C_{20}H_{13}ClN_4O_2S$ (MW 408.86).

3-[6-(2,3-Dihydro-benzo[1,4]dioxin-6-yl)-imidazo[2,1-b][1,3,4]thiadiazol-2-yl]-5-fluoro-1H-indole (27o)

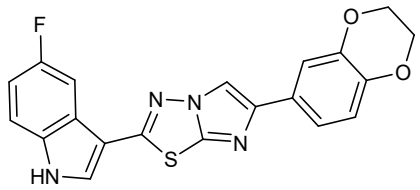

Yield: 50 %; beige solid; m.p.: 330 °C (dec); IR (cm^{-1}): 3193 (NH);^{1}H NMR (200 MHz, DMSO-d6) δ: 4.28 (4H, s, CH_2), 6.90 (1H, d, J = 8.0 Hz, Ar), 7.16 (1H, t, J = 8.5 Hz, Ar), 7.35 (2H, d, J = 8.5 Hz, Ar), 7.56 (1H, dd, J = 8.5, 4.2 Hz, Ar), 7.84 (1H, d, J = 9.8 Hz, Ar), 8.37 (1H, s, Ar), 8.59 (1H, s, Ar), 12.21 (1H, s, NH).^{13}C NMR (50 MHz, DMSO-d6)δ: 64.59 (t), 105.77 (d), 107.24 (s), 110.22 (d), 111.96 (d), 113.60 (d), 114.35 (d), 117.71 (d), 118.13 (d), 124.53 (s), 128.09 (s), 131.43 (d), 133.83 (s), 143.19 (s), 143.97 (s), 145.11 (s), 156.98 (s), 157.14 (s), 160.25 (s). Anal. Calculated for $C_{20}H_{13}FN_4O_2S$ (MW 392.41).

3-[6-(2,3-Dihydro-benzo[1,4]dioxin-6-yl)-imidazo[2,1-b][1,3,4]thiadiazol-2-yl]-1-methyl-1H-indole(27p)

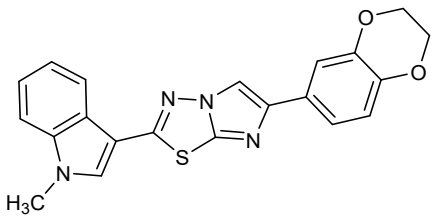

Yield: 38 %; light brown solid; m.p.: 230 °C (dec); ^{1}H NMR (200 MHz, DMSO-d6) δ: 3.90 (3H, s, CH_3), 4.29 (4H,s, CH_2), 6.94 (1H, d, *J* = 8.3 Hz, Ar), 7.35 (4H, dq, J = 13.1, 6.5 Hz, Ar), 7.62 (1H, d, J = 7.4 Hz, Ar), 8.14 (1H, dd, J = 6.6, 1.6 Hz, Ar), 8.40 (1H, s, Ar),8.69 (1H, s, Ar),9.67 (1H, s, Ar). ^{13}C NMR (50 MHz, DMSO-d6) δ: 33.61 (q), 105.62 (d), 105.93 (s), 110.23 (d), 111.52 (d), 112.07 (d), 121.00 (d), 122.27 (d), 123.74 (d), 124.55 (s), 133.48 (d), 137.64 (s), 137.74 (d), 142.38 (s), 149.75 (s), 157.37(s). Anal. Calculated for $C_{19}H_{16}N_4O_2S$ (MW 388.44).

3-[6-(2,3-Dihydro-benzo[1,4]dioxin-6-yl)-imidazo[2,1-b][1,3,4]thiadiazol-2-yl]-5-methoxy-1-methyl-1H-indole (27q)

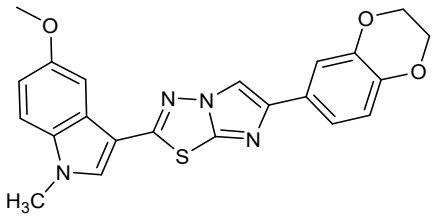

Yield: 27 %; light brown solid; m.p.: 238 °C (dec); ^{1}H NMR (200 MHz, DMSO-d6) δ: 3.86 (6H, s, CH_3), 4.27 (4H, s, CH_2), 6.88 (1H, d, *J* = 8.3 Hz, Ar), 6.99 (1H, dd, J = 8.9, 2.2 Hz, Ar), 7.35 (2H, d, *J* = 7.9 Hz, Ar), 7.51 (1H, d, *J* = 8.9 Hz, Ar), 7.62 (1H, d, *J* = 2.1 Hz, Ar), 8.22 (1H, s, Ar), 8.55 (1H, s, Ar). ^{13}C NMR (50 MHz, DMSO-d6) δ: 33.71 (q), 55.95 (q), 64.60 (d), 102.98 (d), 105.65 (s), 110.21 (d), 112.36 (d), 113.40 (d), 113.59 (d), 117.69 (d), 118.11 (d), 125.17 (s), 128.15 (s), 132.86 (s), 133.45 (s), 143.15 (s), 143.96 (s), 145.00 (s), 155.91 (s), 156.96 (s). Anal. Calculated for $C_{22}H_{18}N_4O_3S$ (MW 418.47)

3-[6-(2,3-Dihydro-benzo[1,4]dioxin-6-yl)-imidazo[2,1-b][1,3,4]thiadiazol-2-yl]-5-fluoro-1-methyl-1H-indole (27r)

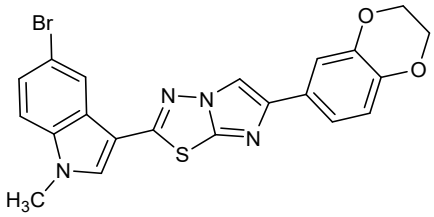

Yield: 35 %; yellow solid; m.p.: 257 °C (dec); ^{1}H NMR (200 MHz, DMSO-d6) δ: 3.88 (3H, s, CH_3) 4.28 (4H, s, CH_2), 6.88 (1H, d, *J* = 8.2 Hz,Ar), 7.33 (1H, d, J = 7.8 Hz, Ar), 7.47 (1H, d, *J* = 8.7 Hz, Ar), 7.59 (1H, d, *J* = 8.7 Hz, Ar), 8.31 (1H, d, J = 9.7 Hz, Ar), 8.58 (1H, s, Ar). Anal. Calculated for $C_{21}H_{15}BrN_4O_2S$ (MW 467.34).

5-Chloro-3-[6-(2,3-dihydro-benzo[1,4]dioxin-6-yl)-imidazo[2,1-b][1,3,4]thiadiazol-2-yl]-1-methyl-1H-indole (27s)

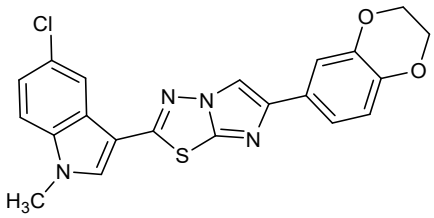

Yield: 44%; brown solid; m.p.: 270 °C (dec); ^{1}H NMR (200 MHz, DMSO-d6) δ: 3.88 (3H, s, CH_3), 4.27 (4H, s, CH_2), 6.89 (1H, d, *J* = 8.1 Hz, Ar), 7.34 (3H, m, Ar), 7.64 (1H, d, *J* = 8.7 Hz, Ar), 8.13 (1H, s, Ar), 8.36 (1H, s, Ar), 8.59 (1H, s, Ar). Anal. Calculated for $C_{21}H_{15}ClN_4O_2S$ (MW 322.89).

3-[6-(2,3-Dihydro-benzo[1,4]dioxin-6-yl)-imidazo[2,1-b][1,3,4]thiadiazol-2-yl]-5-fluoro-1-methyl-1H-indole (27t)

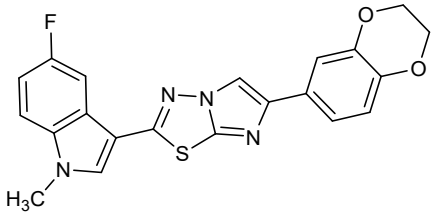

Yield: 55%; beige solid; m.p: 271 °C (dec); ^{1}H NMR (200 MHz, DMSO-d6) δ: 3.89 (3H, s, CH_3) 4.28 (4H, s, CH_2), 6.89 (1H, d, J = 8.0 Hz, Ar), 7.22 (1H, t, J = 8.5 Hz, Ar), 7.35 (1H, s, Ar), 7.63 (1H, dd, *J* = 8.1, 3.7 Hz,Ar), 7.82 (1H,d, J = 9.4 Hz, Ar), 8.35 (1H, s, Ar), 8.54 (1H, s, Ar). ^{13}C NMR (50 MHz, DMSO-d6) δ: 33.92 (q), 105.64 (d), 105.93 (s), 106.14 (d), 110.29 (d), 111.77 (d), 112.04 (d), 113.11 (d), 114.55 (s), 124.94 (s), 134.48(d), 134.96 (s), 137.67(d), 142.39 (s), 143.65 (s), 149.73 (s), 157.03 (s), 157.45 (s),160.57 (s). Anal. Calculated for $C_{21}H_{15}FN_4O_2S$ (MW 406.43).

Biology

Drugs and chemicals.

The synthesized compounds **27** were dissolved in DMSO. The medium, foetal bovine serum (FBS), penicillin (50 IU mL^{-1}) and streptomycin (50 mg mL^{-1}) were from Gibco (Gaithersburg, MD, USA). All other chemicals were from Sigma (Zwijndrecht, the Netherlands).

Cell culture

The cells were cultured in RPMI-1640 (Roswell Park Memorial Institute 1640) supplemented with 10% heat-inactivated FBS, 1% penicillin/streptomycin, or in DMEM (Dulbecco's Modified Eagle's Medium), supplemented with 10% heat-inactivated FBS, 1% HEPES. The cells were kept in a humidified atmosphere of 5% CO2 and 95% air at 37 °C and harvested with trypsin-EDTA. All the PDAC cells, i.e., Panc-1GR, SUIT-2 and PDAC-3, but also Panc-1, Capan-1, Patu-T, BxPC-3 cells were selected for the wound-healing assay because in all these cells the exposure for 24 h with our compounds did not result in pro-apoptotic or necrotic effects, allowing a reliable analysis of the results.

Viability assay *in vitro*

The evaluation of the cytotoxic activity of the two series of imidazothiadiazoles derivatives **27a-t** against differentiated pancreatic cancer cells was determined by the sulforhodamine B (SRB) chemosensitivity assay.

Cells were seeded into a 96-well flat-bottom plates in triplicate in a volume of 100 µL (3 x 10^3 cells/well for SUIT-2, Panc-1, Panc-1GR, Patu-T, and PDAC-3 cell lines, 4 x 10^3 cells/well for BxPC-3 cells, 5 x 10^3 cells/well for Capan-1 cells, and 8 x 10^3 cells/well for Hs27 cells) and incubated for 24 h at 37 °C to create a confluent monolayer. Then, the cells were treated with 100 µL of the compounds dissolved in DMSO at different concentration for 72 h at 37 °C, 5% CO2 and 100% humidity. At the end of incubation period, the cells were fixed with 25 µL of 50% cold trichloroacetic acid (TCA) and kept for at least 60 min at 4 °C. Then, the plates were emptied and washed gently with deionized water, dried at room

temperature (RT) overnight. and stained with 50 µL of 0.4% SRB solution in 1% acetic acid for 15 min at RT. The excess of SRB stain was removed and the plates were washed with a 1% acetic acid solution and let dry at RT overnight. The SRB staining was dissolved in 150 µL of tris(hydroxymethyl)aminomethane solution pH = 8.8 (TRIS base), and the absorbance was measured at wavelengths of 490 nm and 540 nm. Cell growth inhibition was calculated as the percentage of drug treated cells versus vehicle-treated cells ("untreated cells or control") OD (corrected for OD before drug addiction, "day-0"). The comparison of the average optical density of the growth in control wells with that in the sample wells allowed estimating the percentage of cell growth, using the following equation:

% Cell Growth = [(mean ODcompound – mean ODday zero plate)/ mean (ODcontrol cells – mean ODday zero plate)]x100

The results obtained were adjusted by the day zero plate (wells containing cells growing for only 24 hours) and normalized by the control cells (wells with untreated cells) to obtain the rate of viable cells. The 50% inhibitory concentration of cell growth (IC_{50}) was calculated by non-linear least squares curve fitting (GraphPad PRISM, Intuitive Software for Science, San Diego, CA). In the NCI protocol IC_{50} is named GI_{50} (50% growth inhibitory concentration). Data is expressed as mean values ± SEM.

Firstly, cells were exposed to three screening concentrations (0.1 µM, 1 µM, 10 µM) of each compound **27** for 72 hours, and the amount of proliferation was then determined by the sulforhodamine B (SRB) chemosensitivity assay. SRB assay was employed to determine IC_{50} on each PDAC cell line. Cells were treated with eight increasing concentrations (from 0.1 µM to 40 µM) of **27a, 27e, 27f,** and **27s** compounds for 72 hours. The antitumor activity of compounds was measured, using the IC_{50} values, thus the concentration of a compound required to produce 50% growth inhibition relative to the control.

Cell cycle assay

Cell cycle stage was analysed by flow cytometry. Cells were seeded in 6 wells plate (2.5 x 10^5cells/well). After an overnight incubation at 37 °C, the cells were

treated with the compounds **27f** at two concentrations (i.e. 2µM and 4xIC_{50}), and incubated for 24 hours. Drug concentrations were chosen because of the respective IC_{50} values. After treatment, the cells were harvested by trypsinization (0.3 µl/well of trypsin-EDTA), incubated until the cells were detached; cells were resuspended with 1.7ml of medium and collected into FACS tubes. The samples were then centrifuged in order to get cells pellet (5 min at 1200 rpm). Finally, these pellets were fixed in ice-cold 70% ethanol, washed twice with phosphate-buffered saline (20 mM sodium phosphate pH 7.4, 150 mM NaCl) and incubated for 30 min at 37 °C with 50 µl of RNase (100 µg/ml) followed by incubation with 200 µl of propidium iodide solution (PI, 50 µg/ml). The cycle analysis was performed on the FACS (Fluorescence Activated Cell Sorting) Calibur instrument, to evaluate the effects on the cell cycle distribution and cell viability.

Wound healing assay

Cell migration was assessed using a wound healing assay. A total of 5 x 10^4 cells/well were seeded in a 96-well plate and incubated overnight atmosphere of 5% CO_2 and 95% air at 37 °C to form confluent monolayer. Gaps or scratch were created in confluent cell layers using the scratch tool. The detached cell following scratch induction were removed and fresh medium was added to the wells. Cells were next treated at 4xIC_{50} concentration with **27a** and **27f**. After treatment, cells were kept in atmosphere of 5% CO_2 and 95% air at 37 °C. The wound closure was monitored by phase-contrast microscopy and photographed immediately after scratch (T=0) and after 4h, 8h, 20h and 24h. Pictures of the plates were taken using the Universal Grab 6.3 software (DCILabs) from a computer connected to a Leica microscope with a JAI TMC-1327 camera. The percentage of migration was calculated using the following equation:

$\%\ Migration$ = [(Width of the wound at T = 0 − Width of the wound at T = X)/ (Width of the wound at T = 0)]x 100

PamGene array

A PamChip array with 144 kinase peptides substrates was used to test the change in tyrosine kinase activity when using the **27f** compound. This experiment was performed with SUIT-2 and PDAC-3 cells in biological triplicates (three untreated samples and three treated samples with **27f** compound), as described previously.[260]

Cells were grown in 25 cm^2 flasks until they reached 80% of confluence, at 37 °C and 5% of CO2, then both cells line were treated with 5xIC_{50} of **27f**, and the medium of control cells was replaced with fresh medium. Treatment lasted 2 h, and then cells were detached, and 10^6 cells/ml were collected from each replicate in 1.5 mL tubes. Cells were lysed with 100 µL x 10^6 cells of M-PER lysis buffer containing: M-PER Mammalian Extraction Buffer (Thermo Scientific, Rockford, IL, USA), Halt protease Inhibitor cocktail, EDTA free (Complete Mini EDTA-free Protease Inhibitor Cocktail, Roche #11836170001), Halt Phosphatase Inhibitor Cocktail (Thermo Fisher #78420) both diluted 1:100, for at least 15 min at 4 °C. The lysates were collected in 1.5 mL tubes, which were centrifuged (at 4 °C, 16000g) for 15 min, and the supernatants were collected and stored at -80 °C until use. Protein concentration of the samples was determined using Bio-Rad protein Assay, based on the method of Bradford (BioRad, Hercules, CA)

The PamChips were prepared in order to reach a concentration of 10 mg protein/array, and they were added to the MasterMix (PamGene reagent kit 32116) containing: PTK buffer 10x, BSA solution 100x, PTK additive 10x, 1 M DTT solution, Complete Mini EDTA-free Protease Inhibitor Cocktail, Halt Phosphatase Inhibitor Cocktail 400x (Thermo Fisher), PY-20-FITC (fluorescent labelled antibody), 4 mM ATP solution. Samples were added to the MasterMix immediately prior to loading on the chip. Before loading the samples, the PamStation®12 instrument performed a blocking step with 25 µL of 2% BSA on each array followed by three wash steps with PTK buffer, then 40 µL of each sample mix was loaded in duplicate onto the arrays. During incubation at 30 °C, the sample mix was pumped up and down through the array once per minute for 60 cycles. Repeated fluorescent imaging of each array was performed with a 12-

bit CCD camera, monitoring fluorescence intensities in real time described micromethod[261].

Minimum inhibitory concentrations (MICs)

The following Gram-positive and Gram-negative bacterial reference strains were used: *S. aureus ATCC 25923, S. aureus ATCC 6538 and S. epidermidis ATCC 12228, P. aeruginosa ATCC 15442* and *E. coli ATCC 25922*. MICs were determined by a previously described micromethod[261]. Briefly, a series of solutions were prepared with a range of concentrations from 100 to 0.75 μg/mL (obtained by two-fold serial dilution). The serial dilutions were made in tryptic soy broth (TSB, VWR International, Leuven) in a 96- wells plate, starting from a stock solution of 1 mg/mL in NaCl 0.9% w/v. A 10 mL volume of a bacterial suspension from a 24 h culture containing ~106 cfu/mL was added to each well. The plate was incubated at 37 C for 24 h; after this time, the MICs were determined using a microplate reader (Glomax Multidetection System TM297 Promega, Milano, Italy) as the lowest concentrations of the studies compounds whose OD, read at 570 nm, was comparable with the negative control wells (broth only, without inoculum). Each assay was performed in triplicate and repeated at least twice.

Inhibition of biofilm formation assay

The inhibitory activities toward biofilm formation of new oxadiazole derivatives were determined by the Crystal Violet Method. Bacteria were grown in tryptic soy broth (TSB, Sigma) containing 2% w/v glucose overnight a 37 °C in a shaking bath. The obtained culture broth was diluted 1:200 to a suspension of 2% w/v of glucose in TSB, with optical density (OD) between 0.020 and 0.040, at 570 nm. 2.5 μl of diluted suspension were added to the wells of polystyrene 96-well tissue culture plates, previously filled with TSB (200 μL) with 2% w/v glucose. In each of these wells, 1μl of stock solution (10 μg / mL) of different compounds were added, in order to obtain the desired concentrations of substance in each well. Each concentration was evaluated in duplicate within the same experiment. The plates were incubated for 24 h at 37 °C. Then, the wells were emptied, washed twice with sterile NaCl 0.9% and stained with 200 μl of 0.1% v/v crystal violet

solution for 15 mins at 37 °C. The excess stain was rinsed off by placing the plates under running tap water and then the plates were air dried overnight. Stained biofilms were rinsed with 200 µl of ethanol for each well, and the optical density (OD) was read at 600 nm, using a microplate reader (GlomaxMultidetection System Promega). Each assay was performed in triplicate and assays were repeated at least twice. The comparison of the average optical density of the growth in control wells with that in the sample wells allowed to estimate the percentage of inhibition of the biofilm formation at the screening concentration of 10 µg/mL, using the following equation:

% of inhibition = [(OD570 growth control - OD570 sample)/ (OD570 growth control)]x100

Anti-biofilm activity against preformed biofilm

A suspension of bacteria (0.5 McFarland standard) was obtained using the procedure described above for the inhibition of biofilm formation test. 2.5 ml of suspension was added to each well of a 96- well plate containing TSB (100 µl) with 2% w/v glucose. After the growth of a biofilm (24 h old), the content of each well was removed, wells were washed up twice with sterile PBS and then filled with fresh TSB medium (200 µl). After that, different concentrations of compounds were added starting from a concentration equal or greater than MIC obtained against planktonic form of tested strains using TSB as medium. The microtiter plate was sealed and incubated at 37 C for further 24 h. The content of each well was removed, wells were washed up twice with sterile PBS (100 µl to each well) and the 96-weel plate was placed at 60 °C for 1 h before staining with a 0.1% w/v crystal violet solution. After 30 min, plates were washed with tap water to remove any excess stain. Biofilm formation was determined by solubilizing crystal violet as above described and the absorbance was read at 540 nm using a microplate reader (Glomax Multidetection System Promega). The percentages of inhibition were calculated with the above-reported. Each assay was performed in triplicate and repeated at least twice.

References

1. Siegel, R. L., Miller, K. D., Fuchs, H. E. & Jemal, A. Cancer Statistics, 2021. *CA. Cancer J. Clin.* **71**, 7–33 (2021).

2. Ferlay J, Ervik M, Lam F, Colombet M, Mery L, Piñeros M, et al. Global Cancer Observatory: Cancer Today. Lyon: International Agency for Research on Cancer; 2020.

3. Siegel, R. L., Miller, K. D., Fuchs, H. E. & Jemal, A. Cancer statistics, 2022. *CA. Cancer J. Clin.* **72**, 7–33 (2022).

4. Sarantis, P., Koustas, E., Papadimitropoulou, A., Papavassiliou, A. G. & Karamouzis, M. V. Pancreatic ductal adenocarcinoma: Treatment hurdles, tumor microenvironment and immunotherapy. *World J. Gastrointest. Oncol.* **12**, 173–181 (2020).

5. Leung, P. S. Physiology of the Pancreas. in *The Renin-Angiotensin System: Current Research Progress in The Pancreas* vol. 690 13–27 (Springer Netherlands, 2010).

6. Yadav, D. & Lowenfels, A. B. The Epidemiology of Pancreatitis and Pancreatic Cancer. *Gastroenterology* **144**, 1252–1261 (2013).

7. Grant, T. J., Hua, K. & Singh, A. Molecular Pathogenesis of Pancreatic Cancer. in *Progress in Molecular Biology and Translational Science* vol. 144 241–275 (Elsevier, 2016).

8. Verbeke, C. S. Endocrine tumours of the pancreas: Endocrine tumours of the pancreas. *Histopathology* **56**, 669–682 (2010).

9. Chen, X., Zeh, H. J., Kang, R., Kroemer, G. & Tang, D. Cell death in pancreatic cancer: from pathogenesis to therapy. *Nat. Rev. Gastroenterol. Hepatol.* **18**, 804–823 (2021).

10. Rahib, L. *et al.* Projecting Cancer Incidence and Deaths to 2030: The Unexpected Burden of Thyroid, Liver, and Pancreas Cancers in the United States. *Cancer Res.* **74**, 2913–2921 (2014).

11. Ushio, J. *et al.* Pancreatic Ductal Adenocarcinoma: Epidemiology and Risk Factors. *Diagnostics* **11**, 562 (2021).

12. Lynch, S. M. *et al.* Cigarette Smoking and Pancreatic Cancer: A Pooled Analysis From the Pancreatic Cancer Cohort Consortium. *Am. J. Epidemiol.* **170**, 403–413 (2009).

13. Bosetti, C. *et al.* Diabetes, antidiabetic medications, and pancreatic cancer risk: an analysis from the International Pancreatic Cancer Case-Control Consortium. *Ann. Oncol.* **25**, 2065–2072 (2014).

14. Jeune, F. *et al.* Pancreatic cancer surgical management. *Presse Médicale* **48**, e147–e158 (2019).

15. Mavros, M. N. *et al.* Clinical Trials of Systemic Chemotherapy for Resectable Pancreatic Cancer: A Review. *JAMA Surg.* **156**, 663 (2021).

16. Kaur, S., Baine, M. J., Jain, M., Sasson, A. R. & Batra, S. K. Early diagnosis of pancreatic cancer: challenges and new developments. *Biomark. Med.* **6**, 597–612 (2012).

17. Wang, L., Xie, D. & Wei, D. Pancreatic Acinar-to-Ductal Metaplasia and Pancreatic Cancer. *Methods Mol. Biol. Clifton NJ* **1882**, 299–308 (2019).

18. Hruban, R. H., Maitra, A., Kern, S. E. & Goggins, M. Precursors to Pancreatic Cancer. *Gastroenterol. Clin. North Am.* **36**, 831–849 (2007).

19. Berman, J. J. *et al.* Precancer: a conceptual working definition -- results of a Consensus Conference. *Cancer Detect. Prev.* **30**, 387–394 (2006).

20. Moskaluk, C. A., Hruban, R. H. & Kern, S. E. p16 and K-ras gene mutations in the intraductal precursors of human pancreatic adenocarcinoma. *Cancer Res.* **57**, 2140–2143 (1997).

21. Scarpa, A. *et al.* Pancreatic adenocarcinomas frequently show p53 gene mutations. *Am. J. Pathol.* **142**, 1534–43 (1993).

22. Basturk, O. *et al.* A Revised Classification System and Recommendations From the Baltimore Consensus Meeting for Neoplastic Precursor Lesions in the Pancreas. *Am. J. Surg. Pathol.* **39**, 1730–1741 (2015).

23. Yachida, S. & Iacobuzio-Donahue, C. A. Evolution and dynamics of pancreatic cancer progression. *Oncogene* **32**, 5253–5260 (2013).

24. Kanda, M. *et al.* Presence of somatic mutations in most early-stage pancreatic intraepithelial neoplasia. *Gastroenterology* **142**, 730-733.e9 (2012).

25. Wilentz, R. E. *et al.* Inactivation of the p16 (INK4A) tumor-suppressor gene in pancreatic duct lesions: loss of intranuclear expression. *Cancer Res.* **58**, 4740–4744 (1998).

26. Wilentz, R. E. *et al.* Immunohistochemical labeling for dpc4 mirrors genetic status in pancreatic adenocarcinomas : a new marker of DPC4 inactivation. *Am. J. Pathol.* **156**, 37–43 (2000).

27. Sethi, V., Giri, B., Saluja, A. & Dudeja, V. Insights into the Pathogenesis of Pancreatic Cystic Neoplasms. *Dig. Dis. Sci.* **62**, 1778–1786 (2017).

28. Kleeff, J. *et al.* Pancreatic cancer. *Nat. Rev. Dis. Primer* **2**, 16022 (2016).

29. Janes, M. R. *et al.* Targeting KRAS Mutant Cancers with a Covalent G12C-Specific Inhibitor. *Cell* **172**, 578-589.e17 (2018).

30. Canon, J. *et al.* The clinical KRAS(G12C) inhibitor AMG 510 drives anti-tumour immunity. *Nature* **575**, 217–223 (2019).

31. Gillson, J. *et al.* Small Molecule KRAS Inhibitors: The Future for Targeted Pancreatic Cancer Therapy? *Cancers* **12**, 1341 (2020).

32. Bannoura, S. F., Khan, H. Y. & Azmi, A. S. KRAS G12D targeted therapies for pancreatic cancer: Has the fortress been conquered? *Front. Oncol.* **12**, (2022).

33. Liot, S. *et al.* Stroma Involvement in Pancreatic Ductal Adenocarcinoma: An Overview Focusing on Extracellular Matrix Proteins. *Front. Immunol.* **12**, (2021).

34. Park, W., Chawla, A. & O'Reilly, E. M. Pancreatic Cancer: A Review. *JAMA* **326**, 851 (2021).

35. Ansari, D., Gustafsson, A. & Andersson, R. Update on the management of pancreatic cancer: surgery is not enough. *World J. Gastroenterol.* **21**, 3157–65 (2015).

36. Dumont, R. *et al.* A single center experience in resectable pancreatic ductal adenocarcinoma : the limitations of the surgery-first approach. Critical review of the literature and proposals for practice update. *Acta Gastro-Enterol. Belg.* **80**, 451–461 (2017).

37. Kaur, S. *et al.* A Combination of MUC5AC and CA19-9 Improves the Diagnosis of Pancreatic Cancer: A Multicenter Study. *Am. J. Gastroenterol.* **112**, 172–183 (2017).

38. Miquel, M., Zhang, S. & Pilarsky, C. Pre-clinical Models of Metastasis in Pancreatic Cancer. *Front. Cell Dev. Biol.* **9**, (2021).

39. Elnaggar, M., Giovannetti, E. & J. Peters, G. Molecular Targets of Gemcitabine Action: Rationale for Development of Novel Drugs and Drug Combinations. *Curr. Pharm. Des.* **18**, 2811–2829 (2012).

40. Herting, C. J., Karpovsky, I. & Lesinski, G. B. The tumor microenvironment in pancreatic ductal adenocarcinoma: current perspectives and future directions. *Cancer Metastasis Rev.* **40**, 675–689 (2021).

41. Burris, H. A. *et al.* Improvements in survival and clinical benefit with gemcitabine as first-line therapy for patients with advanced pancreas cancer: a randomized trial. *J. Clin. Oncol.* **15**, 2403–2413 (1997).

42. Plunkett, W. *et al.* Gemcitabine: metabolism, mechanisms of action, and self-potentiation. *Semin. Oncol.* **22**, 3–10 (1995).

43. Bergman, A. M., Pinedo, H. M. & Peters, G. J. Determinants of resistance to 2',2'-difluorodeoxycytidine (gemcitabine). *Drug Resist. Updat.* **5**, 19–33 (2002).

44. Ruiz van Haperen, V. W., Veerman, G., Vermorken, J. B. & Peters, G. J. 2',2'-Difluoro-deoxycytidine (gemcitabine) incorporation into RNA and DNA of tumour cell lines. *Biochem. Pharmacol.* **46**, 762–766 (1993).

45. Mini, E., Nobili, S., Caciagli, B., Landini, I. & Mazzei, T. Cellular pharmacology of gemcitabine. *Ann. Oncol.* **17**, v7–v12 (2006).

46. Conroy, T. *et al.* FOLFIRINOX versus Gemcitabine for Metastatic Pancreatic Cancer. *N. Engl. J. Med.* **364**, 1817–1825 (2011).

47. Hoff, D. D. V. *et al.* Increased Survival in Pancreatic Cancer with nab-Paclitaxel plus Gemcitabine. *N. Engl. J. Med.* **369**, 1691–1703 (2013).

48. Frese, K. K. *et al.* nab-Paclitaxel potentiates gemcitabine activity by reducing cytidine deaminase levels in a mouse model of pancreatic cancer. *Cancer Discov.* **2**, 260–269 (2012).

49. Yardley, D. A. nab-Paclitaxel mechanisms of action and delivery. *J. Controlled Release* **170**, 365–372 (2013).

50. Debela, D. T. *et al.* New approaches and procedures for cancer treatment: Current perspectives. *SAGE Open Med.* **9**, 20503121211034370 (2021).

51. Zahreddine, H. & Borden, K. Mechanisms and insights into drug resistance in cancer. *Front. Pharmacol.* **4**, (2013).

52. Zeng, S. *et al.* Chemoresistance in Pancreatic Cancer. *Int. J. Mol. Sci.* **20**, E4504 (2019).

53. Mackey, J. R. *et al.* Functional nucleoside transporters are required for gemcitabine influx and manifestation of toxicity in cancer cell lines. *Cancer Res.* **58**, 4349–57 (1998).

54. Mayati, A. *et al.* mRNA Expression and Activity of Nucleoside Transporters in Human Hepatoma HepaRG Cells. *Pharmaceutics* **10**, 246 (2018).

55. Miao, H., Chen, X. & Luan, Y. Small Molecular Gemcitabine Prodrugs for Cancer Therapy. *Curr. Med. Chem.* **27**, 5562–5582 (2020).

56. Bhutia, Y. D., Hung, S. W., Patel, B., Lovin, D. & Govindarajan, R. CNT1 Expression Influences Proliferation and Chemosensitivity in Drug-Resistant Pancreatic Cancer Cells. *Cancer Res.* **71**, 1825–1835 (2011).

57. Saiki, Y. *et al.* DCK is frequently inactivated in acquired gemcitabine-resistant human cancer cells. *Biochem. Biophys. Res. Commun.* **421**, 98–104 (2012).

58. Apte, M. V. *et al.* Pancreatic cancer: The microenvironment needs attention too! *Pancreatol. Off. J. Int. Assoc. Pancreatol. IAP Al* **15**, S32-38 (2015).

59. Spratlin, J. *et al.* The Absence of Human Equilibrative Nucleoside Transporter 1 Is Associated with Reduced Survival in Patients With Gemcitabine-Treated Pancreas Adenocarcinoma. *Clin. Cancer Res.* **10**, 6956–6961 (2004).

60. Giovannetti, E. *et al.* Transcription analysis of human equilibrative nucleoside transporter-1 predicts survival in pancreas cancer patients treated with gemcitabine. *Cancer Res.* **66**, 3928–35 (2006).

61. Carter, C. J., Mekkawy, A. H. & Morris, D. L. Role of human nucleoside transporters in pancreatic cancer and chemoresistance. *World J. Gastroenterol.* **27**, 6844–6860 (2021).

62. Ohhashi, S. *et al.* Down-regulation of Deoxycytidine Kinase Enhances Acquired Resistance to Gemcitabine in Pancreatic Cancer. *Anticancer Res.* **28**, 2205–2212 (2008).

63. Ohmine, K. *et al.* Attenuation of Phosphorylation by Deoxycytidine Kinase is Key to Acquired Gemcitabine Resistance in a Pancreatic Cancer Cell Line: Targeted Proteomic and Metabolomic Analyses in PK9 Cells. *Pharm. Res.* **29**, 2006–2016 (2012).

64. Ruiz van Haperen, V. W. *et al.* Development and molecular characterization of a 2',2'-difluorodeoxycytidine-resistant variant of the human ovarian carcinoma cell line A2780. *Cancer Res.* **54**, 4138–4143 (1994).

65. Elledge, S. J., Zhou, Z. & Allen, J. B. Ribonucleotide reductase: regulation, regulation, regulation. *Trends Biochem. Sci.* **17**, 119–123 (1992).

66. Bergman, A. M. *et al.* In vivo induction of resistance to gemcitabine results in increased expression of ribonucleotide reductase subunit M1 as the major determinant. *Cancer Res.* **65**, 9510–9516 (2005).

67. Han, Q. L., Zhou, Y. H., Lyu, Y., Yan, H. & Dai, G. H. Effect of ribonucleotide reductase M1 expression on overall survival in patients with pancreatic cancer receiving gemcitabine chemotherapy: A literature-based meta-analysis. *J. Clin. Pharm. Ther.* **43**, 163–169 (2018).

68. Pandey, V. & Storz, P. Targeting the tumor microenvironment in pancreatic ductal adenocarcinoma. *Expert Rev. Anticancer Ther.* **19**, 473–482 (2019).

69. Funamizu, N. *et al.* Is the resistance of gemcitabine for pancreatic cancer settled only by overexpression of deoxycytidine kinase? *Oncol. Rep.* **23**, 471–475 (2010).

70. Cao, F. *et al.* HES 1 is essential for chemoresistance induced by stellate cells and is associated with poor prognosis in pancreatic cancer. *Oncol. Rep.* **33**, 1883–1889 (2015).

71. Firuzi, O. *et al.* Role of c-MET Inhibitors in Overcoming Drug Resistance in Spheroid Models of Primary Human Pancreatic Cancer and Stellate Cells. *Cancers* **11**, 638 (2019).

72. Xu, Z. *et al.* Targeting the HGF/c-MET pathway in advanced pancreatic cancer: a key element of treatment that limits primary tumour growth and eliminates metastasis. *Br. J. Cancer* **122**, 1486–1495 (2020).

73. Paul, M. K. & Mukhopadhyay, A. K. Tyrosine kinase - Role and significance in Cancer. *Int. J. Med. Sci.* **1**, 101–115 (2004).

74. Cohen, P. Protein kinases — the major drug targets of the twenty-first century? *Nat. Rev. Drug Discov.* **1**, 309–315 (2002).

75. Siegel, R. L., Miller, K. D., Fuchs, H. E. & Jemal, A. Cancer statistics, 2022. *CA. Cancer J. Clin.* **72**, 7–33 (2022).

76. Robinson, D. R., Wu, Y.-M. & Lin, S.-F. The protein tyrosine kinase family of the human genome. *Oncogene* **19**, 5548–5557 (2000).

77. Neet, K. & Hunter, T. Vertebrate non-receptor protein-tyrosine kinase families. *Genes Cells Devoted Mol. Cell. Mech.* **1**, 147–169 (1996).

78. Ingley, E. Src family kinases: regulation of their activities, levels and identification of new pathways. *Biochim. Biophys. Acta* **1784**, 56–65 (2008).

79. Manning, G., Whyte, D. B., Martinez, R., Hunter, T. & Sudarsanam, S. The Protein Kinase Complement of the Human Genome. *Science* **298**, 1912–1934 (2002).

80. Blume-Jensen, P. & Hunter, T. Oncogenic kinase signalling. *Nature* **411**, 355–365 (2001).

81. Wiener, J. R. *et al.* Activated SRC protein tyrosine kinase is overexpressed in late-stage human ovarian cancers. *Gynecol. Oncol.* **88**, 73–79 (2003).

82. Lutz, M. P. *et al.* Overexpression and activation of the tyrosine kinase Src in human pancreatic carcinoma. *Biochem. Biophys. Res. Commun.* **243**, 503–508 (1998).

83. Mazurenko, N. N., Kogan, E. A., Zborovskaya, I. B. & Kisseljov, F. L. Expression of pp60c-src in human small cell and non-small cell lung carcinomas. *Eur. J. Cancer Oxf. Engl. 1990* **28**, 372–377 (1992).

84. FDA Approved Protein Kinase Inhibitors: https://brimr.org/protein-kinase-inhibitors/.

85. Cohen, P., Cross, D. & Jänne, P. A. Kinase drug discovery 20 years after imatinib: progress and future directions. *Nat. Rev. Drug Discov.* **20**, 551–569 (2021).

86. Roskoski, R. Properties of FDA-approved small molecule protein kinase inhibitors. *Pharmacol. Res.* **144**, 19–50 (2019).

87. Saraon, P. *et al.* Receptor tyrosine kinases and cancer: oncogenic mechanisms and therapeutic approaches. *Oncogene* **40**, 4079–4093 (2021).

88. Hubbard, S. R. & Till, J. H. Protein tyrosine kinase structure and function. *Annu. Rev. Biochem.* **69**, 373–398 (2000).

89. Ségaliny, A. I., Tellez-Gabriel, M., Heymann, M.-F. & Heymann, D. Receptor tyrosine kinases: Characterisation, mechanism of action and therapeutic interests for bone cancers. *J. Bone Oncol.* **4**, 1–12 (2015).

90. Roskoski, R. VEGF receptor protein–tyrosine kinases: Structure and regulation. *Biochem. Biophys. Res. Commun.* **375**, 287–291 (2008).

91. Solouki, S., August, A. & Huang, W. Non-receptor tyrosine kinase signaling in autoimmunity and therapeutic implications. *Pharmacol. Ther.* **201**, 39–50 (2019).

92. Liu, B. A., Engelmann, B. W. & Nash, P. D. The language of SH2 domain interactions defines phosphotyrosine-mediated signal transduction. *FEBS Lett.* **586**, 2597–2605 (2012).

93. Mayer, B. J. SH3 domains: complexity in moderation. *J. Cell Sci.* **114**, 1253–1263 (2001).

94. Weiner, T. M., Craven, R. J., Cance, W. G. & Liu, E. Expression of focal adhesion kinase gene and invasive cancer. *The Lancet* **342**, 1024–1025 (1993).

95. Focal adhesion kinase: in command and control of cell motility - PubMed. https://pubmed.ncbi.nlm.nih.gov/15688067/.

96. Schaller, M. D. Biochemical signals and biological responses elicited by the focal adhesion kinase. *Biochim. Biophys. Acta* **1540**, 1–21 (2001).

97. Frame, M. C., Patel, H., Serrels, B., Lietha, D. & Eck, M. J. The FERM domain: organizing the structure and function of FAK. *Nat. Rev. Mol. Cell Biol.* **11**, 802–814 (2010).

98. Tapial Martínez, P., López Navajas, P. & Lietha, D. FAK Structure and Regulation by Membrane Interactions and Force in Focal Adhesions. *Biomolecules* **10**, E179 (2020).

99. Chen, H. C. *et al.* Interaction of focal adhesion kinase with cytoskeletal protein talin. *J. Biol. Chem.* **270**, 16995–16999 (1995).

100. Parsons, J. T., Horwitz, A. R. & Schwartz, M. A. Cell adhesion: integrating cytoskeletal dynamics and cellular tension. *Nat. Rev. Mol. Cell Biol.* **11**, 633–643 (2010).

101. Zhou, J. *et al.* Mechanism of Focal Adhesion Kinase Mechanosensing. *PLOS Comput. Biol.* **11**, e1004593 (2015).

102. Hochwald, S. N. *et al.* A novel small molecule inhibitor of FAK decreases growth of human pancreatic cancer. *Cell Cycle Georget. Tex* **8**, 2435–2443 (2009).

103. Golubovskaya, V. M., Zheng, M., Zhang, L., Li, J.-L. & Cance, W. G. The direct effect of Focal Adhesion Kinase (FAK), dominant-negative FAK, FAK-CD and FAK siRNA on gene expression and human MCF-7 breast cancer cell tumorigenesis. *BMC Cancer* **9**, 280 (2009).

104. Chatzizacharias, N. A. *et al.* Evaluation of the clinical significance of focal adhesion kinase and SRC expression in human pancreatic ductal adenocarcinoma. *Pancreas* **39**, 930–936 (2010).

105. Erkan, M. *et al.* Loss of BNIP3 expression is a late event in pancreatic cancer contributing to chemoresistance and worsened prognosis. *Oncogene* **24**, 4421–4432 (2005).

106. Duxbury, M. S., Ito, H., Zinner, M. J., Ashley, S. W. & Whang, E. E. Focal adhesion kinase gene silencing promotes anoikis and suppresses metastasis of human pancreatic adenocarcinoma cells. *Surgery* **135**, 555–562 (2004).

107. Liu, W.-S. *et al.* siRNA directed against survivin enhances pancreatic cancer cell gemcitabine chemosensitivity. *Dig. Dis. Sci.* **54**, 89–96 (2009).

108. Perrone, C. *et al.* FAK Signaling in Rhabdomyosarcoma. *Int. J. Mol. Sci.* **21**, 8422 (2020).

109. Cho, S. Y. & Klemke, R. L. Extracellular-regulated kinase activation and CAS/Crk coupling regulate cell migration and suppress apoptosis during invasion of the extracellular matrix. *J. Cell Biol.* **149**, 223–236 (2000).

110. Zhao, X. & Guan, J.-L. Focal adhesion kinase and its signaling pathways in cell migration and angiogenesis. *Adv. Drug Deliv. Rev.* **63**, 610–615 (2011).

111. Hsia, D. A. *et al.* Differential regulation of cell motility and invasion by FAK. *J. Cell Biol.* **160**, 753–767 (2003).

112. Lim, S.-T. *et al.* Nuclear FAK promotes cell proliferation and survival through FERM-enhanced p53 degradation. *Mol. Cell* **29**, 9–22 (2008).

113. Dar, A. C. & Shokat, K. M. The Evolution of Protein Kinase Inhibitors from Antagonists to Agonists of Cellular Signaling. *Annu. Rev. Biochem.* **80**, 769–795 (2011).

114. Roskoski, R. Classification of small molecule protein kinase inhibitors based upon the structures of their drug-enzyme complexes. *Pharmacol. Res.* **103**, 26–48 (2016).

115. Lamba, V. & Ghosh, I. New Directions in Targeting Protein Kinases: Focusing Upon True Allosteric and Bivalent Inhibitors. *Curr. Pharm. Des.* **18**, 2936–2945.

116. Golubovskaya, V. M. Focal Adhesion Kinase as a Cancer Therapy Target. *Anticancer Agents Med. Chem.* **10**, 735–741 (2010).

117. Wu, X. *et al.* Recent progress on FAK inhibitors with dual targeting capabilities for cancer treatment. *Biomed. Pharmacother.* **151**, 113116 (2022).

118. Wu, Y. *et al.* Focal adhesion kinase inhibitors, a heavy punch to cancer. *Discov. Oncol.* **12**, 52 (2021).

119. Study of Pembrolizumab with or Without Defactinib Following Chemotherapy as a Neoadjuvant and Adjuvant Treatment for Resectable Pancreatic Ductal Adenocarcinoma.

120. Phase I Trial of Defatcinib and VS-6766. https://clinicaltrials.gov/ct2/show/NCT03875820.

121. Harbarth, S. *et al.* Antimicrobial resistance: one world, one fight! *Antimicrob. Resist. Infect. Control* **4**, 49 (2015).

122. Christaki, E., Marcou, M. & Tofarides, A. Antimicrobial Resistance in Bacteria: Mechanisms, Evolution, and Persistence. *J. Mol. Evol.* **88**, 26–40 (2020).

123. Tamma, P. D. *et al.* Infectious Diseases Society of America Guidance on the Treatment of AmpC β-Lactamase-Producing Enterobacterales, Carbapenem-Resistant Acinetobacter baumannii, and Stenotrophomonas maltophilia Infections. *Clin. Infect. Dis. Off. Publ. Infect. Dis. Soc. Am.* **74**, 2089–2114 (2022).

124. Price, R. O'Neill report on antimicrobial resistance: funding for antimicrobial specialists should be improved. *Eur. J. Hosp. Pharm.* **23**, 245–247 (2016).

125. Parrino, B. *et al.* Synthetic small molecules as anti-biofilm agents in the struggle against antibiotic resistance. *Eur. J. Med. Chem.* **161**, 154–178 (2019).

126. Oliveira, D. M. P. D. *et al.* Antimicrobial Resistance in ESKAPE Pathogens. (2020) doi:10.1128/CMR.

127. Founou, R. C. *et al.* The COVID-19 pandemic: a threat to antimicrobial resistance containment. *Future Sci. OA* **7**, FSO736 (2021).

128. Costello, E. J., Erkanli, A., Copeland, W. & Angold, A. Association of Family Income Supplements in Adolescence With Development of Psychiatric and Substance Use Disorders in Adulthood Among an American Indian Population. *JAMA* **303**, 1954–1960 (2010).

129. Lee, J.-H. Perspectives towards antibiotic resistance: from molecules to population. *J. Microbiol. Seoul Korea* **57**, 181–184 (2019).

130. Anderson, G. G. & O'Toole, G. A. Innate and induced resistance mechanisms of bacterial biofilms. *Curr. Top. Microbiol. Immunol.* **322**, 85–105 (2008).

131. Zankari, E. *et al.* Identification of acquired antimicrobial resistance genes. *J. Antimicrob. Chemother.* **67**, 2640–2644 (2012).

132. Fernández, L., Breidenstein, E. B. M. & Hancock, R. E. W. Creeping baselines and adaptive resistance to antibiotics. *Drug Resist. Updat.* **14**, 1–21 (2011).

133. Rizi, K., Ghazvini, K. & Kouhi Noghondar, M. Adaptive Antibiotic Resistance: Overview and Perspectives. *J. Infect. Dis. Ther.* **06**, (2018).

134. Sandoval-Motta, S. & Aldana, M. Adaptive resistance to antibiotics in bacteria: a systems biology perspective. *WIREs Syst. Biol. Med.* **8**, 253–267 (2016).

135. Holmes, A. H. *et al.* Understanding the mechanisms and drivers of antimicrobial resistance. *Lancet Lond. Engl.* **387**, 176–187 (2016).

136. Munita, J. M. & Arias, C. A. Mechanisms of Antibiotic Resistance. *Microbiol. Spectr.* **4**, (2016).

137. Stoodley, P., Sauer, K., Davies, D. G. & Costerton, J. W. Biofilms as complex differentiated communities. *Annu. Rev. Microbiol.* **56**, 187–209 (2002).

138. Abdalla, A. K. *et al.* Exopolysaccharides as Antimicrobial Agents: Mechanism and Spectrum of Activity. *Front. Microbiol.* **12**, 664395 (2021).

139. Fleming, D. & Rumbaugh, K. P. Approaches to Dispersing Medical Biofilms. *Microorganisms* **5**, E15 (2017).

140. Rumbaugh, K. P., Griswold, J. A., Iglewski, B. H. & Hamood, A. N. Contribution of Quorum Sensing to the Virulence ofPseudomonas aeruginosa in Burn Wound Infections. *Infect. Immun.* **67**, 5854–5862 (1999).

141. Costerton, J. W., Stewart, P. S. & Greenberg, E. P. Bacterial biofilms: a common cause of persistent infections. *Science* **284**, 1318–1322 (1999).

142. Koo, H., Allan, R. N., Howlin, R. P., Stoodley, P. & Hall-Stoodley, L. Targeting microbial biofilms: current and prospective therapeutic strategies. *Nat. Rev. Microbiol.* **15**, 740–755 (2017).

143. Høiby, N., Bjarnsholt, T., Givskov, M., Molin, S. & Ciofu, O. Antibiotic resistance of bacterial biofilms. *Int. J. Antimicrob. Agents* **35**, 322–332 (2010).

144. Hall, C. W. & Mah, T.-F. Molecular mechanisms of biofilm-based antibiotic resistance and tolerance in pathogenic bacteria. *FEMS Microbiol. Rev.* **41**, 276–301 (2017).

145. Schembri, M. A., Hjerrild, L., Gjermansen, M. & Klemm, P. Differential expression of the Escherichia coli autoaggregation factor antigen 43. *J. Bacteriol.* **185**, 2236–2242 (2003).

146. Secor, P. R., Michaels, L. A., Ratjen, A., Jennings, L. K. & Singh, P. K. Entropically driven aggregation of bacteria by host polymers promotes antibiotic tolerance in Pseudomonas aeruginosa. *Proc. Natl. Acad. Sci. U. S. A.* **115**, 10780–10785 (2018).

147. Tang, P. *et al.* Effect of Superhydrophobic Surface of Titanium on *Staphylococcus aureus* Adhesion. *J. Nanomater.* **2011**, e178921 (2011).

148. Pogodin, S. *et al.* Biophysical model of bacterial cell interactions with nanopatterned cicada wing surfaces. *Biophys. J.* **104**, 835–840 (2013).

149. Kim, S. *et al.* Nanostructured Multifunctional Surface with Antireflective and Antimicrobial Characteristics. *ACS Appl. Mater. Interfaces* **7**, 326–331 (2015).

150. Pereira, Maria Olívia · Machado, Idalina · Simões, M. Vieira, M. J. *Preventing biofilm formation using surfactants*. (2017).

151. Song, D. *et al.* Pseudomonas aeruginosa quorum-sensing metabolite induces host immune cell death through cell surface lipid domain dissolution. *Nat. Microbiol.* **4**, 97–111 (2019).

152. Rabin, N. *et al.* Agents that inhibit bacterial biofilm formation. *Future Med. Chem.* **7**, 647–671 (2015).

153. Rémy, B. *et al.* Interference in Bacterial Quorum Sensing: A Biopharmaceutical Perspective. *Front. Pharmacol.* **9**, (2018).

154. Gao, L. *et al.* Nanocatalysts promote Streptococcus mutans biofilm matrix degradation and enhance bacterial killing to suppress dental caries in vivo. *Biomaterials* **101**, 272–284 (2016).

155. Kumar, R., Chhibber, S. & Harjai, K. Quorum sensing is necessary for the virulence of Pseudomonas aeruginosa during urinary tract infection. *Kidney Int.* **76**, 286–292 (2009).

156. Gupta, R. K., Chhibber, S. & Harjai, K. Quorum sensing signal molecules cause renal tissue inflammation through local cytokine responses in experimental UTI caused by Pseudomonas aeruginosa. *Immunobiology* **218**, 181–185 (2013).

157. Bjarnsholt, T. *et al.* Pseudomonas aeruginosa tolerance to tobramycin, hydrogen peroxide and polymorphonuclear leukocytes is quorum-sensing dependent. *Microbiology* **151**, 373–383.

158. Hentzer, M. Attenuation of Pseudomonas aeruginosa virulence by quorum sensing inhibitors. *EMBO J.* **22**, 3803–3815 (2003).

159. Frei, R., Breitbach, A. S. & Blackwell, H. E. 2-Aminobenzimidazole Derivatives Strongly Inhibit and Disperse *Pseudomonas aeruginosa* Biofilms. *Angew. Chem. Int. Ed.* **51**, 5226–5229 (2012).

160. Park, J. S., Ryu, E.-J., Li, L., Choi, B.-K. & Kim, B. M. New bicyclic brominated furanones as potent autoinducer-2 quorum-sensing inhibitors against bacterial biofilm formation. *Eur. J. Med. Chem.* **137**, 76–87 (2017).

161. Römling, U. Cyclic di-GMP, an established secondary messenger still speeding up. *Environ. Microbiol.* **14**, 1817–1829 (2012).

162. Boyd, C. D. & O'Toole, G. A. Second Messenger Regulation of Biofilm Formation: Breakthroughs in Understanding c-di-GMP Effector Systems. *Annu. Rev. Cell Dev. Biol.* **28**, 439–462 (2012).

163. Jung, H.-I. *et al.* Mutation of the cyclic di-GMP phosphodiesterase gene in Burkholderia lata SK875 attenuates virulence and enhances biofilm formation. *J. Microbiol.* **55**, 800–808 (2017).

164. Nakayama, S., Kelsey, I., Wang, J. & Sintim, H. O. c-di-GMP can form remarkably stable G-quadruplexes at physiological conditions in the presence of some planar intercalators. *Chem. Commun.* **47**, 4766–4768 (2011).

165. Römling, U. & Balsalobre, C. Biofilm infections, their resilience to therapy and innovative treatment strategies. *J. Intern. Med.* **272**, 541–561 (2012).

166. Corrigan, R. M. *et al.* Systematic identification of conserved bacterial c-di-AMP receptor proteins. *Proc. Natl. Acad. Sci.* **110**, 9084–9089 (2013).

167. Wexselblatt, E. *et al.* ppGpp analogues inhibit synthetase activity of Rel proteins from Gram-negative and Gram-positive bacteria. *Bioorg. Med. Chem.* **18**, 4485–4497 (2010).

168. Cascioferro, S. *et al.* Sortase A Inhibitors: Recent Advances and Future Perspectives. *J. Med. Chem.* **58**, 9108–9123 (2015).

169. Cascioferro, S., Totsika, M. & Schillaci, D. Sortase A: An ideal target for anti-virulence drug development. *Microb. Pathog.* **77**, 105–112 (2014).

170. Totsika, M. *et al.* A FimH Inhibitor Prevents Acute Bladder Infection and Treats Chronic Cystitis Caused by Multidrug-Resistant Uropathogenic Escherichia coli ST131. *J. Infect. Dis.* **208**, 921–928 (2013).

171. Ryu, J.-H. & Beuchat, L. R. Biofilm Formation by *Escherichia coli* O157:H7 on Stainless Steel: Effect of Exopolysaccharide and Curli Production on Its Resistance to Chlorine. *Appl. Environ. Microbiol.* **71**, 247–254 (2005).

172. Uhlich, G. A., Cooke, P. H. & Solomon, E. B. Analyses of the Red-Dry-Rough Phenotype of an *Escherichia coli* O157:H7 Strain and Its Role in Biofilm Formation and Resistance to Antibacterial Agents. *Appl. Environ. Microbiol.* **72**, 2564–2572 (2006).

173. Vega, N. M., Allison, K. R., Khalil, A. S. & Collins, J. J. Signaling-mediated bacterial persister formation. *Nat. Chem. Biol.* **8**, 431–433 (2012).

174. Soukarieh, F. *et al.* In Silico and in Vitro-Guided Identification of Inhibitors of Alkylquinolone-Dependent Quorum Sensing in Pseudomonas aeruginosa. *Molecules* **23**, 257 (2018).

175. Wagner, S. *et al.* Novel Strategies for the Treatment of *Pseudomonas aeruginosa* Infections. *J. Med. Chem.* **59**, 5929–5969 (2016).

176. Sahner, J. H. *et al.* Exploring the chemical space of ureidothiophene-2-carboxylic acids as inhibitors of the quorum sensing enzyme PqsD from Pseudomonas aeruginosa. *Eur. J. Med. Chem.* **96**, 14–21 (2015).

177. Zender, M. *et al.* Dissecting the Multiple Roles of PqsE in *Pseudomonas aeruginosa* Virulence by Discovery of Small Tool Compounds. *ACS Chem. Biol.* **11**, 1755–1763 (2016).

178. Oniga, S. *et al.* New 2-Phenylthiazoles as Potential Sortase A Inhibitors: Synthesis, Biological Evaluation and Molecular Docking. *Molecules* **22**, 1827 (2017).

179. Wurpel, D. J., Beatson, S. A., Totsika, M., Petty, N. K. & Schembri, M. A. Chaperone-Usher Fimbriae of Escherichia coli. *PLoS ONE* **8**, e52835 (2013).

180. Conover, M. S. *et al.* Inflammation-Induced Adhesin-Receptor Interaction Provides a Fitness Advantage to Uropathogenic E. coli during Chronic Infection. *Cell Host Microbe* **20**, 482–492 (2016).

181. Diggle, S. P. *et al.* The galactophilic lectin, LecA, contributes to biofilm development in Pseudomonas aeruginosa. *Environ. Microbiol.* **8**, 1095–1104 (2006).

182. Hauck, D. *et al.* Discovery of Two Classes of Potent Glycomimetic Inhibitors of *Pseudomonas aeruginosa* LecB with Distinct Binding Modes. *ACS Chem. Biol.* **8**, 1775–1784 (2013).

183. Sommer, R. *et al.* Glycomimetic, Orally Bioavailable LecB Inhibitors Block Biofilm Formation of *Pseudomonas aeruginosa*. *J. Am. Chem. Soc.* **140**, 2537–2545 (2018).

184. Anderson, J. K. *et al.* Chemorepulsion from the Quorum Signal Autoinducer-2 Promotes Helicobacter pylori Biofilm Dispersal. *mBio* **6**, e00379-15 (2015).

185. Lauderdale, K. J., Malone, C. L., Boles, B. R., Morcuende, J. & Horswill, A. R. Biofilm dispersal of community-associated methicillin-resistant *Staphylococcus aureus* on orthopedic implant material: DISPERSAL OF MRSA BIOFILMS. *J. Orthop. Res.* **28**, 55–61 (2010).

186. Christensen, L. D. *et al.* Clearance of Pseudomonas aeruginosa Foreign-Body Biofilm Infections through Reduction of the Cyclic Di-GMP Level in the Bacteria. *Infect. Immun.* **81**, 2705–2713 (2013).

187. Assefa, M. & Amare, A. Biofilm-Associated Multi-Drug Resistance in Hospital-Acquired Infections: A Review. *Infect. Drug Resist.* **15**, 5061–5068 (2022).

188. Loiselle, M. & Anderson, K. W. The Use of Cellulase in Inhibiting Biofilm Formation from Organisms Commonly Found on Medical Implants. *Biofouling* **19**, 77–85 (2003).

189. Barraud, N. *et al.* Involvement of Nitric Oxide in Biofilm Dispersal of Pseudomonas aeruginosa. *J. Bacteriol.* **188**, 7344–7353 (2006).

190. Kim, S.-K. & Lee, J.-H. Biofilm dispersion in Pseudomonas aeruginosa. *J. Microbiol.* **54**, 71–85 (2016).

191. Gilbert, P., Maira-Litran, T., McBain, A. J., Rickard, A. H. & Whyte, F. W. The physiology and collective recalcitrance of microbial biofilm communities. *Adv. Microb. Physiol.* **46**, 202–256 (2002).

192. Parrino, B., Carbone, D., Cirrincione, G., Diana, P. & Cascioferro, S. Inhibitors of antibiotic resistance mechanisms: clinical applications and future perspectives. *Future Med. Chem.* **12**, 357–359 (2020).

193. Cascioferro, S. *et al.* 2,6-Disubstituted imidazo[2,1-b][1,3,4]thiadiazole derivatives as potent staphylococcal biofilm inhibitors. *Eur. J. Med. Chem.* **167**, 200–210 (2019).

194. Noolvi, M. N., Patel, H. M., Kamboj, S., Kaur, A. & Mann, V. 2,6-Disubstituted imidazo[2,1-b][1,3,4]thiadiazoles: Search for anticancer agents. *Eur. J. Med. Chem.* **56**, 56–69 (2012).

195. Khan, I. *et al.* Synthesis, antioxidant activities and urease inhibition of some new 1,2,4-triazole and 1,3,4-thiadiazole derivatives. *Eur. J. Med. Chem.* **45**, 5200–5207 (2010).

196. Aouali, M. *et al.* Synthesis, antibacterial, and antifungal activities of imidazo[2,1-c][1,2, 4]triazoles and 1,2,4-triazolo[4,3-a]pyrimidinones. *Synth. Commun.* **44**, 748–756 (2014).

197. Almajan, G. L. *et al.* Synthesis and antimicrobial evaluation of some fused heterocyclic [1,2,4]triazolo[3,4-b][1,3,4]thiadiazole derivatives. *Eur. J. Med. Chem.* **45**, 6139–6146 (2010).

198. Jatav, V., Mishra, P., Kashaw, S. & Stables, J. P. CNS depressant and anticonvulsant activities of some novel 3-[5-substituted 1,3,4-thiadiazole-2-yl]-2-styryl quinazoline-4(3H)-ones. *Eur. J. Med. Chem.* **43**, 1945–1954 (2008).

199. Andreani, A. *et al.* Synthesis and antihypertensive activity of imidazo[2,1-b]-thiazoles bearing a 2,6-dichlorophenyl group. *Acta Pharm. Nord.* **4**, 93–96 (1992).

200. Andreani, A. *et al.* Synthesis and antitubercular activity of imidazo[2,1-b]thiazoles. *Eur. J. Med. Chem.* **36**, 743–746 (2001).

201. Askin, S. *et al.* Design, synthesis, characterization, in vitro and in silico evaluation of novel imidazo[2,1-b][1,3,4]thiadiazoles as highly potent acetylcholinesterase and non-classical carbonic anhydrase inhibitors. *Bioorganic Chem.* **113**, 105009 (2021).

202. Gadad, A. K., Mahajanshetti, C. S., Nimbalkar, S. & Raichurkar, A. Synthesis and antibacterial activity of some 5-guanylhydrazone/thiocyanato-6-arylimidazo[2,1-b]-1,3, 4-thiadiazole-2-sulfonamide derivatives. *Eur. J. Med. Chem.* **35**, 853–857 (2000).

203. Terzioglu, N. & Gürsoy, A. Synthesis and anticancer evaluation of some new hydrazone derivatives of 2,6-dimethylimidazo[2,1-b][1,3,4]thiadiazole-5-carbohydrazide. *Eur. J. Med. Chem.* **38**, 781–786 (2003).

204. Dhepe, S., Kumar, S., Vinayakumar, R., Ramareddy, S. A. & Karki, S. S. Microwave-assisted synthesis and antimicrobial activity of some imidazo[2,1-b][1,3,4]thiadiazole derivatives. *Med. Chem. Res.* **21**, 1550–1556 (2012).

205. Kumar, S. *et al.* Synthesis and antiproliferative activity of imidazo[2,1-b][1,3,4]thiadiazole derivatives. *Bioorg. Med. Chem. Lett.* **24**, 4682–4688 (2014).

206. Kumar, S. *et al.* 2-(4-Chlorobenzyl)-6-arylimidazo[2,1-b][1,3,4]thiadiazoles: Synthesis, cytotoxic activity and mechanism of action. *Eur. J. Med. Chem.* **84**, 687–697 (2014).

207. Kamal, A. *et al.* Synthesis and biological evaluation of imidazo[2,1-b][1,3,4]thiadiazole- linked oxindoles as potent tubulin polymerization inhibitors. *ChemMedChem* **9**, 1463–1475 (2014).

208. Patel, H. M. *et al.* Design, synthesis and evaluation of small molecule imidazo[2,1-b][1,3,4]thiadiazoles as inhibitors of transforming growth factor-β type-I receptor kinase (ALK5). *Eur. J. Med. Chem.* **93**, 599–613 (2015).

209. Cascioferro, S. *et al.* Imidazo[2,1-b] [1,3,4]thiadiazoles with antiproliferative activity against primary and gemcitabine-resistant pancreatic cancer cells. *Eur. J. Med. Chem.* **189**, 112088 (2020).

210. Cascioferro, S. *et al.* 3-(6-Phenylimidazo [2,1-b][1,3,4]thiadiazol-2-yl)-1H-Indole Derivatives as New Anticancer Agents in the Treatment of Pancreatic Ductal Adenocarcinoma. *Molecules* **25**, 329 (2020).

211. Petri, G. L. *et al.* New Imidazo[2,1-b][1,3,4]Thiadiazole Derivatives Inhibit FAK Phosphorylation and Potentiate the Antiproliferative Effects of Gemcitabine Through Modulation of the Human Equilibrative Nucleoside Transporter-1 in Peritoneal Mesothelioma. *Anticancer Res.* **40**, 4913–4919 (2020).

212. Randazzo, O. *et al.* SF3B1 modulators affect key genes in metastasis and drug influx: A new approach to fight pancreatic cancer chemoresistance. *Cancer Drug Resist.* **4**, 904–922 (2021).

213. Kumar, S. & Ritika. A brief review of the biological potential of indole derivatives. *Future J. Pharm. Sci.* **6**, 121 (2020).

214. Gummidi, L., Kerru, N., Adeniyi, A. A., Dhawan, S. & Singh, P. Comparative experimental and DFT analysis of novel indole tagged [1,3,4]thiadiazolo[3,2-a]pyrimidin-5-one hybrid. *J. Mol. Struct.* **1263**, 133159 (2022).

215. Sirakanyan, S. N. *et al.* Synthesis and Neurotropic Activity of New Heterocyclic Systems: Pyridofuro[3,2-d]pyrrolo[1,2-a]pyrimidines, Pyridofuro[3,2-d]pyrido[1,2-a]pyrimidines and Pyridofuro[3',2':4,5]pyrimido[1,2-a]azepines. *Molecules* **26**, 3320 (2021).

216. Wusiman, A. & Mulati, A. Facile One-Pot Synthesis of Cyclic N-Sulfonylamidines from Lactam and Sulfonamide. *HETEROCYCLES* **91**, 2163 (2015).

217. Gupta, P., Gupta, S., Sachar, A. & Sharma, R. L. Synthesis of novel and biologically potent heteropolycyclics containing bridge head nitrogen. *J. Heterocycl. Chem.* **47**, 1188–1199 (2010).

218. Nazarenko, K. G., Shyrokaya, T. I. & Tolmachev, A. A. Lactim Ethers in the Synthesis of 1,2-Polymethylene-4-quinazolones. *Synth. Commun.* **33**, 303–310 (2003).

219. Hermecz, I. *et al.* Nitrogen bridgehead compounds. 66. Bronchodilator nitrogen bridgehead compounds with a pyrimidinone moiety. *J. Med. Chem.* **30**, 1543–1549 (1987).

220. Kim, B. *et al.* Trapidil induces osteogenesis by upregulating the signaling of bone morphogenetic proteins. *Cell. Signal.* **49**, 68–78 (2018).

221. El-Gendy, M. M. A., Shaaban, M., Shaaban, K. A., El-Bondkly, A. M. & Laatsch, H. Essramycin: A First Triazolopyrimidine Antibiotic Isolated from Nature†. *J. Antibiot. (Tokyo)* **61**, 149–157 (2008).

222. Azab, M. E., Abdel-Wahab, S. S., Mahmoud, N. F. & Elsayed, G. A. Novel Bridgehead Thiadiazolopyrimidine Derivatives with Antimicrobial and Antitumor Activities: 1,3,4-Thiadiazolo[3,2- *a*] Pyrimidine. *J. Heterocycl. Chem.* **55**, 2349–2359 (2018).

223. Andreani, A. *et al.* Imidazo[2,1-b]thiazole guanylhydrazones as RSK2 inhibitors [1]. *Eur. J. Med. Chem.* **46**, 4311–4323 (2011).

224. Kamal, A. *et al.* Synthesis of Imidazothiazole–Chalcone Derivatives as Anticancer and Apoptosis Inducing Agents. *ChemMedChem* **5**, 1937–1947 (2010).

225. Moraski, G. C. *et al.* Arrival of Imidazo[2,1-b]thiazole-5-carboxamides: Potent Anti-tuberculosis Agents That Target QcrB. *ACS Infect. Dis.* **2**, 393–398 (2016).

226. Park, J.-H., El-Gamal, M. I., Lee, Y. S. & Oh, C.-H. New imidazo[2,1-b]thiazole derivatives: synthesis, in vitro anticancer evaluation, and in silico studies. *Eur. J. Med. Chem.* **46**, 5769–5777 (2011).

227. Ali, A. R., El-Bendary, E. R., Ghaly, M. A. & Shehata, I. A. Synthesis, in vitro anticancer evaluation and in silico studies of novel imidazo[2,1-b]thiazole derivatives bearing pyrazole moieties. *Eur. J. Med. Chem.* **75**, 492–500 (2014).

228. Sharma, N. & Anurag. 7-Azaindole Analogues as Bioactive Agents and Recent Results. *Mini-Rev. Med. Chem.* **19**, 727–736.

229. Heinrich, T. *et al.* Fragment-Based Discovery of New Highly Substituted 1H-Pyrrolo[2,3-b]- and 3H-Imidazolo[4,5-b]-Pyridines as Focal Adhesion Kinase Inhibitors. *J. Med. Chem.* **56**, 1160–1170 (2013).

230. Ayati, A., Emami, S., Asadipour, A., Shafiee, A. & Foroumadi, A. Recent applications of 1,3-thiazole core structure in the identification of new lead compounds and drug discovery. *Eur. J. Med. Chem.* **97**, 699–718 (2015).

231. Djukic, M. *et al.* In vitro antioxidant activity of thiazolidinone derivatives of 1,3-thiazole and 1,3,4-thiadiazole. *Chem. Biol. Interact.* **286**, 119–131 (2018).

232. Sharma, R. N., Xavier, F. P., Vasu, K. K., Chaturvedi, S. C. & Pancholi, S. S. Synthesis of 4-benzyl-1,3-thiazole derivatives as potential anti-inflammatory agents: an analogue-based drug design approach. *J. Enzyme Inhib. Med. Chem.* **24**, 890–897 (2009).

233. Bondock, S., Naser, T. & Ammar, Y. A. Synthesis of some new 2-(3-pyridyl)-4,5-disubstituted thiazoles as potent antimicrobial agents. *Eur. J. Med. Chem.* **62**, 270–279 (2013).

234. Lino, C. I. *et al.* Synthesis, molecular modeling studies and evaluation of antifungal activity of a novel series of thiazole derivatives. *Eur. J. Med. Chem.* **151**, 248–260 (2018).

235. Bhagat, K. *et al.* Design, Synthesis, Antimicrobial Evaluation, and Molecular Modeling Studies of Novel Indolinedione–Coumarin Molecular Hybrids. *ACS Omega* **4**, 8720–8730 (2019).

236. Ahangar, N. *et al.* 1-[(2-arylthiazol-4-yl)methyl]azoles as a new class of anticonvulsants: design, synthesis, in vivo screening, and in silico drug-like properties. *Chem. Biol. Drug Des.* **78**, 844–852 (2011).

237. Keating, G. M. Dasatinib: A Review in Chronic Myeloid Leukaemia and Ph+ Acute Lymphoblastic Leukaemia. *Drugs* **77**, 85–96 (2017).

238. Puszkiel, A. *et al.* Clinical Pharmacokinetics and Pharmacodynamics of Dabrafenib. *Clin. Pharmacokinet.* **58**, 451–467 (2019).

239. Duan, Y.-T. *et al.* Synthesis, biological evaluation, and molecular docking studies of novel 2-styryl-5-nitroimidazole derivatives containing 1,4-benzodioxan moiety as FAK inhibitors with anticancer activity. *Bioorg. Med. Chem.* **22**, 2947–2954 (2014).

240. Sun, J. *et al.* Synthesis, biological evaluation and molecular docking studies of 1,3,4-thiadiazole derivatives containing 1,4-benzodioxan as potential antitumor agents. *Bioorg. Med. Chem. Lett.* **21**, 6116–6121 (2011).

241. Sun, J. *et al.* Discovery of a series of 1,3,4-oxadiazole-2(3H)-thione derivatives containing piperazine skeleton as potential FAK inhibitors. *Bioorg. Med. Chem.* **25**, 2593–2600 (2017).

242. Luchini, C. *et al.* KRAS wild-type pancreatic ductal adenocarcinoma: molecular pathology and therapeutic opportunities. *J. Exp. Clin. Cancer Res.* **39**, 227 (2020).

243. Di Martino, M. T. *et al.* From single gene analysis to single cell profiling: a new era for precision medicine. *J. Exp. Clin. Cancer Res. CR* **39**, 48 (2020).

244. Gradiz, R., Silva, H. C., Carvalho, L., Botelho, M. F. & Mota-Pinto, A. MIA PaCa-2 and PANC-1 – pancreas ductal adenocarcinoma cell lines with neuroendocrine differentiation and somatostatin receptors. *Sci. Rep.* **6**, 21648 (2016).

245. Amrutkar, M. & Gladhaug, I. P. Pancreatic Cancer Chemoresistance to Gemcitabine. *Cancers* **9**, E157 (2017).

246. Elsässer, H. P., Lehr, U., Agricola, B. & Kern, H. F. Structural analysis of a new highly metastatic cell line PaTu 8902 from a primary human pancreatic adenocarcinoma. *Virchows Arch. B Cell Pathol. Incl. Mol. Pathol.* **64**, 201–207 (1993).

247. Giovannetti, E. *et al.* MicroRNA-21 in pancreatic cancer: correlation with clinical outcome and pharmacologic aspects underlying its role in the modulation of gemcitabine activity. *Cancer Res.* **70**, 4528–4538 (2010).

248. Chirumamilla, C. S. *et al.* Profiling Activity of Cellular Kinases in Migrating T-Cells. in *T-Cell Motility* (ed. Verma, N. K.) vol. 1930 99–113 (Springer New York, 2019).

249. Hilhorst, R. *et al.* Peptide Microarrays for Profiling of Serine/Threonine Kinase Activity of Recombinant Kinases and Lysates of Cells and Tissue Samples. in *Gene Regulation* (ed. Bina, M.) vol. 977 259–271 (Humana Press, 2013).

250. Chen, J. *et al.* Palladium-Catalyzed Asymmetric Hydrogenation of α-Acyloxy-1-arylethanones. *Angew. Chem. Int. Ed.* **52**, 11632–11636 (2013).

251. Li, K. *et al.* Inhibiting NF-κB-inducing kinase (NIK): Discovery, structure-based design, synthesis, structure–activity relationship, and co-crystal structures. *Bioorg. Med. Chem. Lett.* **23**, 1238–1244 (2013).

252. Diana, P. *et al.* Synthesis and Antitumor Activity of 3-(2-Phenyl-1,3-thiazol-4-yl)-1H-indoles and 3-(2-Phenyl-1,3-thiazol-4-yl)-1H-7-azaindoles. *ChemMedChem* **6**, 1300–1309 (2011).

253. Shehab, W. S. & Mouneir, S. M. Design, synthesis, antimicrobial activity and anticancer screening of some new 1,3-thiazolidin-4-ones derivatives. *Eur. J. Chem.* **6**, 157–162 (2015).

254. Pedras, M. S. C. & Hossain, M. Design, synthesis, and evaluation of potential inhibitors of brassinin glucosyltransferase, a phytoalexin detoxifying enzyme from Sclerotinia sclerotiorum. *Bioorg. Med. Chem.* **15**, 5981–5996 (2007).

255. Bahekar, R. H. *et al.* Synthesis and antidiabetic activity of 2,5-disubstituted-3-imidazol-2-yl-pyrrolo[2,3-b]pyridines and thieno[2,3-b]pyridines. *Bioorg. Med. Chem.* **15**, 6782–6795 (2007).

256. Carbone, A. *et al.* Synthesis and Antiproliferative Activity of Thiazolyl-bis-pyrrolo[2,3-b]pyridines and Indolyl-thiazolyl-pyrrolo[2,3-c]pyridines, Nortopsentin Analogues. *Mar. Drugs* **13**, 460–492 (2015).

257. Bandarage, U. K. *et al.* ROCK inhibitors 4: Structure-activity relationship studies of 7-azaindole-based rho kinase (ROCK) inhibitors. *Bioorg. Med. Chem. Lett.* **33**, 127721 (2021).

258. Bellale, E. *et al.* Diarylthiazole: An Antimycobacterial Scaffold Potentially Targeting PrrB-PrrA Two-Component System. *J. Med. Chem.* **57**, 6572–6582 (2014).

259. Xue, W. *et al.* N-thiadiazole-4-hydroxy-2-quinolone-3-carboxamides bearing heteroaromatic rings as novel antibacterial agents: Design, synthesis, biological evaluation and target identification. *Eur. J. Med. Chem.* **188**, 112022 (2020).

260. Vandersteen, N *et al.* Molecular mechanism underlying the pharmacological interactions of the protein kinase C-β inhibitor enzastaurin and erlotinib in non-small cell lung cancer cells. *Am. J. Cancer Res.* **7**, 816–830 (2017).

261. Schillaci, D. *et al.* A peptide from human β thymosin as a platform for the development of new anti-biofilm agents for Staphylococcus spp. and Pseudomonas aeruginosa. *World J. Microbiol. Biotechnol.* **32**, 124 (2016).